Teknillinen korkeakoulu
Laivalaboratorio

Helsinki University of Technology
Ship Laboratory

Espoo 2000

M-251

MARITIME RESEARCH SEMINAR 2000

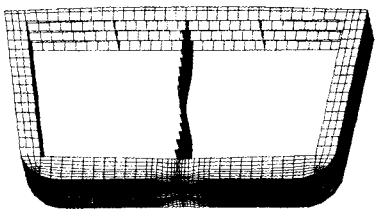

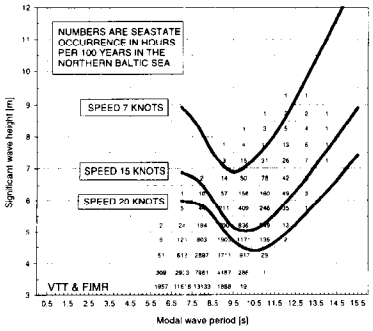

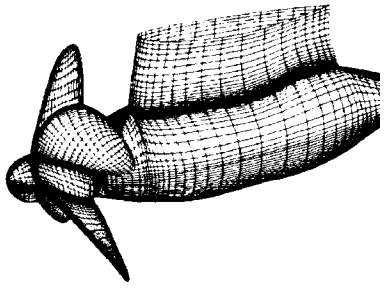

TEKNILLINEN KORKEAKOULU
HELSINKI UNIVERSITY OF TECHNOLOGY

M-251

MARITIME RESEARCH SEMINAR 2000

Seminar held in Espoo, Finland, 16 March 2000

Edited by Jukka Tuhkuri
Helsinki University of Technology

Organized by Maritime Institute of Finland:
Helsinki University of Technology
Technical Research Centre of Finland

Helsinki University of Technology
Ship Laboratory

Teknillinen korkeakoulu
Laivalaboratorio

Espoo 2000

Distribution:
Helsinki University of Technology
Ship Laboratory
P.O.Box 4100
FIN-02015 HUT, Finland
Tel. +358 9 451 3501
Fax +358 9 451 4173
E-mail: leila.silonsaari@hut.fi

ISBN 951-22-5101-9
ISSN 1456-3045

Picaset Oy
Espoo 2000

PREFACE

This annual seminar was the sixth one organized by the Maritime Research Institute of Finland. This time the idea was to make it more a workshop type; i.e. to provide a more informal discussion forum between researchers and the whole maritime community in Finland. No special theme was selected, but the presentations covered several actual topics, currently under active research at the Helsinki University of Technology (HUT) or at the Technical Research Centre of Finland (VTT).

Although the main aim of this seminar was to highlight current maritime research activities, it is essential that the needs and expectations of the industry are taken into account. The opening presentation, given by Mr. Renny Salminen, Design Manager of Kvaerner Masa-Yards, Turku New Shipyard, contributed excellently to this purpose. The "new economy" is already present in shipbuilding, too, requiring each of the actors to focus on their core competence, which makes networking with other players a must. Universities and research institutes like VTT have their own role in this maritime network.

The first four technical presentations dealt with safety aspects of maritime transport. Bow impact loads on passenger ferries, ship stability in waves, grounding loads and effects on the ship structure are all so complicated phenomena that a thorough understanding of the underlying physics is needed. Modern simulation and computer techniques allow the use of these first principles methods more and more relevant in practical applications. Simulation techniques are also of great importance, when possible emergency situations are practised in the way described in the fourth technical presentation.

The latter part the seminar topics covered structural as well as hydrodynamic issues. Fatigue in ship structures is especially important, when high tensile steel is used or novel structural concepts are applied. In hydrodynamics, computational methods (CFD) are approaching the level, at which they can be used to assist ship hull and propeller design in demanding applications. The real time simulation of ship motions in six degrees-of freedom is developing into a level, where it can be used in ship handling simulators, thus enabling the "man-in-the-loop" approach, i.e. the effect of man is taken into account e.g. in loads simulation instead of the conventional "blind ship" approach. The last presentation deals with the applications of novel power methods in vibration and noise control of ships.

The discussion from the floor during and after the presentations was enthusiastic. The general feeling was that these kind of annual seminars are very fruitful get-togethers within the Finnish maritime community.

Last but not least, I would like to thank all the people involved in organizing this occasion, all the speakers as well as the active audience for a very successful maritime session.

Espoo, May 2000 Matti K. Hakala

CONTENTS

MARITIME RESEARCH SEMINAR 2000

Renny Salminen
Kvaerner Masa-Yards

Mr Chairman, ladies and gentlemen,

First I would like to express my appreciation at being invited to this seminar and for the opportunity to say a few words at its opening. I shall use the time given me to give a few of my views on what the situation of Finnish shipbuilding and the shipyard industry is today.

This seminar, organised by the Maritime Institute of Finland, is already a tradition; I believe we can call it that when this is the sixth occasion on which we have gathered together to discuss the latest research and its results. This seminar is an excellent expression of the successful cooperation of the parties involved, who work together on an everyday basis to produce the results that we shall hear about today.

The scope of the topics covered this time is extremely broad and varied. As the invitation mentioned, the idea is to have a workshop approach to finding out about the projects going on in different research areas. The subjects range from the development of calculation and simulation methods to structural research and transport research. Several of the subjects are linked in some way to safety. We can see from the programme that this is going to be a very interesting day.

At present, world shipbuilding is booming. There are more modern cargo vessels, bulk and container ships, on the order books than ever before. At the same time, the price level has dropped so low that it is rarely possible for European shipyards to be competitive with this type of vessel. In central Europe there are still orders on the books, but new orders are difficult to get. Shipyards that build smaller tonnage are in a slightly better position. This situation means that European shipyards are moving more in the direction of special vessels, which means stiffening competition for Finnish shipyards.

At the same time, shipyards in the Far East will notice that the present boom in cargo vessels will fade within the next two to four years. Demand is decreasing. This has already meant that Korea and Japan are moving actively into the field of specialist vessels. Several RoPax and cruiser orders have gone to the Far East. Simultaneously, the USA is reviving its passenger vessel industry. This means that the territory that has belonged relatively peacefully to Finland and several European partners in recent years is threatened.

It is good to notice that national cooperation with different parties – industry, design offices, suppliers, VTT, Helsinki University of Technology – functions well. A good example of this is this seminar and Seatech 2000+. The foundation is the successful regular cooperation in everyday operations. It is vital to preserve in Finland all the factors involved in marine and maritime technology. The industry cannot manage without high quality education and

research, and similarly the maintenance of research and continuation in general would be difficult without an active industry.

Universities and VTT are primarily concerned that the basic conditions are in order. Education is world class, and research ensures that expertise in marine technology, marine theory and the technology applied in ships is the very best available in the world. On the other hand, it has been pleasing to notice the will and effort to extend the fields of activity very much over the years from what it was say, twenty years ago. Changes in products and production methods put the focus on different kinds of problems. The application of mechanical and electrical engineering to ships has long been a subject of training and research. Research into the use of ships in different situations is also advanced, as we can see from the seminar programme. There has also been a cautious start in the application of interior design and HVAC to ships. In these areas, the nature of the education differs from that in conventional marine areas. It's a question of applying the achievements of another scientific discipline in a new environment. Applications to the conditions in ships and at sea require their own knowledge, their own research. These interdisciplinary matters are central to the final product: taking into account costs and the end-user, the passenger.

In addition to the construction part of shipyard operation, there is a need to study and define the new networked environment in the shipbuilding industry. The actual assembly of the ship naturally takes place at the shipyard. In the vicinity and at the shipyard itself there is a many-layered network of suppliers. The role of ships' outfitters has also grown significantly with the concentration on cargo vessels. These changes have meant that control of operations and costs has become a vital factor alongside the conventional "welding" side of the industry.

These extensions to the field are also evident in the subjects of academic theses and dissertations, as well as in the topics of research. In addition, there is some indication of increased interest in research into the networking of the shipbuilding industry in other higher education institutions, for example, schools of economics and business administration and in the universities. Their research focuses more on working methods, costs and relations between the various parties than on the conventional technology. It is my belief that cooperation in this field is only in its infancy at the moment.

It has been my intention to draw attention to the importance of education, research and cooperation; the broad nature of the field in which we have to work, and the direction in which it still has to expand.

Finally, I would like to thank all the speakers and organisers of this seminar. I'm sure we have ahead of us a very interesting and rewarding day.

For my own part, it is a great pleasure to welcome you all to this seminar.

FINNISH FLAG PASSENGER SHIP BOW STRUCTURAL DESIGN AGAINST WAVE INDUCED LOADS AT THE NORTHERN BALTIC AND SURVEY OF THE BOWS

Harri Soininen
VTT Manufacturing Technology

ABSTRACT

A detailed survey was performed for all passenger ships under Finnish flag (16 ships in all) having bow doors. The wave statistics of the Northern Baltic was updated for this project. Calculations were performed individually for each ship of the sea conditions, significant wave height/modal period and the ship speed for meeting the design loads according to the unified Classification regulations, IACS-95. A semi-empirical method calibrated with model test results was used. The method was further validated with direct simulation calculations. Based on the combinations of design load levels and the wave statistics some operative recommendations were proposed.

1. INTRODUCTION

The International Accident Investigation Commission investigating the capsizing of MV Estonia proposed in its final report that the design criteria of old passenger and Ro-Ro passenger vessels should be studied. The new knowledge of ship safety and new safety standards should be taken into account.

The Finnish Institute of Marine Research has continuously measured during the past 3 years the sea state in the Northern Baltic. As a result it is now possible to check more precisely if the measured wave conditions are equal with the wave conditions that have been used as a basis for the design loads. In October 1998 some damages occurred at the bow areas of 2 Ro-Ro passenger ferries during heavy weather in the Northern Baltic. A discussion has taken place regarding possible weather limits for Ro-Ro passenger vessels equipped with bow doors. The first study recommended by the Estonia accident report accorded a critical assessment of bow designs and load criteria. The Finnish Maritime Administration ordered this study from VTT Manufacturing Technology in November 1998. Parts of it were performed by the Finnish Institute of Marine Research and Engineering Company ILS Oy.

The aim of the study was to develop a rational basis for assessing the adequate strength of a passenger ship bow construction in the environmental conditions of the Northern Baltic. The aim is reached when the design sea state of the sea area is assessed, together with the loads induced to bow by that sea state and, on the other hand, the sea states corresponding to the design loads of every Finnish passenger ship bow. A detailed survey of all Finnish passenger ships equipped with a bow door or visor (16 ships in all) was performed paying attention to a critical review of the balance of the structure.

2. THE RESEARCH PROGRAMME

2.1 Scantling calculations

The development of the classification requirements of passenger ships under the Finnish flag was reviewed from 1970'ies to the present day regarding the bow strength. The original individual design calculations when available as well as the calculations according to unified classification regulations, IACS-95, were reviewed. New requirements were studied paying attention to details that are essential for the structural strength and that are not valid for older ships. Both fatigue and limit strength were taken into account. The existing plate thicknesses and stiffener section moduli were compared to the present requirements - in some cases it was found quite clear underdimensioning. Fulfilling these scantling requirements is not, however, obligatory for vessels built before IACS-95. The requirements for additional strenghtenings of old ships apply to the locking devices.

2.2 The survey

Bow parts, especially the bow door locks and supportive constructions, of all Finnish passenger ships equipped with bow doors were surveyed. All the bow constructions have been designed and strengthened in accordance with the IACS-95 requirements, some of the strengthenings have been quite extensive. On the other hand the surveys showed more defects in construction details than were expected. In quite many cases the actual design differed from the one in the approved drawings.

2.3 The wave statistics

New data from measurements in the Northern Baltic Proper, as well as wave model calculations have been used to obtain more accurate statistics than have been available in the past.The probability for the various combinations of significant wave heights and periods were predicted for a critical location, south of Utö, at the Northern Baltic. The worst situations occur during south-westerly winds. Ships that meet these conditions are heading from Helsinki or Tallinn towards Stockholm. The 1% probability of exceedance for the significant wave height is 4.1 m at Bogskär and, on the other hand, only 2.6 m at the Åland Sea. The 1% exceedance means about 70 hours per year. In addition this time is not continuous but is split into short storms. While high waves can exist in all seasons, in practise they are restricted to the autumn and winter periods.

2.4 The wave conditions where design loads are met

The wave conditions - H_S/T combination -where the IACS-95 load level will be met for each vessel were calculated. The calculations are based on a semi-empirical method. First the wave-induced motions for a set of wave conditions in head and oblique head seas were assessed. Based on experience of some model tests the load was assumed to depend besides of the bow geometry and speed of the ship from the vertical relative speed of the wave and bow in power two and relative position of the wave and bow in power one. The following formula was developed:

$$p = CZ_R V_R^2 f_{IACS}(V, L, \alpha, \beta) \quad (1)$$

where: p is the wave pressure (averaged to the whole area of the bow doors or visor), C is a constant, Z_R is the relative position between the wave and the bow, V_R is the vertical relative speed of the wave and bow, $f_{IACS}(V, L, \alpha, \beta)$ is the formula in IACS-95 rules for the calculations of bow load taking into account the ship size, ship speed and bow geometry. The method was calibrated by the model test results from Estonia (Trägårdh1995) and the SSPA (Lundgren 1996) measurements to define the constant C.

The operability-limiting significant wave heights with regard to the IACS-95 design pressure were calculated using the following procedure:

1. The design pressure obtained by the IACS-95 formula is calculated.
2. The significant motions of a ship bow in irregular seas are calculated using the Jonswap wave spectrum. The ratio of the significant relative velocity and relative motion is obtained.
3. The significant relative velocity corresponding to the IACS-95 design pressure is calculated.
4. The significant wave height corresponding to the significant relative velocity is calculated.
5. The procedure is repeated for different wave periods and ship speeds.

The loads were calculated to correspond three hours exposure for each sea state. For most of the ships the significant wave height between 4 to 5 meters will result to the design load level at full speed. Typical result for a medium-size of a vessel combined with the wave statistics is shown in Figure 1.

2.5 Time domain simulation of impact loads, validation of load calculations

Direct simulations of impact loads on bow doors or visors were carried out in order to verify the semi-empirical results. The theoretical background is given in more detail in Palkama (1996), and Kukkanen & Matusiak (1999). The main features of the applied method are as follows:

1. The impact force perpendicular to the stem of the ship bow is calculated. The relative velocity and acceleration components are determined separately in the longitudinal and vertical directions in order to obtain resultant that is perpendicular to the stem. The velocity potential of the water impact is also calculated in the co-ordinate system that is related to the stem. This takes into account the approximate vertical and longitudinal components of the relative velocity and accelerations.
2. The impact forces on the bow doors and visors are evaluated in three stages. Firstly the velocity potentials are determined for the bow sections at different submergence values. This is done for the bow sections that are perpendicular to the stem and applying the two-dimensional so-called close-fit method. At the second stage, transfer functions of the vertical relative motions, velocities, and accelerations at the bow are determined using thelinear strip theory. Finally the impact pressures and forces are simulated in irregular

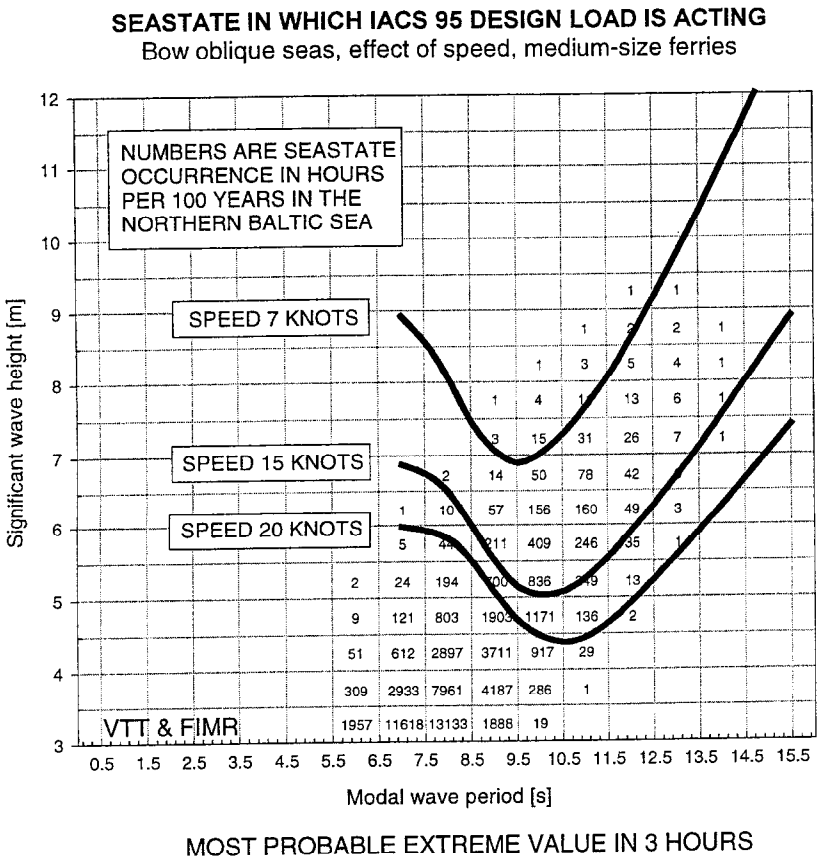

Figure 1. Typical design level curves for an average sized vessel

waves using the pre-calculated transfer functions and velocity potentials. As ship motions are computed using the linear strip theory they are not affected by impact wave loads. Total hydrodynamic pressure is evaluated on the instantaneous wetted surface. This pressure comprises the effect of the wave impact load. Integration of pressures is conducted for each time step yielding time histories of impact force.

Direct simulation of the bow loads was performed for 2 ships representing typical bow geometries. For each ship, simulations were conducted for 3 vessel speeds, and three heading angles and a few different sea states. Results of the time domain simulation together with the semi-empirical results for one ship are given in Figure 2. Directly simulated loads are in good agreement with the semi-empirical estimates in terms of the ship operation limiting sea state parameters.

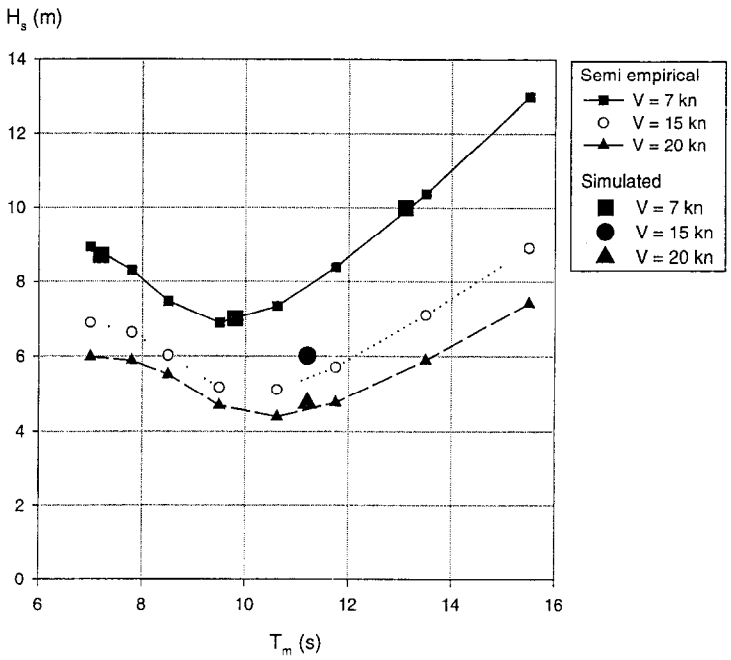

Figure 2. The results of time domain simulations compared to the semi-empirical estimation.

2.6 Criteria of load levels

The design load level applied should give adequate strength for the construction in the operation environment. However, it is not so obvious what is strong enough. A very low level of failure risk may lead to an unpractical and expensive construction while frequent reports of bow door failure incidents may have a negative effect on the popularity of passenger ferry traffic. To assess what is an adequate level for the design load boundaries, criteria developed for risk levels generally applied in the society were used. A review of risk levels and a specific application to high-speed passenger craft operation is presented in the report by the SSPA (1998).

The development of the criterion is based on the following basic assumptions:

1. Although the loss of a passenger ferry is as such not acceptable, applying general risk criteria give a limit of about 1 loss in 10^6 ship years.
2. One in a hundred exceedances of the IACS-95 bow door design level causes significant damage to the bow door construction.
3. One in a hundred cases of significant damage to bow door construction leads to foundering.

Taking into account the time that an individual ship spends on the critical area and the average yearly ice coverage the acceptable probability for an exceedance of the IACS-95 design level, P_{design}, is reached :

$$P_{design} < 33\ ppm \qquad (2)$$

On the basis of the above consideration, it seems that a reasonable criterion is in the range of $P_{design} < 30$ to 300 ppm. Thus, the order of magnitude should be hundreds of ppm, not thousands of ppm. In applying this criterion to individual ships, it should be taken into account that the numbers of ppm increase quickly with decreasing significant wave height. Thus, a relatively small error in the level of the boundary may cause an order of magnitude error in the risk level. On the other hand, the bow load increases very quickly with increasing significant wave height and if the vessel has a chance of encountering sea states significantly above the design boundary, it may be necessary to wipe out the probabilities of encountering these sea states by defining operational restrictions.

2.7 Operative recommendations

Operative recommendations individually for each ship were proposed by the Maritime Administration as a result of the study. The restrictions are based on the calculated design load curves combined with wave statistics taking into account the margins between damage load and design load etc. The recommendations are illustrated roughly for three size categories small, average and large in Figure 3. The speed is limited as function of significant wave height and extreme conditions not allowed for average size and small ships.

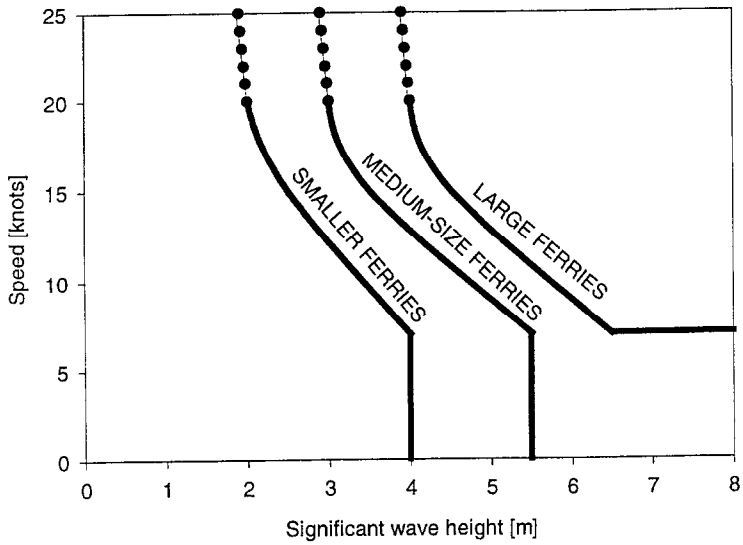

Figure 3. Speed recommendations for small, medium-size and large ferries as function of significant wave height.

2.8 Monitoring the load

To help the officer in charge to better assess the level of loads at the bow the current level and trend of bow door or visor loads could be monitored onboard the ship. The load itself is difficult to measure directly. The measuring instrumentation is complex and expensive and the calibration of the system is laborious. However, the calculations of the relation between the

load and ship motions make it possible to estimate the loads indirectly utilising the easily measurable global vertical acceleration at the bow as an indicator of the load. The significant wave height can be estimated using the type of information given in Figure 4A where the limiting significant wave heights with regard to criterion of 0.25 g vertical acceleration at the bow are presented for various ferries in non-dimensional form. The corresponding curves with regard to the IACS-95 design loads shown in Figure 4B are used when the load is estimated.

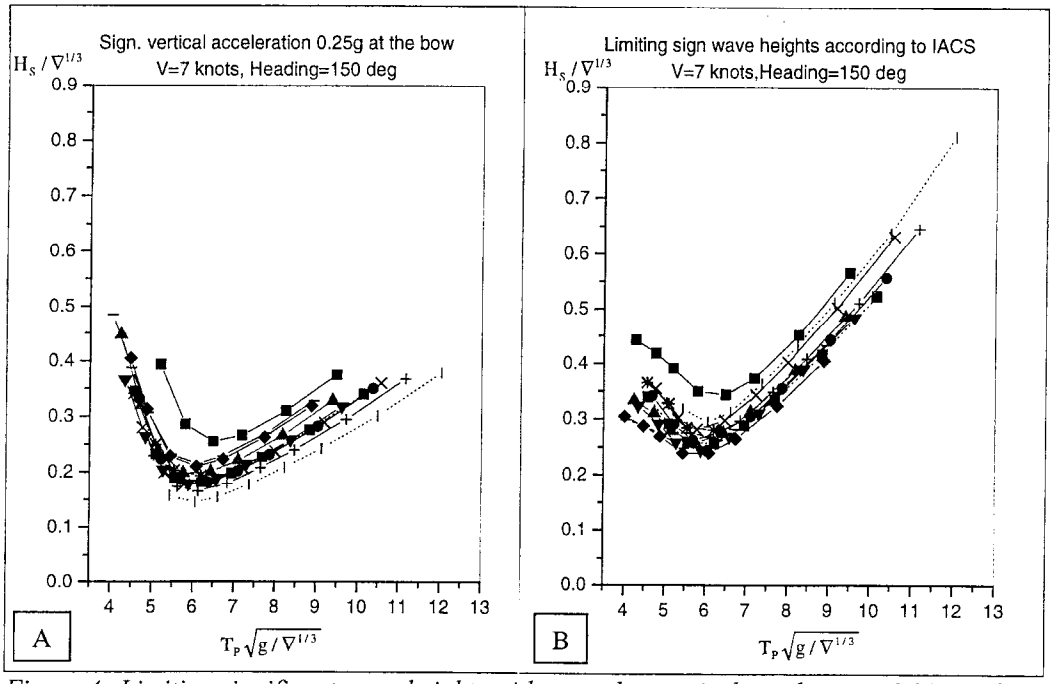

Figure 4. Limiting significant wave heights with regard to vertical acceleration 0.25 g at bow (A) and the IACS-95 design load (B) for various ferries.

3. CONCLUSIONS

The results show that for most ships the significant wave height between 4 to 5 meters will result to the design load level at full speed. The typical ship size and wave height, wave modal period combination at the Baltic on the other hand, are such that the design load level is met at these conditions that are far from being extreme. Increasing the load level to double (the margin between the design load and ultimate load) will increase the critical wave height with about one meter. Dropping the speed from 20 knots to 7 knots will increase the critical wave height with 2 to 3 meters. It has to be noticed that 20 knots speed is somewhat theoretical in rough seas, the speed drops due to the added resistance of the waves and the speed has to be dropped to maintain some comfort level onboard.

The combined wave statistics load curves show that without considerable speed reduction the design load level would be exceeded for average sized vessels for some 3 hours a year at the trade in question. The wave statistics show, however, that wave conditions of critical wave

height in the Northern Baltic do not usually last long, i.e. the limiting effect to the trade is marginal.

The results of direct simulation of impact loads for 2 vessels support the results obtained by the semi-empirical method. It would be beneficial to calculate some more validation cases.

The similarity of the dimensionless bow vertical acceleration and load curve shapes supports the idea of a simple monitoring system that is based on acceleration measurements.

Based on the results of the design load calculations as a function of wave conditions it is natural that operative recommendations are given. The Finnish Maritime Administration has given speed/wave height recommendations individually for each ship. It is, of course clear that there exists a certain margin above the design loads before any damage takes place. On the other hand, it cannot be claimed that the load curve calculations give exact results. If the inaccuracy against wave height is as much as 1 metre it would mean considerable changes in the wave condition occurrence probabilities.

4. ACKNOWLEDGEMENTS

The Finnish Maritime Administration, and especially the Maritime Safety Director Heikki Valkonen is thanked for giving the opprtunity of working with this interesting subject. The project has been performed by a group of individuals at VTT. The constructive attitude of the shipping companies is acknowledged.

5. REFERENCES

Kukkanen, T. and Matusiak, J. 1999. Passenger ship bow structural design against wave induced loads at the Northern Baltic. Simulation of impact loads on bow doors and visors of car-ferries. VTT Manufacturing Technology, Research Report No. VAL32-992742.

Lundgren, J. 1996. Bow loads on RoRo ships. RORO96 Conference Lubeck, 21-23 May 1996. Proceedings, VOL 2, Session 11.

Palkama, H. 1996. Impact wave loads on bow doors of car-ferries. Master thesis, Helsinki University of Technology. 110 p.

SSPA (co-ordinator). 1998. Joint Nordic Project for Safety Assessment of High-Speed Craft Operations, Final Report, SSPA Maritime Consulting, Sweden, October.

Trägårdh, P. 1995. Model test with M/S ESTONIA. Sea loads on bow visor and yawing behaviour due to heel. SSPA Maritime Consulting. Report 7524. Gothenburg 1995.

Dynamic stability of a fast Ropax vessel in following waves

M. Mattila[1]
[1]Helsinki University of Technology, Espoo, Finland

ABSTRACT

Transverse stability of a fast Ropax-vessel in following seas is investigated experimentally. A transom stern vessel experiences large waterplane area changes in waves that the vessel is encountering stern-on and this may lead to pure loss of stability on a wave crest. Model experiments were made using a modern twin screw transom stern type hull form. All experiments were made using three different metacentric height (GM) values. In order to determine the form stability of the model at different speeds, inclining experiments were performed in a Froude number range of 0 to 0.4. Pure loss of stability experiments were done for the model with seven different wavelengths and four different speed values in regular following waves. Pure loss of stability in a wave crest was observed only when the model had a Froude number of 0.35. This was partly due to strong growth of the form stability as a function of speed.

1. INTRODUCTION

The interest towards fast Ropax vessels has increased strongly during past ten years. The hull form for this kind of vessel is usually open type transom stern. This type hull form results in large variation of waterplane area in following seas. When waterplane area is reduced ships initial stability is also reduced and this might even lead to total loss of stability. This situation is called loss of stability on wave crest. This is especially dangerous situation if vessel travelling with nearly same speed as wave phase velocity and wavelength is equal to length of vessel.

This paper describes shortly model tests conducted with a model of modern fast Ropax vessel and some results obtained from analysis of tests. Testing program included testing of vessels initial stability as a function of a speed in calm water and tests in steep following waves. Tests were performed in Helsinki University of Technology's 130 meters long towing tank. Testing program included also testing of parametric resonance of rolling, but these are not presented in this paper.

2. GENERAL

Model used in tests was so called Seatech D-model, which full and model scale main dimensions are presented in Table 1. Table also presents three different positions of centre of gravity (COG). All the tests were performed by using all three positions of COG.

Table 1. Main dimensions of ship and model.

	Ship	Model
Scale	1	39,024
L_{WL} (m)	158,6	4,064
B_{WL} (m)	25	0,641
L_{PP} (m)	158	4,049
D_P (m)	4,80	0,123
T (m)	6,1	0,156
D (m)	15	0,384
∇ (m^3)	13766	0,232
C_B	0,571	0,571
GM_1 (m)	2,8	0,072
GM_2 (m)	2,2	0,056
GM3 (m)	1,7	0,044

Model was equipped with twin shaft arrangement and twin rudders. These were controlled remotely from the towing carriage. Model was fitted with bilge keels and the length of keels were 30% of L_{PP}.

3. FORM STABILITY AT SPEED

3.1 Testing arrangements

In order to measure ships initial stability at different velocities, inclination test was performed at eight different speeds (Fn=0, 0.25, 0.28, 0.30, 0.33, 0.35, 0.38 and 0.40). During these tests model was towed with carriage. A weight was placed off the centre line producing an inclining moment. While towing model at desired speed, inclination angle and model speeds were recorded. From this measured inclination angle could initial stability GM value be calculated. From this value it was possible to calculate form stability at speed BM_V, when models height of COG from baseline is known.

3.2 Results

By analysing values obtained with three different heights of COG, Figure 1 could be drawn. In Figure 1 are presented relative height of metacentre KM values. Also relative change of form stability obtained from tests with lowest COG is presented.

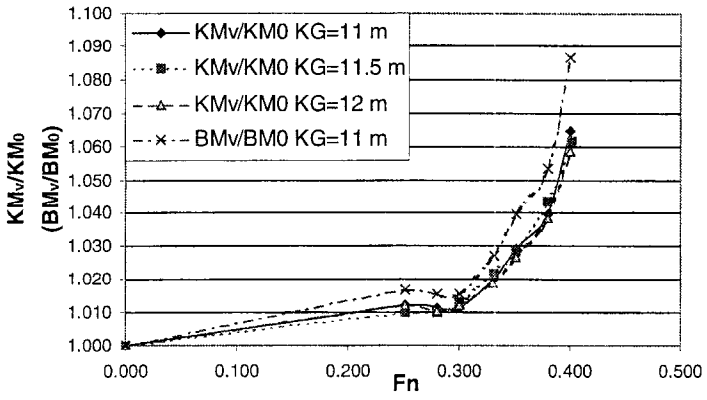

Figure 1. Relative change of initial stability and form stability change as function of speed.

Different KM-curves represent values obtained from tests performed with different height of COG. In Figure 1 can be seen strong growth of vessels initial stability as function of speed. This growth of initial stability is mainly due change of wave pattern along the hull. Especially this change happens in aft part of the hull where wave fills stern of the model producing more waterplane area. This growth is very strong and is dependent of hull form.

4. STABILITY IN WAVE CREST

4.1 Testing arrangements

Testing of stability on wave crest is very difficult due large encounter period. Model encounters only few waves during one run. This is why length of towing tank is very critical, because tank ends easily before model reaches wave crest. In addition model has to be moving freely with own propulsion and model has to be steered. Model can't be towed, because rope forces affect easily to results.

Tests were performed in regular waves, because only one wave is required for loosing vessel stability on wave crest. Waves were chosen to be as steep as wave machine could generate. This way wave height wavelength relation was 20 and increased so that longest wave relation was about 35. There were six different wavelengths (λ=0.75L_{PP}, 0.86L_{PP}, L_{PP}, 1.25L_{PP}, 1.5L_{PP} and 1.75L_{PP}) and four different speeds (Fn=0.25, 0.30, 0.35 and 0.40) chosen for the tests. In addition all speed- and wavelength combinations were tested with all three height of COG values. This way there were 72 different combinations. It was required to perform totally 167 runs, out of which only 100 were good enough for analysis.

Model were equipped with six degrees of freedom gyro in COG and capasitive tapes on both sides of largest frame. Also rudder angle and motor Rpm's were recorded. From towing carriage speed and wave height were recorded. Gyro measured accelerations in co-ordinate system, which was attached to ship. This caused so called g-error in to accelerations and made impossible to get accurate model position in inertial co-ordinate system.

4.2 Results

In result figures inclination angle is made dimensionless by dividing angle with wave slope. Inclination angle as function of speed is presented in Figure 2. It can be seen that largest inclination is reached already at Froude number of 0.35. This can be explained by looking change of form stability in Figure 1. As ship speed increases form stability increases strongly resulting in good enough stability. On the other hand Figure 2 can be explained with Figure 3, which represents relative draft at largest frame (#4) as function of speed. As it can be seen (Figure 3) relative draft doesn't reach that high values at largest speed as one could expect. This is mainly due strong surge motion generated by wave and this way model is accelerated into sagging condition where stability is higher than in calm water.

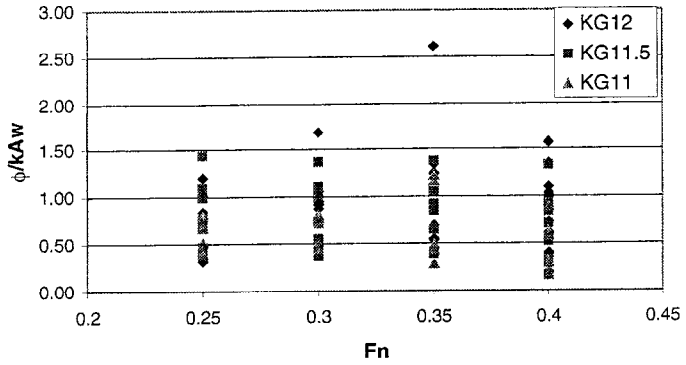

Figure 2. Dimensionless maximum angle as function of Froude number.

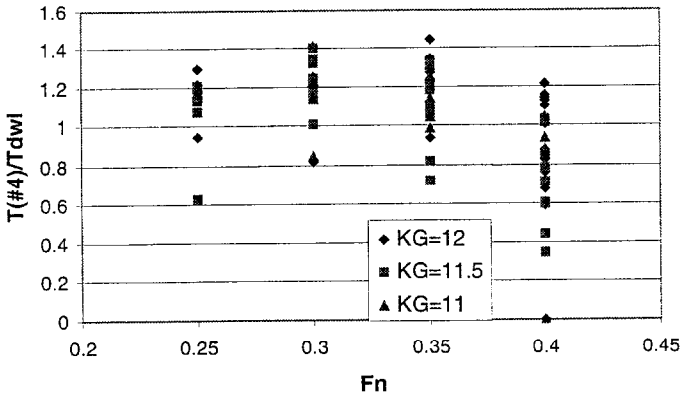

Figure 3. Relative draft at frame four (#4) as function of speed.

Finally for the vessel were calculated GZ-curves at critical situations by using GZ-curves generated with NAPA-program. In NAPA-program vessel was situated in different static

waves, which were same as tested. Calculated GZ-curves were corrected with vessels measured form stability at different speeds by using equation (1). This calculation doesn't take count heave generated by wave motion. It is assumed also that change of form stability is constant at different inclination angles.

$$GZ_{cor.}(\phi) = (GZ_{Wave}(\phi) + B_0 G \sin\phi)\frac{BM_v}{BM_0} - B_0 G \sin\phi \qquad (1)$$

In equation (1) term GZ_{Wave} refers to value calculated in static wave with NAPA-program. Term BM_V refers to measured form stability values (Figure 1) at different speeds. Corrected CZ-curves for the measured critical situations are represented in Figures 4-5.

In measurements were noticed strongest inclination angle at Froude number of 0.35, although according to theory (Matusiak 1995) this should have happened at Froude number of 0.4. Figure 4 explains why there weren't large inclination angles at Froude number of 0.4. As it can be seen, in lower speeds stability is worst, but velocity difference too large and ship doesn't have time to roll before wave has gone by. At Froude number 0.4 initial stability is twice as big as at Froude number of 0.35 and this way there can't be large inclination. Height of the COG has even more clear impact on stability than the speed. This kind of quasi-static stability check can be seen as decent enough way to estimate ships stability in wave crest. Defining ships form stability can be done with simple model test. In addition there is clear signs that this form stability could be obtained by defining wave profile along ships hull and calculating new form stability BM value with this new waterplane. Wave profile could be obtained by using some CFD-program using free surface boundary conditions.

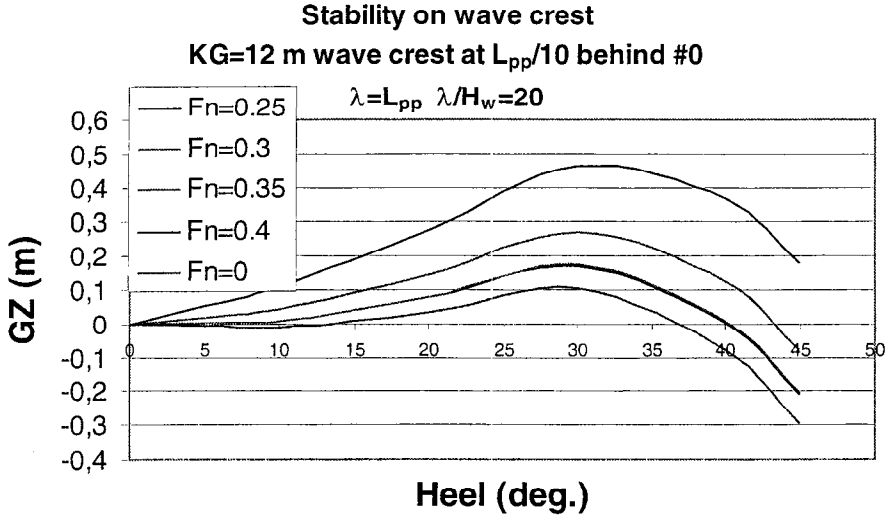

Figure 4. Calculated corrected GZ-curves at different speeds with wavelength being same as ships (Fn=0 not corrected) in full scale.

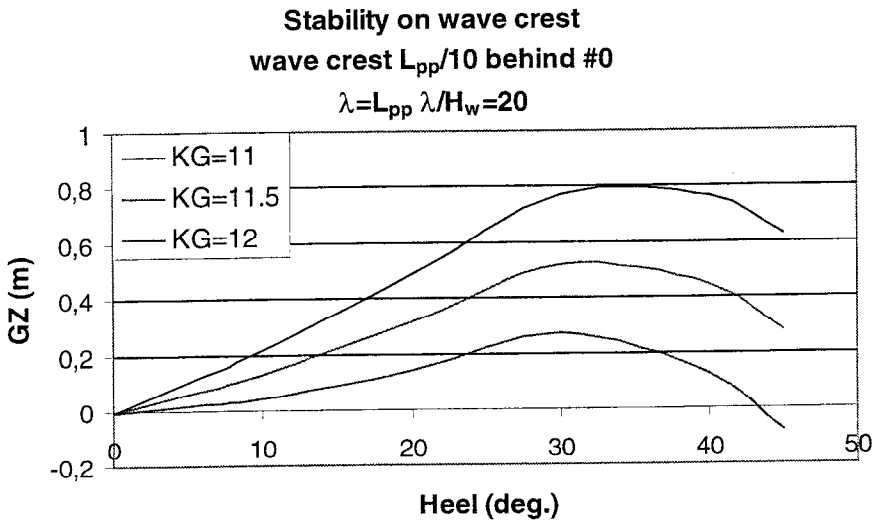

Figure 5. Calculated corrected GZ-curves with different heights of COG and wavelength being same as ships in full scale (Fn=0.35).

5. CONCLUSIONS

Stability of modern fast Ropax vessel has been studied with model tests. Also a calculation method to determine ships stability in wave crest has been proposed.

Form stability of the model at different speeds was tested by towing model with known inclining moment at several speeds. Strong growth of form stability was detected and this is due large growth of waterplane area in stern of the vessel. This change of waterplane area is caused by vessels own wave profile, which fills stern of the vessel.

Loss of stability on wave crest –tests were performed in regular waves with three different heights of COG. Tests were done with using model free to move in all six degrees of freedom and equipped with own propellers and rudders. Model inclined strongly only at the Froude number of 0.35. While model was moving at the Froude number of 0.4, Form stability had increased strongly and no strong inclination were detected. During model tests model didn't capsize.

6. REFERENCES

Matusiak, J. 1995. Ships buoyancy and stability. Espoo Otatieto Oy (in Finnish).

FE APPROACH TO THE SHIP GROUNDING EVENT

J. Kajaste-Rudnitski and P. Kujala
University of Technology, Helsinki, Finland

ABSRTACT

According to statistics, ship grounding is a fairly frequent type of accident in Finnish waters. The structural innovations, such as double bottom hull and internal subdivisions, improve ship safety and diminish risk of environmental disasters (oil spilling). Actually, dynamics of this kind of cargo vessel collision with a rigid obstacle (rock) is considered in terms of contact problem using the FE program ABAQUS (Explicit version). Preliminary buckling analysis enables to find possible distorted shape of the hull and, after superposition with initial intact form, to create its initial imperfect configuration. ABAQUS explicit contact algorithm may help to evaluate quantitatively (in terms of stress and deformation state, kinetic energy dissipation due to plastic strain accumulation etc.) the extent and nature of damages.

1. INTRODUCTION

As an example of ship FE meshing a tanker is chosen. This ship has had a grounding accident and consequent damages were examined and measured providing thus a kind of qualitative comparison to the numerical data.
Meshing the whole hull of the ship over 100 m long is an impossible task, especially having in mind the contact formulation of the problem where fine element mesh is needed around contact area. The middle part of the ship is meshed comprising three sections with 2.1 m long each between transverse web frames. Meshing the whole hull of the ship over 100 m long is an impossible task, especially having in mind the contact formulation of the problem where fine element mesh is needed around contact area. The middle part of the ship is meshed comprising three sections with 2.1 m long each between transverse web frames. It should be noted that a model does not follow exactly the configuration and dimensions of the real tanker and presents only generally this type of vessel. The general view of this meshed part is shown in Fig. 1. To expose the internal structures of the hull the front transverse web frame is not shown as well as masses and spring elements. Since all load bearing elements of the ship are made from the thin steel plate the hull structure may get large initial elastic deformations due to buckling of its sheet constructions when the ship hits an obstacle. The right hand co-ordinate system is chosen so that z- axis coincides with the longitudinal direction of the ship.
So first, the buckling analysis is performed using the ABAQUS Standard routine (implicit version) (Hibbit, Karlsson and Sorensen, 1998) and eigenmodes are superimposed with initial undeformed form of the structure yielding thus an imperfect initial structural form. Next, the static stress-strain analysis is carried out in attempt to estimate a bearing capacity of the unit length (or typical section) of a ship hull. Finally, the dynamic analysis of a ship-grounding event considered as a contact between deformable ship hull and rigid body (obstacle) is successfully performed.

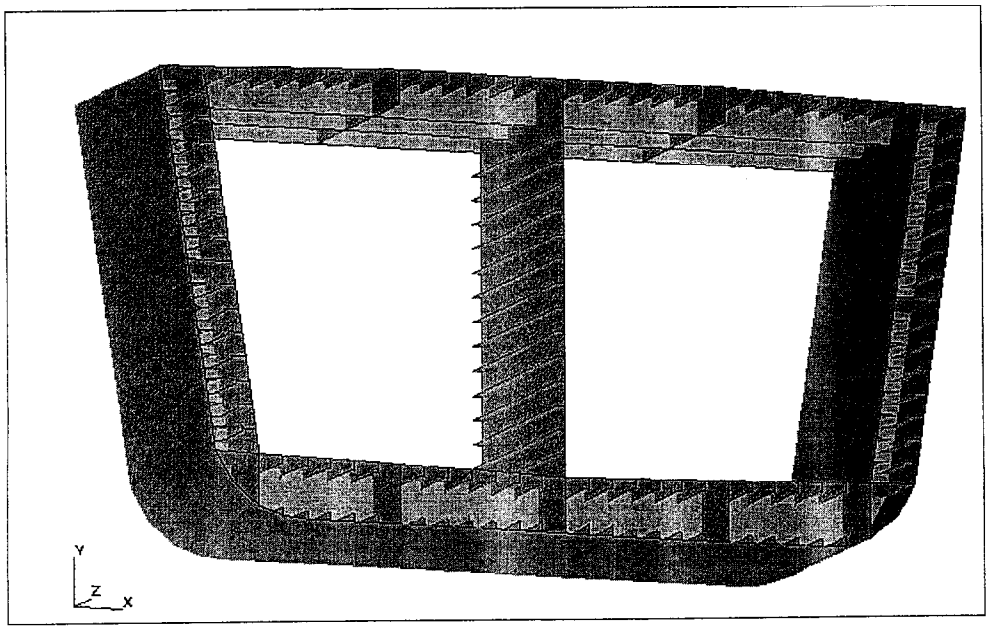

Fig. 1.Meshed section of the ship hull. Front frame is removed to show details of internal structure.

2. FE MODEL

2.1 Geometrical and mechanical characteristics of the model.

To create the element mesh of the main section of the ship the pre-processing program ABAQUS/Pre (Hibbit, Karlsson and Sorensen, 1998) is used. All bearing steel structures including longitudinal beams are modelled with 3D shell elements. The geometry and topology of the mesh, as well as tolerance, is checked automatically and corrected if needed. As it is seen from Fig. 1 the cross-section of the ship is not symmetric, so FE meshing is extended over whole cross-section. It is supposed that a contact touch happens along the middle axis of the ship. Within this area the element mesh is denser. As to structural material, it is elastic-plastic steel with isotropic hardening. The following material properties are needed for further analysis: Young's modulus $E=2.1\cdot10^5$ MPa, Poisson's ratio $\nu=0.3$, strength $\sigma=280$ MPa, yield strength after hardening $\sigma_{pl}=290$ MPa, plastic strain at 1% strain point $\varepsilon_{pl}=0.8$ %. After reaching this yield stress level material becomes perfectly plastic.

2.2 Imperfect configuration of the ship hull.

Distorted eigenmodes of the meshed section are superimposed with initially intact shape yielding thus the initial imperfection. The buckling analysis is performed on a meshed section of the ship only, the other parts being replaced by spring and mass elements.

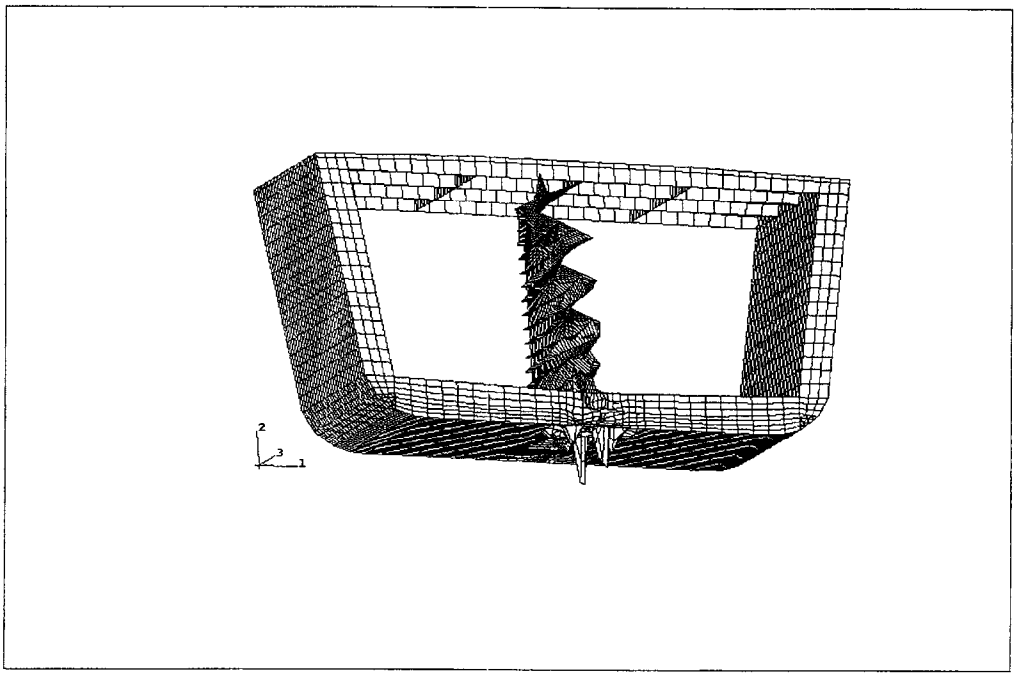

Fig. 2. 15th eigenmode.

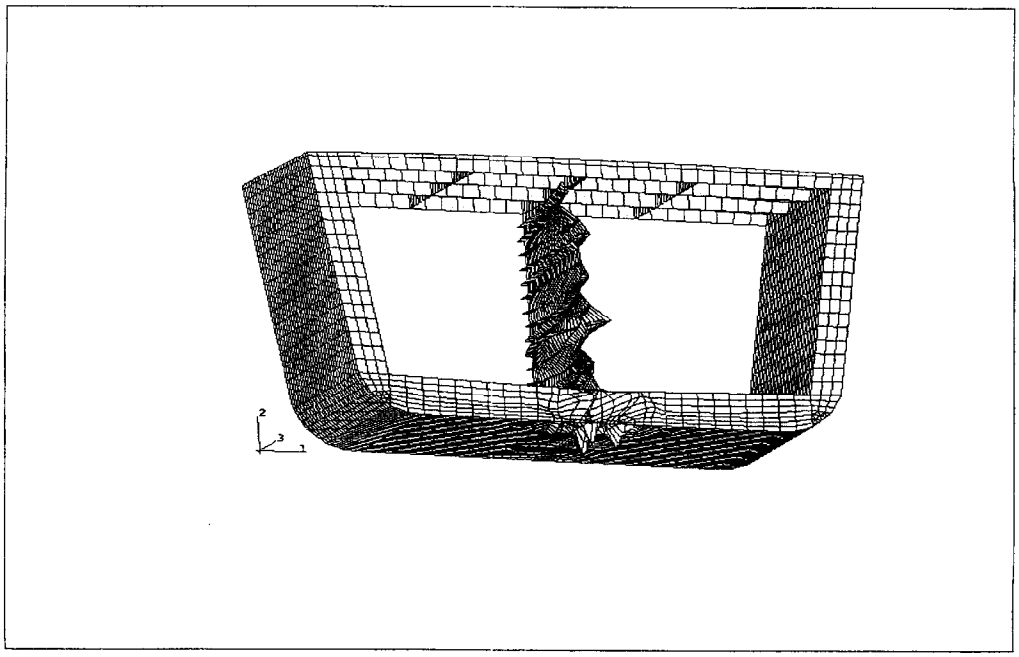

Fig. 3. 19th eigenmode

It is proved that this approach is adequate. Eigenmode amplitudes are normalised to unity (1 m in actual units) and scaling is needed for superposition with initial form. Typically the scaling magnitude is a few percent of shell thickness. Actually the scaling coefficient is 2.1E-3 to 1.0E-3 depending on the mode number. Totally 20 eigenvalues (all of them positive) and corresponding eigenmodes are extracted. The most significant of them, namely 6, 8, 10, 13, 14, 15, 17 and 19^{th} modes, are used for superposition with initial geometry. In a buckling analysis all inelastic effects are ignored. As an example Fig. 2 and Fig. 3 present 15^{th} and 19^{th} eigenmodes respectively. For contact analysis the magnitude of critical load is irrelevant, only probable distorted shape is important.

3. DYNAMIC GEOMETRICALLY NON-LINEAR CONTACT PROBLEM

3.1 General remarks about non-linear contact algorithm.

ABAQUS/Explicit option is used to perform a dynamic analysis. The explicit dynamic procedure deals with a large number of small time increments. An explicit central difference integration rule is used. The explicit central difference operator satisfies the dynamic equilibrium equations at the beginning of the increment t, the accelerations at the time t are used to advance the velocity solution to time $t + \Delta t/2$ and the displacement solution to time $t + \Delta t$. The central difference operator is conditionally stable. The approximation to the stability limit of the operator is defined as the smallest transit time of a dilatational wave across any element in the mesh $\Delta t = L_{min}/c$, where L_{min} is the smallest element dimension and c is a dilatational wave speed in the material. Another estimation of the stability limit is given in terms of highest frequency of the system as $\Delta t \leq 2/\omega_{max}$. The actual automatic time incrementation algorithm uses both these estimations when default option is requested. The use of small increments defined by stability limits is advantageous since it allows the solution to proceed without iterations and without requiring tangent stiffness matrices to be formed.

3.2 Contact with analytically defined rigid body

Now consider an event when a ship 104.2 m long and 22700 tons of buoyancy hits at its middle the rigid obstacle in the form of the obtuse cone. Initial imperfection due to possible buckling is taken into account. At the moment of impact the velocity components are as follows: horizontal component in z-direction V_z =5 m/s and vertical downward component in y-direction V_y = 1 m/s. These data are introduced as initial conditions and can not be changed during analysis. It means that initially the ship moves with some inclination relative immobile rigid cone. Of course, as a consequence of collision the direction and magnitude of velocity change. The rigid body is analytically defined as a revolution of two circular arcs (r_1=0.24 m and r_2=0.14 m) and an inclined straight line around vertical y-axis. Initially there is a gap of 0.05 m between bottom surface and the cone tip. Friction with constant coefficient of 0.3 is introduced into surface interaction model for each defined contact pair. Large displacement option is also used. The overall view of the meshed section of the ship at the end of analysis is shown in Fig. 4.

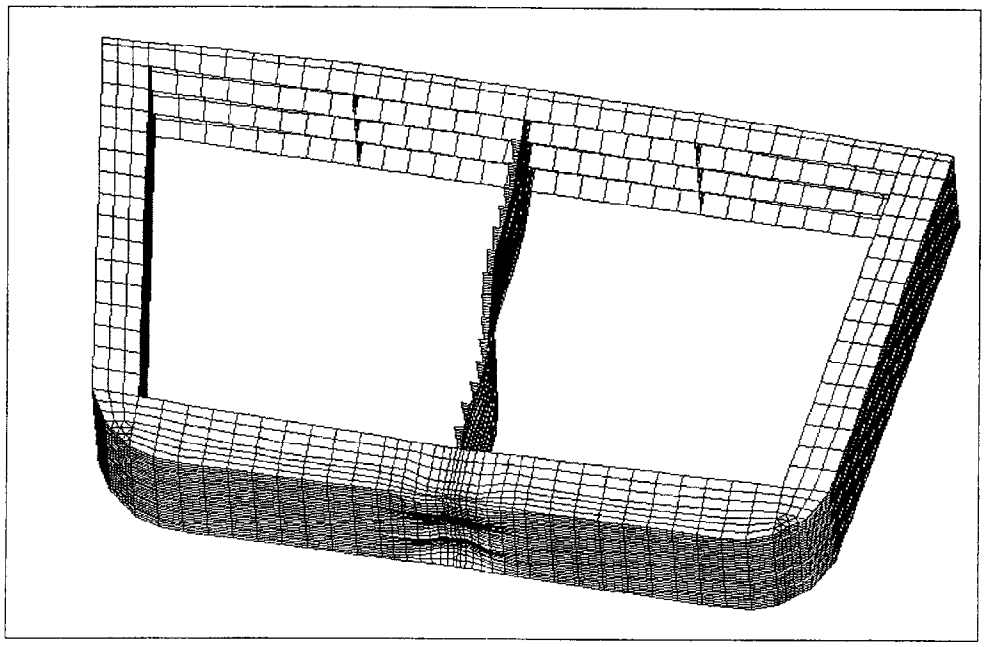

Fig. 4. Overall view of the meshed section at the end of analysis

As it is seen from Fig. 4 the narrow strip of steel constructions along the path of rigid body is distorted leaving the bulk of the hull undisturbed (except a thin vertical wall in the middle). When the ship hits an obstacle its initial kinetic energy dissipates as far as the bottom structures deform. Part of this dissipated energy is elastic recoverable, another part is accumulated by plastic residual deformations.

Fig. 5 shows dissipation of kinetic energy of the whole model. Fig. 6 presents plastic loss of that initial kinetic energy. For such a short period of grounding process only a small part of initial kinetic energy is lost $E_{lost} = (E_{initial} - E_{final})/E_{initial} = 3.77\%$. Energy dissipation through residual plastic deformations is $E_{pl}/E_{initial} = 1.5\%$ and through contact friction 2.05%. The rest of lost energy, namely 0.22%, is accounted for recoverable elastic and strain energy associated with constraints used to remove singular modes.

The total force applied to the ship bottom during grounding process is equal to the to the rigid body reaction. Its components are shown in Fig. 7 to 9.

As it is seen from the example above the ABAQUS contact algorithm provides a reasonably good means to estimate the damages due to ship grounding close enough to reality. The actual numerically simulated grounding damages may be compared qualitatively to the real ones, see Fig. 10 (J. Luukkonen, 1999). Only contact surfaces are shown. It is not the same ship and the same obstacle they hit and not the same event circumstances. But the general nature of damages is similar.

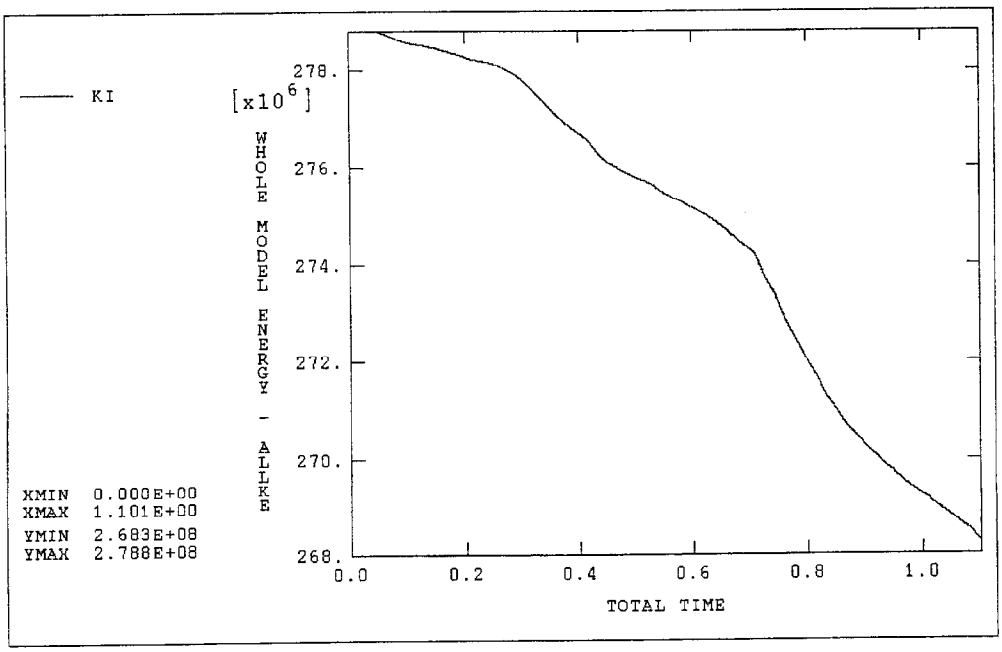

Fig. 5. Kinetic energy dissipation for the whole model.

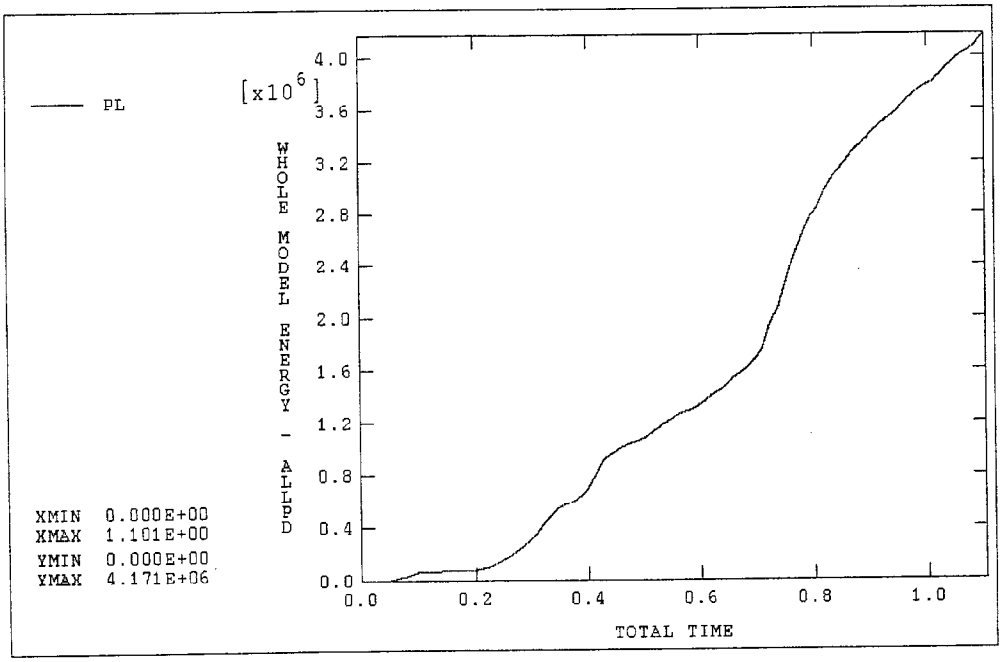

Fig. 6. Plastic energy accumulation for the whole model.

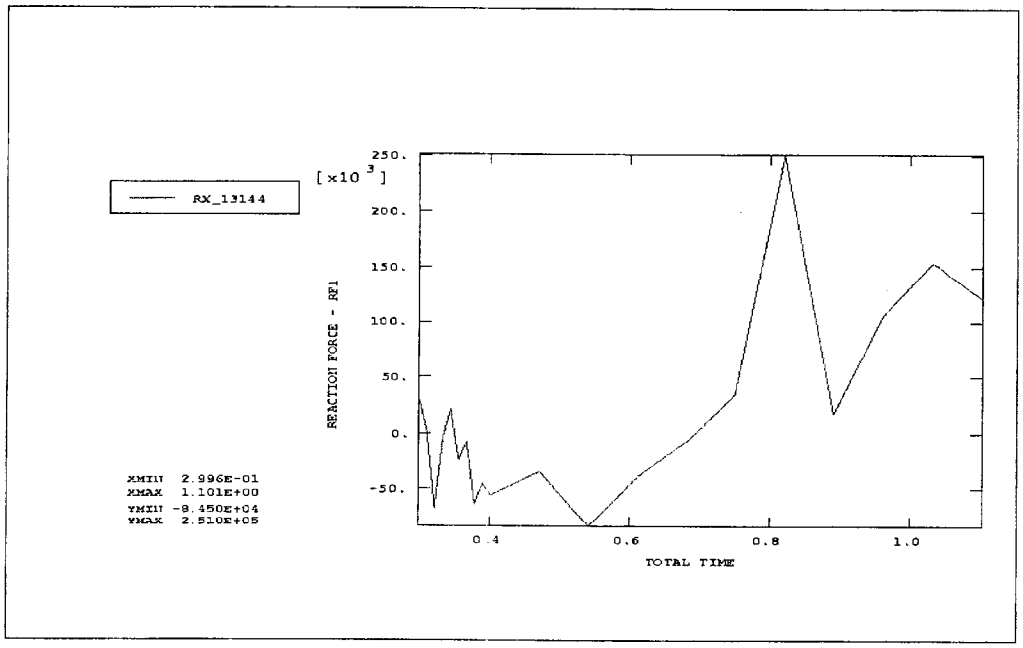

Fig. 7. Time history of the total force x-component

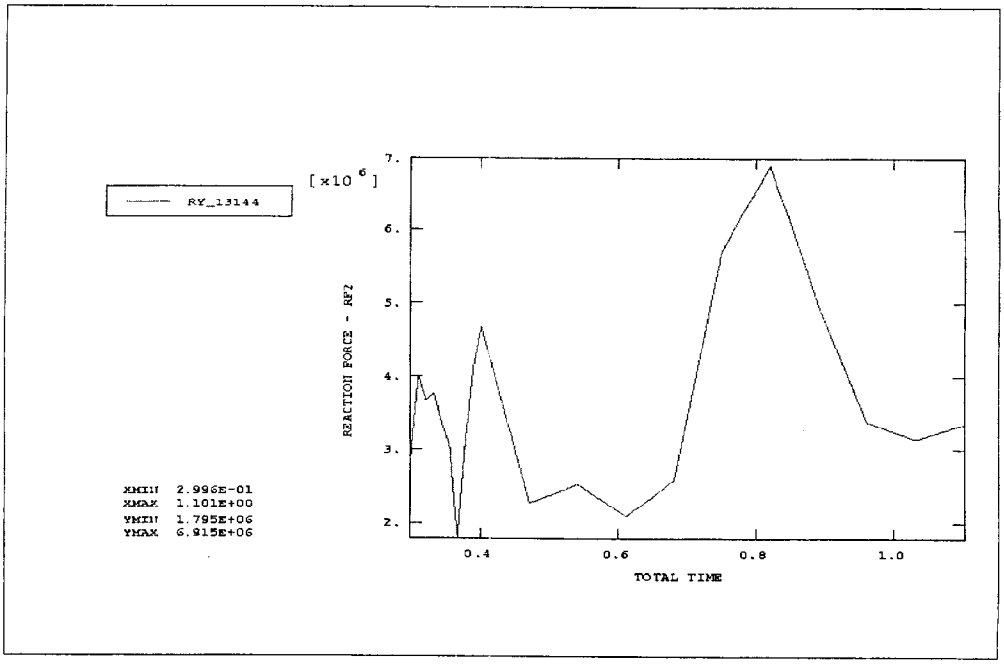

Fig.8. Time history of the total force y-component.

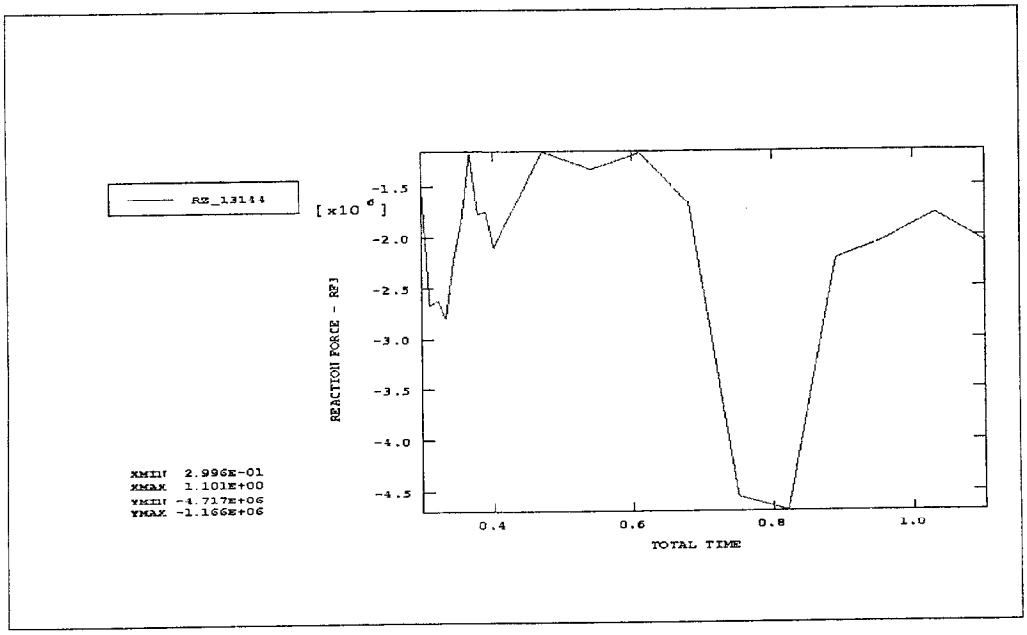

Fig. 9. Time history of the total force z-component

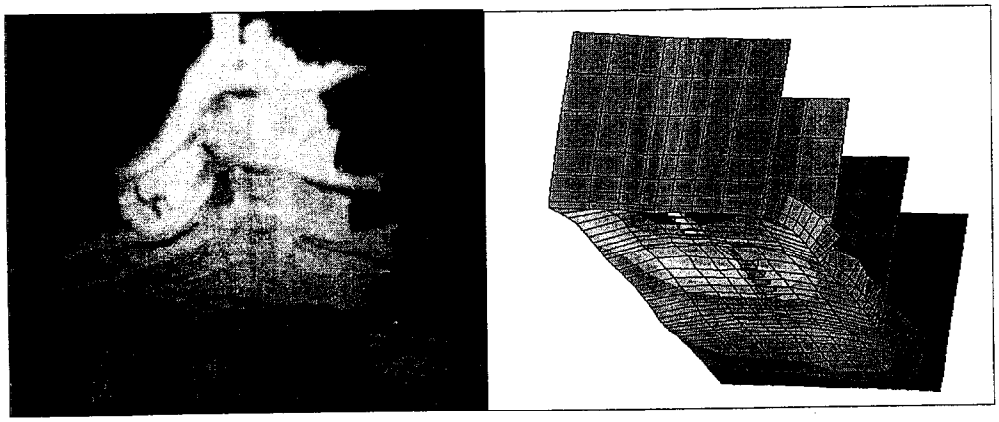

Fig. 10. The real and simulated damages to the ship bottom surface

4 . CONCLUSION

It seems that ABAQUS/Explicit contact algorithm is suitable for solution of such complicated problems as ship grounding. Of course it is limited to the cases when ship structures remain continuous. Actual examples are not associated with any real ship and real grounding situation. They just show the possibility of this numeric approach. Some

simplifications are assumed, such as difference in bow and aft constructions, and some structural details (certain beams, columns) are omitted. Because of these simplifications the inclined movement of the ship relative the rigid obstacle should be given to ensure the contact interaction of the surfaces. For commercial purposes all these discrepancies can be removed.

5. REFERENCES

Hibbit, Karlsson and Sorensen, Inc. 1988, ABAQUS/Standard, version 5.8, Manual.
Hibbit, Karlsson and Sorensen, Inc. 1988, ABAQUS/Explicit, version 5.8, Manual.
Hibbit, Karlsson and Sorensen, Inc. 1988, ABAQUS/Post, version 5.8, Manual.
J. Luukkonen. 1999.Damage of ship bottom structures in grounding accident. Diploma in shipbuilding engineering, University of Technology, Finland.

A NEW SIMULATOR FOR NEW TRAINING DEMANDS – RECOVERING FROM EQUIPMENT MALFUNCTION IN AN INTEGRATED NAVIGATION SYSTEM

Göran Granholm
VTT Manufacturing technology

1. INTRODUCTION

Since decades simulators have been used for ship handling and navigation training. The design, capabilities and performance of the simulations have, of course, changed as computer hardware and software complexity and performance have developed. Also user demands change over time as new bridge equipment and ship designs are taken into use. Full mission simulators are, however, expensive to build and to operate and changing bridge layout and navigation systems is not easily done. Because of this, a new generation of ship simulators has emerged. Low installation cost, ease of use and targeting on strictly specified training objectives seems to be the trend. While full mission simulators are being used typically for training basic navigation skills at nautical schools, the new low cost, task focused simulators suite the specific training needs of ship owners directly.

As integrated navigation systems with advanced autopilot options and detailed electronic route planning possibilities are taken into everyday use the risk increases that the understanding of underlying technologies and the roles and contributions of different subsystems become blurred. Records show incidents where the initial trigger has been a technical fault that could have been quickly corrected but wrong or missing actions instead escalated the problems.

Simulators can be used to practice operation of such systems in normal operation modes e.g. switching between steering modes and selecting backup systems but also to detect and correctly interpret abnormal function and alarms.

At VTT Manufacturing technology a new simulation facility has been installed and taken into use, focusing on handling system and equipment malfunctions in an integrated navigation system. The project was carried out in co-operation between two major Finnish shipping companies, Silja Line and FG Shipping as end users, Finnish Safety Training Centre as training provider, VTT and the software company Simulco Oy as developers and FINNTECH Finnish Technology Ltd who commissioned the project.

2. BACKGROUND

Narrow fairways, increasing ship size, new fast vessels and growing traffic densities all contribute to decreasing safety margins at sea. In the case of a system failure the right action must be taken quickly and second chances may not be given. As shown in picture 1, the time left for action is the time between the recognition of the situation and the point of no return. From the viewpoint of a single vessel the possibilities to increase total time margins are limited. By effective training it may be possible to shorten the time from the occurrence of

the failure to the time when the person understands the situation and knows how to deal with the problem.

For several years VTT has been working closely together with shipping companies developing small-
scale simulators for specific training tasks, such as joystick handling, using new electronic chart display systems etc. At the same time, research on manoeuvring characteristics and ship hydrodynamics have been an important issue.

On initiative from the shipping industry, a project was started to create a simulator facility which would enable training safety procedures in emergency situations caused by technical faults in the navigation system or in devices directly connected to this. A logical step was to extend existing simulator capabilities further and to integrate an actual integrated navigation system with the simulator. At the same time VTT identified the need to renew its previous simulator architecture in order to make subsequent modifications easier.

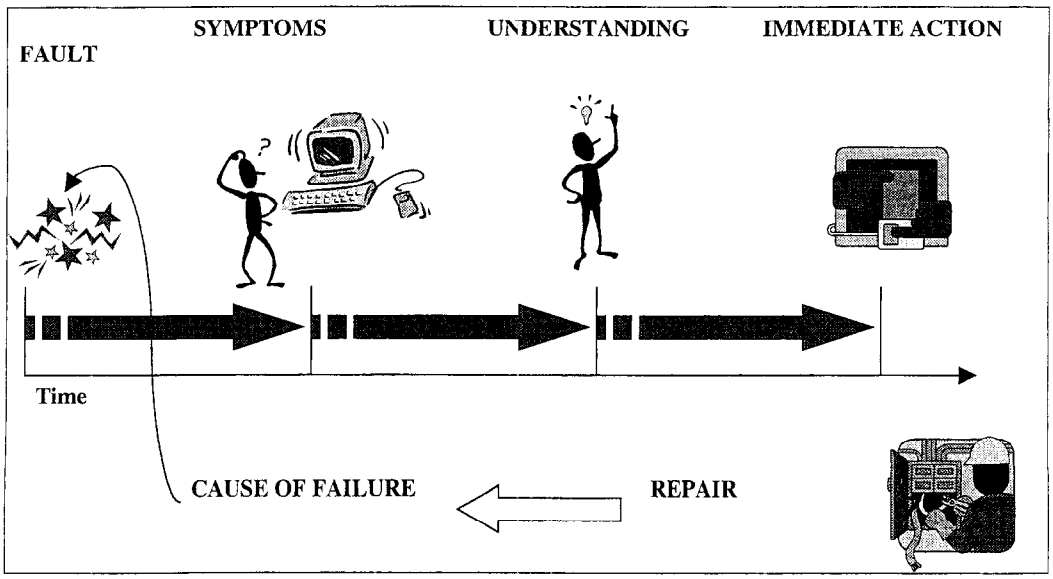

Figure 1.

3. GENERAL REQUIREMENTS

The simulator was developed in close co-operation with the shipping companies Silja Line and FG-shipping and was designed to meet very specified demands. The overall objective was to create a training environment to be used for:

- improving the understanding of system dependencies in an integrated navigation environment
- establishing safe operating procedures, and
- identifying hidden safety hazards in existing systems

To achieve this the following basic requirements were agreed:

1. The simulator must be built around an integrated navigation system of the same type that is used onboard the ships. In this case the system is the Atlas Nacos 35-2. It was recognised that learning to handle a different system from the one in use onboard is not only useless, it could also lead to unforeseen risks. This requirement automatically rules out ships with different bridge configurations.

2. It must be possible to simulate malfunction of instruments, displays and sensors connected to the navigation system as well as to equipment and machinery affecting ships manoeuvring capabilities. All instruments must be connected using standard interfaces in the same manner as onboard so that the simulated malfunctions cause the same response in the system.

3. The ship's hydrodynamics must be accurately modelled. It is important that the systems credibility is not negatively affected by unrealistic behaviour in normal navigation. The trainee must be able to identify his ship from its behaviour. On the other hand it is also important that engine and rudder faults for example affect the performance in a realistic manner. The simulator must be capable of correctly handle shallow water and bank effects, wind and sea current.

4. Other traffic. It must be possible to introduce other traffic that needs to be taken in consideration during the training run. It must be possible to communicate with other vessels and these must have the capability to change their navigation plan during the run. The traffic ships should be controlled by the simulation controller or be manoeuvred by independent simulators.

5. The simulator must be easy to operate. This requirement is based partly on cost saving but also on the aim to involve the shipping company's own training staff in the operation of the simulator. This is intended to produce a tighter integration to existing in-house training schemes.

6. The installation cost must be moderate. The simulator is to be run on a commercial basis and the users will eventually pay any investments. For technology development the project got support from the National Technology Agency TEKES.

Because the system was to be used for system handling and system assisted navigation it was concluded that a visual system was not necessary at this point. For future extension of the simulator an interface to an existing virtual reality based visual system was implemented.

4. FUNCTIONAL REQUIREMENTS

Before the development work started a set of functional requirements had to be agreed. These include required fault modes and requirements for the systems user interface. Faults can be applied to following units:

Mechanical units:

- Thrusters
- Rudders
- Clutches
- Main engines

Sensors and indicators:

- GPS
- Gyro compass
- Turning rate gyro
- Doppler log
- Echo sounder
- Radar antennae
- Power and pitch indicators
- Rudder indicators
- Wind indicators

Note that faults can occur on a physical device or to an indicator of the device's state.

5. OPERATION

The simulator bridge is located in a separate room. The instructor sits in the operating room. He supervises and controls the simulation exercise using a special software that is the only access point to the simulation process. The instructor can communicate with the bridge team through VHF radio and telephone lines. The bridge can also be observed through video and audio surveillance.

For each training scenario the initial situation describing vessels in the exercise and their positions and speeds, environmental conditions etc can be saved. Saved scenario set-ups can be recalled so that subsequent runs start from exactly the same situation. During the simulation the instructor controls the traffic ships using the instructor's interface to the simulation.

All motion and attitude information of the vessels in the exercise is recorded together with fault status, environmental conditions and internal forces. Complete replays can be shown using the simulation software and an analysis tool pack has been created for detailed studies of the simulation results.

The primary users of the simulator are the original consortium partners. Excess capacity is made availavble to other customers.

6. INSTALLATIONS

The current installation works on a Windows NT based local network and consists of 8 PC computers dedicated to specific tasks in the simulation. The same software can be adapted to

different set-ups and if a navigation system is not used all processes necessary to perform complete multiple ship simulations can fit into one PC. A portable version with a joystick interface has been developed and demonstrated e.g. at the Cruise&Ferry exhibition in London 1999.

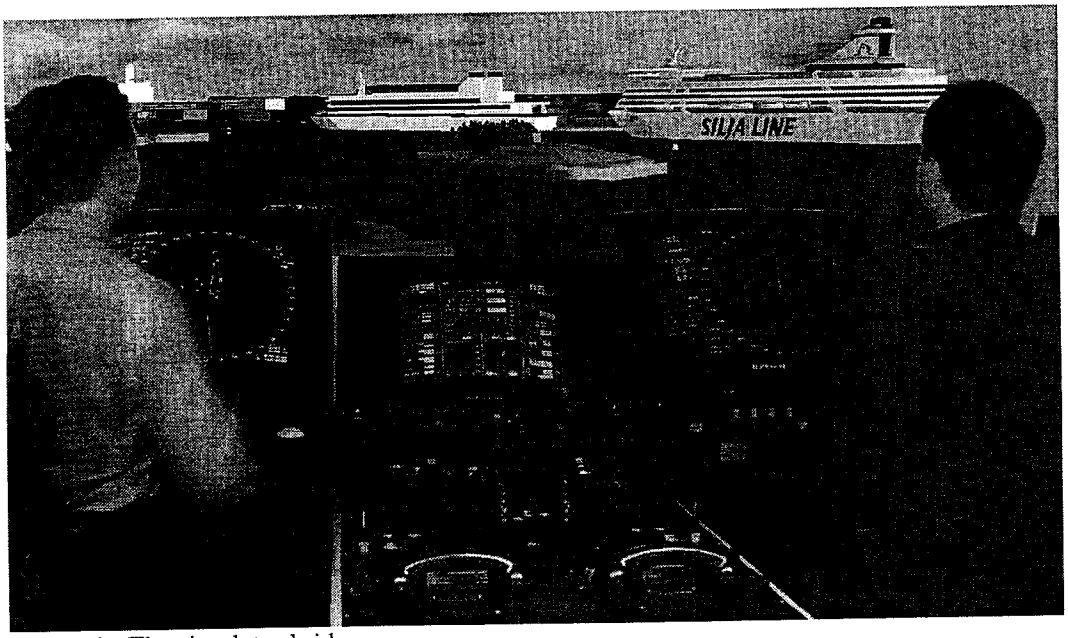

Figure 2. The simulator bridge.

7. SUMMARY

A new simulation facility has been taken into use at VTT in Otaniemi. The project was commissioned by Finntech and training activities started in January 2000. The simulator enables training operation procedures in situations where navigation is affected by malfunctioning sensors, instruments or power units. Also conventional ship handling training is possible. The goal was to replicate navigation systems of existing vessels with special focus on user interfaces and system logic.

THE WINTER NAVIGATION STUDIES IN FINNISH INLAND CANALS

J.Laasonen
VTT Manufacturing Technology, P.O.Box 1705, 02044 VTT, FINLAND

ABSTRACT

In 1996 VTT Manufacturing Technology started to investigate the possibility of extending the navigation season in Lake Saimaa and Saimaa Canal. The studies were extended to the planned Kymijoki and Mäntyharju Canals. Over 20 research reports has been completed during this five year period. The main difficulty in the winter navigation will be the ice formation in the excavated channel or in the restricted cross-section. The estimation of the ice formation in the frequently transited channel is presented in this paper.

1. INTRODUCTION

In 1996 VTT Manufacturing Technology started to investigate the possibility of extending the navigation season in Lake Saimaa and Saimaa Canal. The studies were extended to the planned Kymijoki and Mäntyharju Canals (Figure 1). Over 20 research reports has been completed during this five year period.

The environment of the study area has three different and separable characteristics. The first environment is Lake Saimaa, which is an area of large lakes. The cross-section of the fairway can be considered wide. The second environment is the excavated channels and small lake areas, like Saimaa Canal and the proposed Mäntyharju Canal. The cross-section due the economical considerations has limited water area and the formation of the ice is considerable. The third environment is the river area (the proposed Kymijoki Canal), where the navigation will be carried out in flowing water and will have an influence on the use of twelve hydropower plants.

The collection of the environmental, hydrological and meteorological data was a significant part of the studies. The data of the period of several decades like air temperatures, discharges, ice thicknesses and dates of freezing and break-ups were received from the Finnish Meteorological Institute and Finnish Environment Institute. Probably the most important data, the measurements of the ice thicknesses of the Saimaa Canal, were received from Finnish Maritime Administration. Ice thickness measurements were carried out in the study area during the winter 1998/99. The observations and the measurements during the breaking of a fairway in the Saimaa Canal and Lake Saimaa were very valuable. Other research activitivies comprised e.g. ice reconnaisence flights, ground penetrating radar surveys and ADCP flow measurements.

The preliminary designs of the canal plans were detailly inspected and improvments for the plan were suggested. The favourable canal routing for the winter navigation were determined by comparing ice, discharge, environmental etc. conditions of the canal plans. Environmental conditions were decisive in some alternative routings in Mäntyharju Canal although the ice conditions would preferable be by choosing other routing. The conjunctions of the river and the channel should be carefully designed so that they are suitable for the

vessel navigation and the floating ice will not form any ice jams. These research studies will also help the decision making of the canalization projects.

The fairways in the deep lake areas can be transited through the winter. The main difficulty in the winter navigation will be the ice formation in the excavated channel or in the restricted cross-section. The estimation of the ice formation in the frequently transited channel is presented in this paper.

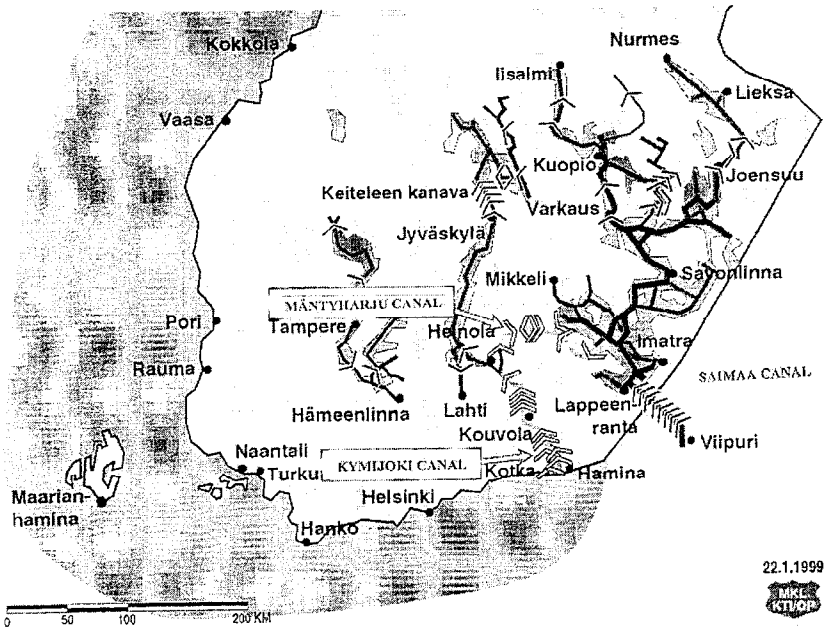

Figure 1. The location of the Saimaa Canal and the proposed Kymijoki and Mäntyharju Canals (Finnish Maritime Institute).

2. SOME HYDROLOGICAL AND METEOROLOGICAL DATA

2.1 Air Temperatures

The daily air temperatures from seven observation stations were received from the Finnish Meteorological Institute. The calculated sums of freezing degree-days in period 1961/62 - 1998/99 are presented in the Figure 2.

The mean value of the sum of freezing degree-days at the River Kymijoki and at the western part of the Mäntyharju Canal is app. 860 degree-days (max. 1430 degree-days), at the Saimaa Canal app. 940 degree-days (max. 1470 degree-days), at the southern part of the Saimaa fairway and at the eastern part of the Mäntyharju Canal 1000 - 1050 degree-days (max. 1670 degree-days) and at the northern part of the Saimaa fairway 1100 - 1200 degree-days (max. 1950 degree-days).

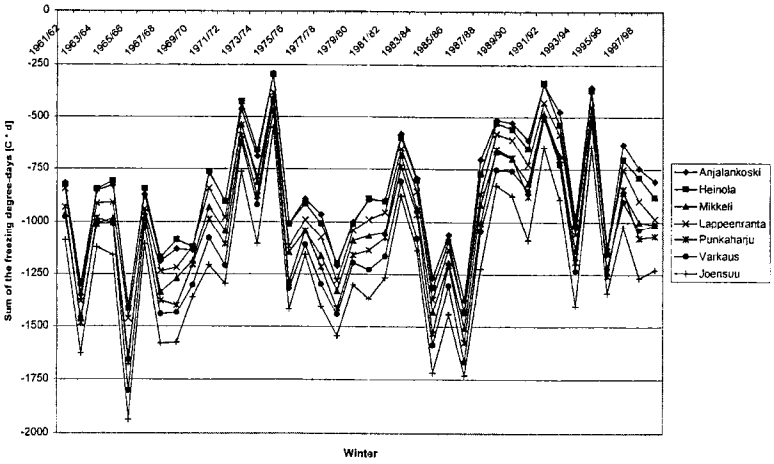

Figure 2. *The sum of the freezing degree-days during the winters 1961/62 - 1998/99 calculated from the data of Finnish Meteorological Institute [VTT Manufacturing Technology, 1999].*

2.2 **Discharges**

The mean discharge (MQ) during the winter months in River Kymijoki is app. 300 m^3/s. The catchment areas of the water systems along the proposed Mäntyharju Canal are small and the areal percentage of lakes is considerable (15...20 %). Therefore average winter runoff is only 8,4 $l/s*km^2$ and the winter discharges are usually small, less than 10 m^3/s. Only lockage waters are discharged through the Saimaa Canal. The mean discharges during the winter months at the Saimaa fairway (at Savonlinna) is app. 480 m^3/s.

The impact of the the proposed winter navigation on Kymijoki hydropower plants were studied. It was found out that it is not economically feasible to melt the ice cover by discharging river water into the excavated channel. The spring floodwater, part of which anyway will bypass the turbines, will accelerate the melting in the excavated channel.

2.3 **Ice Conditions**

In normal winters, the thickness of ice in the River Kymijoki varies between 20 and 50cm. In a winter of heavy ice conditions, ice thickness in some places may be as high as 80–90cm. The mean ice thicknesses of the lakes in the canal areas are same order of magnitude. In normal winter app. 50-55 cm of ice is formed and it will vary between 30-75 cm.

Inland Waterway District of the Finnish Maritime Administration has measured the ice formation in the Saimaa Canal since 1985. The measurements have been carried out in Kansola, in the rock cutting in Nuijamaa and at the Lake Nuijamaa. Over 2,5 meters of ice has been measured in the rock cutting of Nuijamaa.

The drifting ice broken by the vessels in River Kymijoki was preliminary calculated. According to the ice reconnaisance flights the percentage of the open water areas in the River

Kymijoki (between Susikoski and Lake Pyhäjärvi) is more than 50 %. The border is formed in those open water areas. The power of the waste and warm water discharges in this part of the river is app. 325 MW, which has an influence on the ice formation. Therefore numerical 1-D river ice modeling is needed in order to obtain more accurate estimation of the drifting ice.

3. THE ESTIMATION OF THE ICE THICKNESS IN THE FREQUENTLY TRANSITED CHANNELS

Most methods of calculating the ice formation in transited channels are based on Stefan's equation. The empirical growth coefficient is multiplied with the square root of the accumulated freezing degree-days. These methods does not take into account the growth of the brash ice i.e. the growth of the ice thickness is the same in the beginning and at the end of the winter.

The ice thickening process in the transited channel can be considered as a heat conduction from the water through the brash ice into the atmosphere. This thermal conductivity through the brash ice is function of the conductivity of ice, snow and water. The ice formation can be calculated step-wise by the equation (1).

$$\rho_i \, L_i \frac{\partial d}{\partial t} = \frac{T_{water} - T_{air}}{\frac{d_{brash}}{k_{brash}}} \qquad (1)$$

where T_{water}, T_{air} is the temperature of water and air, respectively, d_{brash} is the average depth of brash, k_{brash} is thermal conductivity of brash, ρ_i is the density of ice and L_i is the latent heat of the fusion of the water.

The value of the thermal conductivity was determined with the data measured from the frequently operated channels in the Saimaa Canal. The measured ice cross-section data of ten winters were used. The transition frquencies varied from 2,4 to 5,3 vessels / day. There was a lot of variation in the calculated values (3,7 ... 12,2 J / m * s * °C). The mean thermal conductivity was 6,9 J / m * s * °C, which is 3,1 times the thermal conductivity of ice.

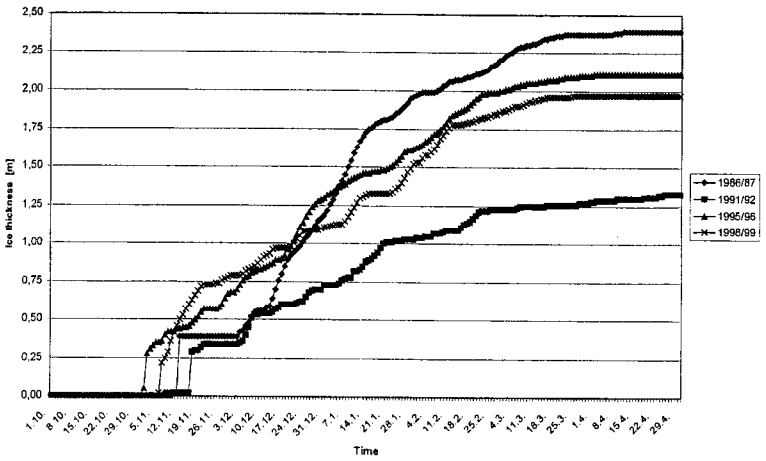

Figure 3. The calculated ice thicknesses in the frequently transited channel (VTT Manufacturing Technology, 1999).

In Figure 3 is presented the formation of the ice in three different winter (mild, average, hard). The ice thicknesses in the frequently transited channel were calculated using air temperature data of the winters 1960/61-1998/99. The average ice thickness was app. 1,9 meters and the maximum app. 2,4 meters (Figure 4). The extreme values of the thermal conductivity will have an influence of ± 35 % to the ice thickness. Also the navigation season of Saimaa Canal will usually end at January, which will cause some uncertainty in the calculation.

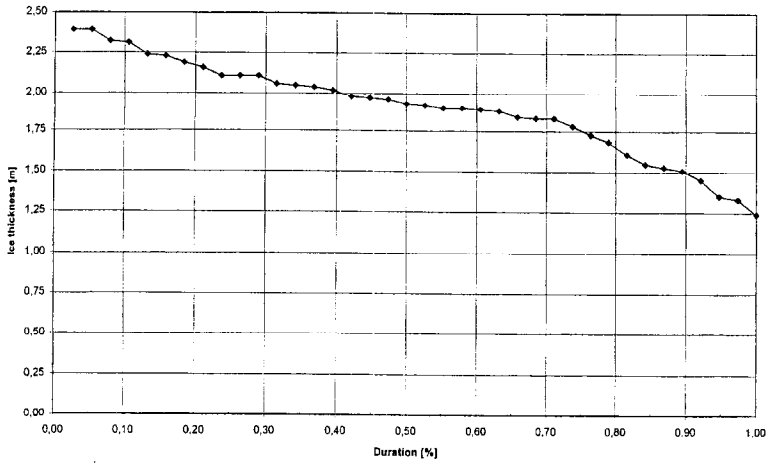

Figure 4. The duration curve of the ice thickness in the frequently transited channel. The air temperature data of the winters 1960/61-1998/99 were used (VTT Manufacturing Technology, 1999).

The depth of the channel will have an influence on the navigation of the conventional vessel in the excavated channel. If the ice thickness is 1,8 meters, the vessel (water-line length 109, width 16 m and draft 4,5 m) with the ice class of I A Super (3200 kW) will not be able to operate in the 6 meter deep channel (Figure 5). The necessary power of the ice-breaker in this depth is app. 5 MW. However it seems that the vessels with the new type azimuth propulsion systems and with innovative hull form can operate by backing in the ice thickness of 3 meters.

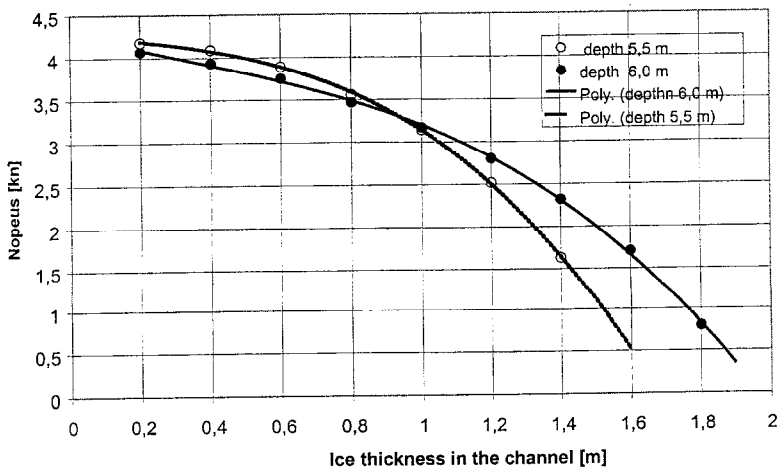

Figure 5. *The speed of the conventional vessel in the frequently transited channel. The results of the ice model studies (VTT Manufacturing Technology, 1999).*

7. REFERENCES

Laasonen, J. & Holm, O. The impact of the proposed winter navigation on Kymijoki hydropower plants.POAC 99, August 23-27, 1999. Helsinki.

Rytkönen, J. & Kostiainen, K. 1999. The Improvement Plans for Finnish Inland Winter Navigation. POAC 99, August 23-27, 1999. Helsinki.

Nyman, T. & Kokkonen, J. Ice Performance Measurements onboard MS Pionier. POAC 99, August 23-27, 1999. Helsinki.

VTT Manufacturing Technology. 1999. Jäätietojen keräys ja analysointi. Saimaan syväväylä, Kymijoen ja Mäntyharjun kanavalinjat talvella 1998/1999. Research Report (confidental) VAL34-992519.

HATTUPROFIILILLA JÄYKISTETYN LEVYKENTÄN VÄSYMISLUJUUS

H. Remes
Teknillinen korkeakoulu, Laivalaboratorio

TIIVISTELMÄ

Tässä julkaisussa esitetyt tulokset perustuvat hiljattain Teknillisen korkeakoulun laivalaboratoriossa tehtyyn diplomityöhön /Remes, 1999/. Työssä tutkittiin hattuprofiililla jäykistetyn levykentän väsymislujuutta sekä laskennallisesti että kokeellisesti. Laskennallinen tutkimus tehtiin FE-menetelmällä käyttäen rakenteesta idealisoitua elementtimallia. FE-analyysin pohjalta hattuprofiilirakenteen liitosta kehitettiin paremmin kuormiakantavaksi. Vahvistamattomalle sekä nurkka- ja pystypolviolla vahvistetuille hattuprofiililiitoksille tehtiin väsytyskokeet. Vahvistamattoman hattuprofiililiitoksen väsymisluokaksi saatiin 16 MPa. Nurkka- ja pystypolviorakenteilla väsymislujuutta saatiin kasvatettua yli kaksinkertaiseksi. Nurkka- ja pystypolviorakenteilla väsymisluokka oli noin 36 MPa. Saatuja väsymiskoetuloksia on verrattu eri standardien ja luokituslaitoksien väsymismitoitusmenetelmiin. Hattuprofiililla jäykistetyn kansirakenteen toteuttamiskelpoisuutta on arvioitu risteilijäaluksen kansirakenteessa. Nurkka- tai pystypolviolla vahvistetun hattuprofiilirakenteen käyttö olisi mahdollista Royal Princess:in kansirakenteissa Karibianmeren liikennöintialueella sekä osittain Pohjois-Atlantilla.

1 JOHDANTO

Laivan, erityisesti risteilijäaluksen painopistekriittisyys on aiheuttanut tarvetta lujuus- ja painooptimaalisemmalle kansirakenteelle. Kotelorakenteen käyttö jäykisteenä tarjoaa laivan kansirakenteen keventämismahdollisuuden. Teknillisen korkeakoulun laivalaboratoriossa on tutkittu hattuprofiililla jäykistetyn kansirakenteen väsymislujuutta. Tutkimuksen tavoitteena oli rakenteen kehittäminen paremmin kuormiakantavaksi sekä rakenteen väsymislujuuden määritys. Lisäksi työssä on arvioitu hattuprofiililla jäykistetyn kansirakenteen käyttömahdollisuuksia risteilijäaluksen ylemmissä kansirakenteissa.

Rakenteen keventämiseen ja uusiin rakenneratkaisuihin liittyy oleellisina tekijöinä valmistettavuus, taloudellisuus ja rakenteen turvallisuus käyttöiän aikana. Ajan suhteen muuttuvasti kuormitettujen rakenteiden väsymismitoituksen tarve on kasvanut merkittävästi viime vuosikymmeninä. Syyt laivan väsymismitoituksen merikittävään korostumiseen on korkealujan teräksen käyttö sekä suoramitoituksen yleistyminen.

2 TUTKITTAVA RAKENNE

2.1 Yleistä

Nykyisin laivan kansirakenne on yleensä jäykistetty palkolattatangolla eli HP-profiililla (kuva 1). Kuvassa 2 esitetyllä hattuprofiililla on pyritty saavuttamaan HP-profiililla jäykistettyä kansirakennetta kilpailukykyisempi rakenne muuttamalla jäykisteen geometria kotelomaiseksi. Hattuprofiililla jäykistetyn kansirakenteen kansilevyn ja laipioiden hitsiliitokset ovat tyypillisesti väsymislujuuden kannalta kriittisiä. Kuvassa 2 esitetyn hattuprofiililla jäykistetyn kansirakenteen ongelmakohta on epäsymmetrisen hattuprofiilin ja poikittaislaipion liitos. Hattuprofiili ja pitkittäislaipio muodostavat huomattavan pituussuuntaisen epäjatkuvuuskohdan.

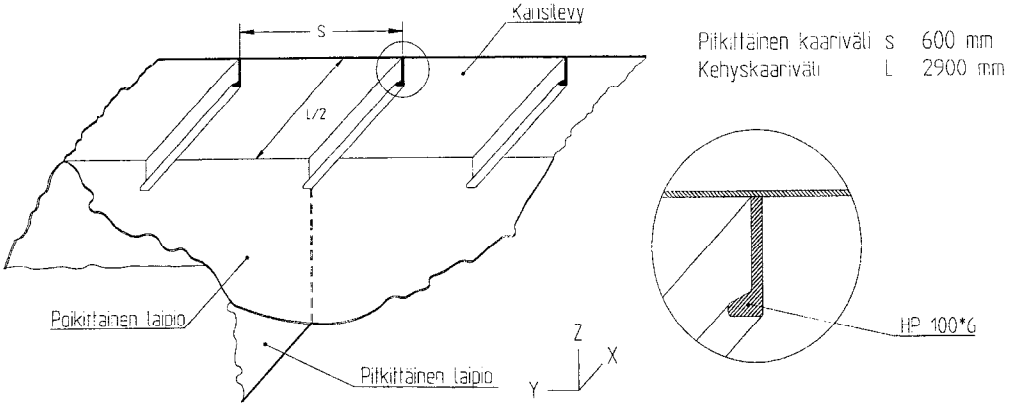

Kuva 1 HP-profiililla jäykistytty kansirakenne

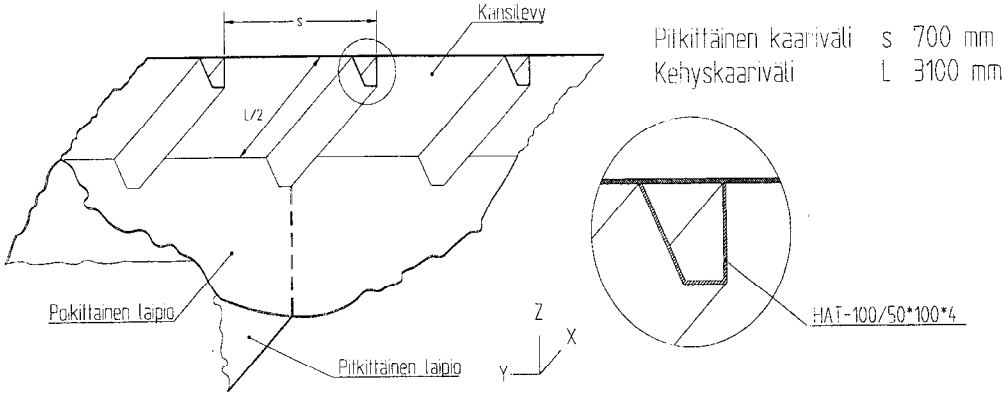

Kuva 2 Hattuprofiililla jäykistetty kansirakenne

2.2 Hattuprofiilin vahvikerakenteet

Hattuprofiili on suljettu kotelorakenne, jolloin profiilin sisäpuoliset hitsaukset ovat hyvin vaikeasti toteutettavissa perinteisillä hitsausmenetelmillä. Valmistusteknillisten tekijöiden ja FE-analyysin pohjalta suunniteltiin vahvikerakenteet hattuprofiilin ja poikittaislaipion liitokseen (kuva 3). Eri rakennevaihtoehdoilla on pyritty jännityskeskittymien pienentämiseen, jolloin profiilin suuntainen vetokuormitus ohjautuu mahdollisimman jouhevasti pitkittäiselle laipiolle.

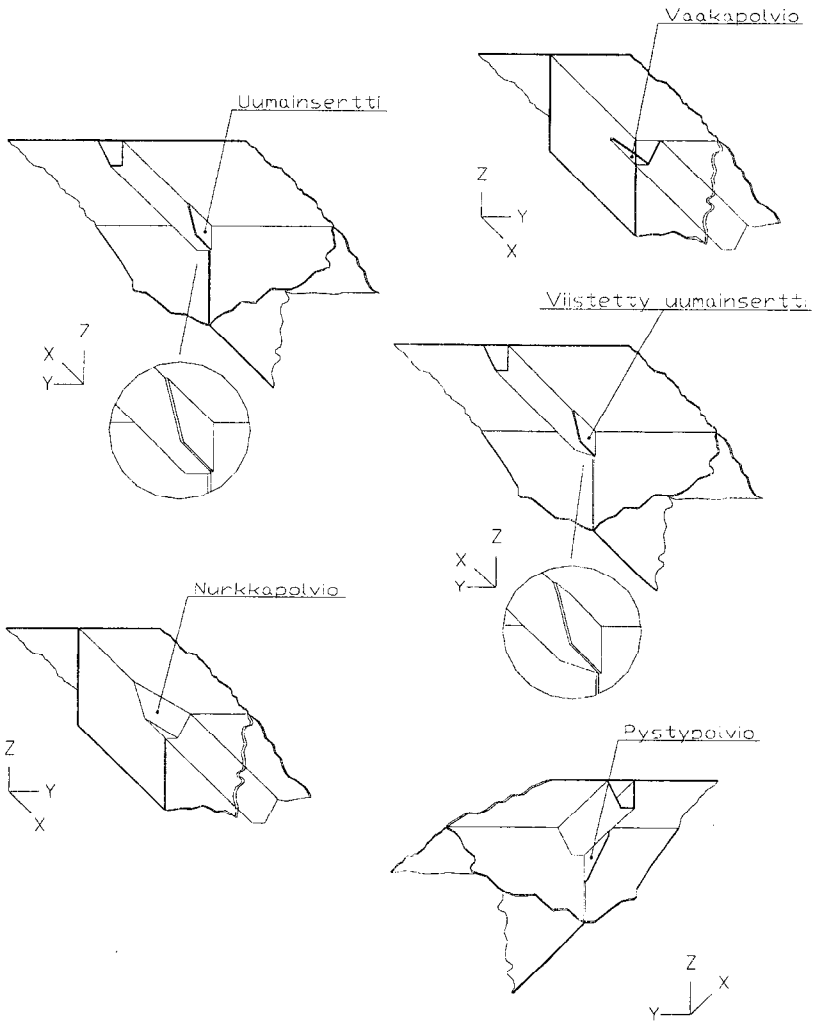

Kuva 3 Hattuprofiililiitoksen vahvikerakenteet

3 FEM-LASKELMAT

3.1 Mallinnus ja reunaehdot

Risteilijäaluksen kansirakenteeseen kohdistuvat kuormitustapaukset sekä kuormitustasojen keskinäiset suhteet voidaan arvioida riittävällä tarkkuudelle, joten tutkimus on rajattu käsittelemään erityisesti paikallislujuutta profiilin ja laipioiden liitoskohdan alueella (kuvat 1 ja 2). Laivan kansirakenteesta mallinnettiin leveyssuunnassa yhden jäykkääjän käsittävä pitkittäisleikkaus ja pituussuunnassa puolet kehyskaaren pituudesta sekä hieman pitkittäisestä laipiosta. Rakennemallit tehtiin käyttäen kuorielementtejä, jolloin rakenteen geometria idealisoitiin levyn keskipinnan mukaisesti. Malleissa käytettävät elementit olivat paraboolisia kahdeksan- ja kuusisolmuisia kuorielementtejä (S8R, STRI65) /Hibbit et al., 1998/. Mallit luotiin I-DEAS Master serias -ohjelmistolla. Mallien ratkaisemisessa ja jälkikäsittelyssä käytettiin Abaqus -ohjelmaa. Laskelmat perustuvat lineaaris-elastiseen teoriaan ja staattiseen analyysiin.

Aaltokuormitus aiheuttaa laivan taipumisen ja laivapalkkiin taivutusjännitystilan. Laivan kansirakenteessa vallitsee tällöin likimain puhdas vetojännitys. Kansirakenteeseen kohdistuu lisäksi kansikuormitusta. Kansirakenteen vetokuormituksena käytettiin kuormitusta, joka aiheutti kansirakenteeseen pituussuuntaisen vakiosiirtymätilan ja 100 MPa:n nimellisjännityksen. Kuvassa 4 on esitetty rakenteen reunaehdot ja kuormitustapaukset: painekuormitus (P=5 kPa) ja vetojännitystilaa (σ_{xx}) vastaava vetokuormitus.

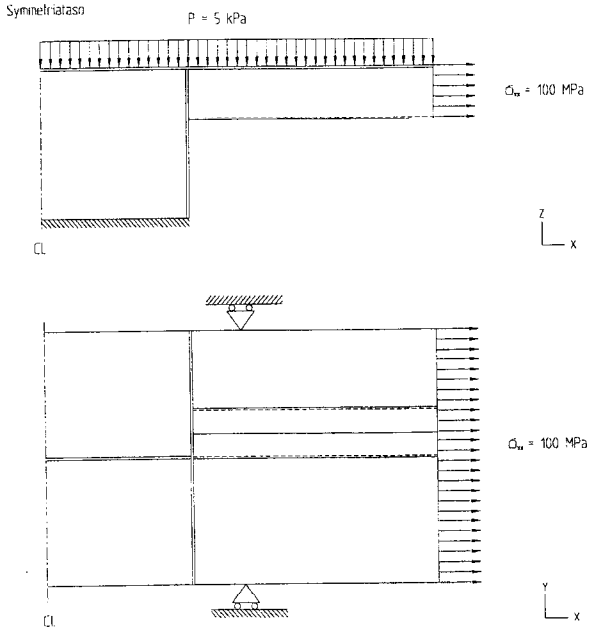

Kuva 4 Rakenteen reunaehdot ja kuormitustapaukset

3.2 Laskentatulokset

Hattuprofiilin ja poikittaislaipion liitoksessa on huomattava rakenteen epäjatkuvuuskohta. Tämä ja epäsymmetrinen hattuprofiili aiheuttivat rakenteeseen huomattavia paikallisia siirtymiä vetokuormituksella (kuva 5). Hattuprofiili pyrki vääntymään liitoskohdan läheisyydessä. Vahvike- ja polviorakenteet tasaavat jännityshuippuja suuremmalle alueelle sekä pienentävät muodonmuutoksia. Painekuormituksella laipion ja profiilin liitokseen ei syntynyt huomattavia siirtymiä eikä leikkausjännityksiä rakenteen epäsymmetriasta johtuen, vaan kuormitus jakautui tasaisemmin koko liitoksen alueelle.

Tutkittavissa rakenteissa maksimijännitys muodostui rakenteen epäjatkuvuuskohtaan eli hattuprofiilin liitoksen nurkkapisteeseen. Vetojännitys ohjautui hattuprofiilin pystyuumaan ja aiheutti huomattavan normaalijännityksen kasvun ennen profiilin nurkkaa, jossa pitkittäinen laipio jatkuu poikittaisen laipion takana. Taulukossa 1 on esitetty eri rakenteiden suhteelliset jännityskonsentraatiokertoimet. HP-profiilirakenteelle (vertailumalli) on annettu lukuarvo 100.

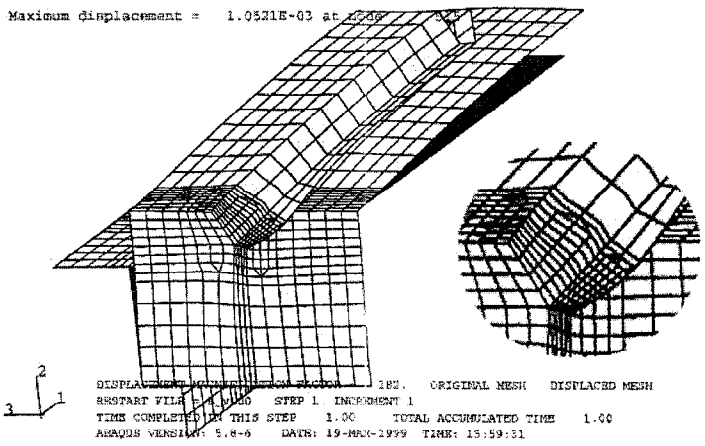

Kuva 5 Hattuprofiililla jäykistetyn kansirakenteen siirtymätila vetokuormituksella

Taulukko 1 Rakennemallien suhteelliset jännityskonstraatiokertoimet

Rakennemalli	ks,xx [%]
HP-profiili	100
Hattu-profiili	230
Hattu-profiili vaakapolviolla	180
Hattu-profiili uumainsertillä	140
Hattu-profiili viistetyllä uumainsertillä	170
Hattu-profiili nurkkapolviolla	110
Hattu-profiili pystypolviolla	100

4 VÄSYTYSKOKEET

4.1 Koejärjestelyt

FE-analyysin pohjalta tehtiin väsytyskokeet kolmelle hattuprofiilirakenteelle: hattuprofiili ilman vahvistusta, nurkkapolviolla vahvistettu hattuprofiili ja pystypolviolla vahvistettu hattuprofiili. Kussakin koesarjassa oli neljä koekappaletta, joten kuormituskokeet käsittivät yhteensä 12 koekappaletta.

Koekappale on rakenne yksityiskohta hattuprofiililla jäykistetyn kansilevyn, poikittais- ja pitkittäislaipion liitoskohdasta. Kansilevyn leveys oli 500 mm käsittäen yhden jäykisteen. Koekappaleen pituus oli 1600 mm. Kuvassa 6 on esitetty hattuprofiilikoekappale kuormituskehään asennettuna. Koekappale kiinnitettiin vetokorvakkeista liukulaakeroitujen nivelvarsien välityksellä kuormituskehään ja voima-anturiin. Voima-anturin toinen pää oli kiinnitetty koekappaletta kuormittavan hydraulisylinterin männänvarteen. Väsytyskokeet olivat voimaohjattuja vetotykytys kuormituskokeita, jossa kuormitusvoiman vaihteluväli pidettiin vakiona.

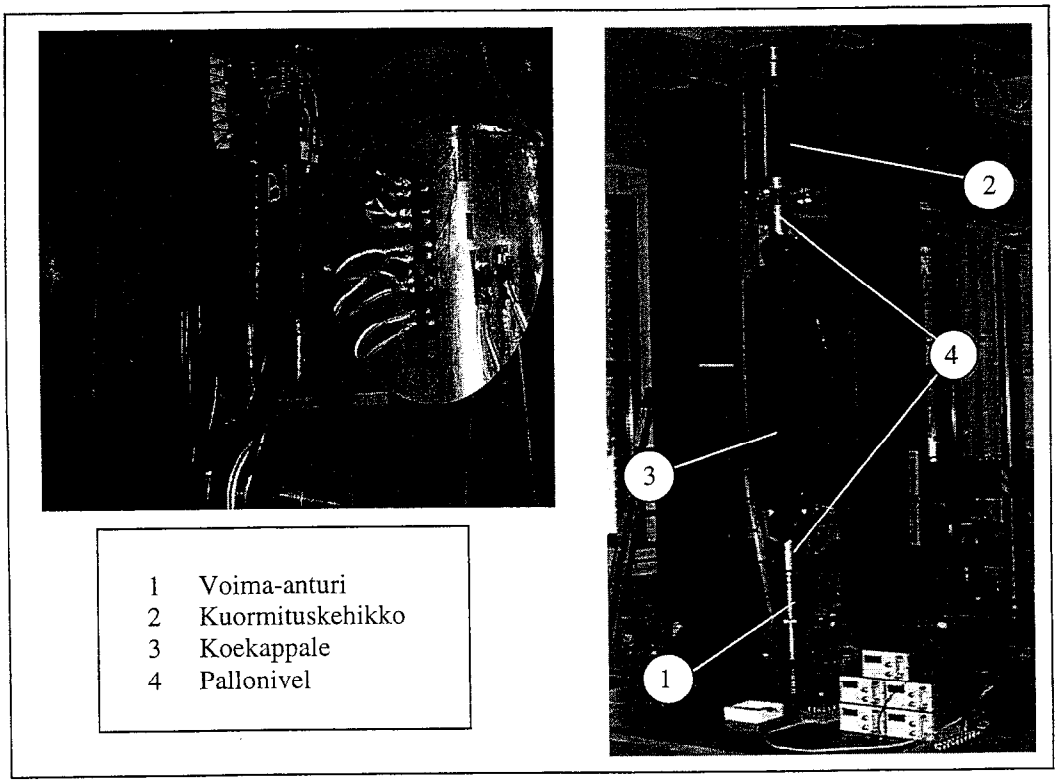

Kuva 6 Hattuprofiililla jäykistetyn kansilevyn koejärjestely

4.2 Tulokset

Väsymisvauriot syntyivät rakenteiden hitsiliitoksiin. Vahvistamattomalla ja nurkkapolviolla vahvistetulla rakenteilla säröt syntyivät hattuprofiilin pystyuuman ja poikittaislaipion liitokseen (kuva 7A). Nurkkapolviorakenteella väsymisvaurioita havaittiin lisäksi hattuprofiilin vinouuman ja poikittaislaipion hitsiliitoksessa (kuva 7B). Nänä väsymisvauriot ydintyivät hitsin juuren puolelta. Pystypolviorakenteella väsymissärö ydintyi polvion kärkeen hitsin ja hattuprofiilin rajapinnalle (kuva 7C).

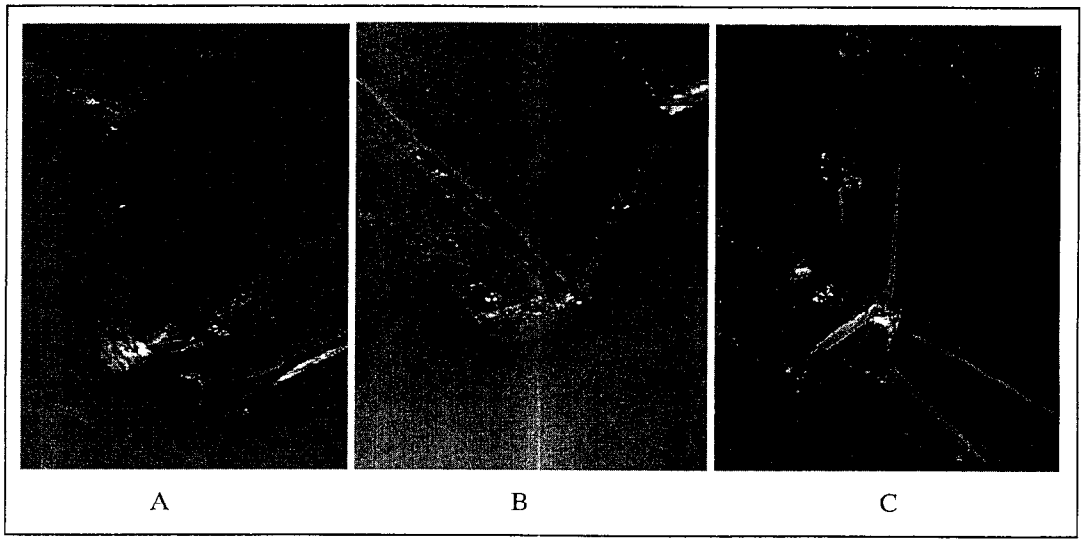

Kuva 7 Syntyneet väsymisvauriot

Kuvassa 8 on esitetty eri rakenteiden väsytyskoetulokset. Kuvassa 8 on esitetty katkoviivalla koetuloksiin sovitettu S-N käyrä

$$NS^m = C, \tag{1}$$

missä N on vaurioon johtaneiden jännitysjaksojen lukumäärä jännityksen vaihteluvälin arvolla S. C ja m ovat kokeellisesti määritettyjä parametrivakioita. Koetuloksiin sovitettujen S-N –käyrän parametrivakioiden arvot sekä koesarjaa vastaava väsymisluokka on esitetty taulukossa 2. Koetuloksien hajonta oli melko pieni. Jotta standardin mukainen FAT-luokka voitaisiin määrittää, koesarjan toistojen lukumäärää tulisi kasvattaa. Esitettyjä FAT-luokkia voidaan pitää suuntaa antavina abroksimaatioina. Vahvistamattoman hattuprofiilin teoreettinen väsymisluokka on melko pieni, 16 MPa. Nurkka- tai pystypolvio vahvikerakenteilla hattuprofiililiitoksen väsymislujuutta saatiin kasvatettua noin 220 %. Nurkka- ja pystypolviorakenteen väsymisluokka on likimain 36 MPa. Kuvassa 8 on esitetty lisäksi pienahitsatun neliöprofiilin ja laippaliitoksen S-N –käyrät /GL, 1997/.

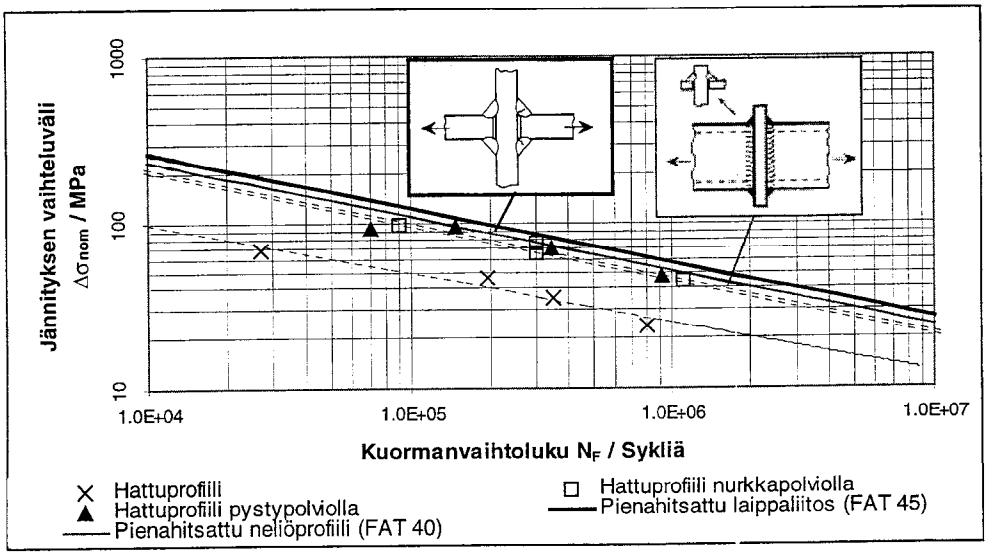

Kuva 8 Hattuprofiililiitoksien väsytyskoetulokset

Taulukko 2 Eri koesarjoille määritettyjen parametrivakioiden arvot sekä FAT-luokka

Koesarja	Kokeelliset vakiot		FAT-luokka
	m	C	
		(MPa)^3*sykliä	[MPa]
Hattuprofiili	3	8.789E+09	16
Hattuprofiili nurkkapolviolla	3	8.418E+10	35
Hattuprofiili pystypolviolla	3	1.001E+11	37

Pystypolviorakenteelle, jolla särö ydintyi hitsin rajaviivalle, on esitetytty hot spot S-N -käyrä sekä verrattu sitä kirjallisuudessa esitettyihin tuloksiin (kuva 9). Hot spot –jännitys σ_{hs} eli rakenteellinen jännitys hitsin rajaviivalla on ekstrapoloitu 0,4*t, 0,9*t ja 1,4*t etäisyyksillä olevien mittapisteiden kautta, missä t on levynpaksuus /Niemi, 1996/. Kuvassa 9 on esitetty lisäksi 95 % ja 50 % todennäköisyyttä vastaavat hot spot S-N -käyrä (hot spot: 4-10 mm), jotka soveltuvat 4-10 mm levynpaksuuksille /Niemi et all, 1998/. IIW:n suosituksen mukainen hot spot -käyrä (FAT 100) soveltuu poikittaiselle pienahitsille, jonka hitsin rajaviiva on hitsatussa tilassa /Hobbacher, 1996/.

Kuvassa 10 on esitetty DNV:n väsymismitoituskäyrä ja pystypolviorakenteen mittaustulokset. Saatuja koetuloksia on verrattu luokituslaitoksen väsymismitoitusmenetelmään, jossa käytetään jännityksen vaihteluvälinä teoreettista lovijännitystä $\Delta\sigma_0$ /DNV, 1998/. Jännityskonsentraatiokerroin on määritetty 1/2*t ja 3/2*t ekstrapolointipisteiden jännitysten avulla, missä t on levynpaksuus. Teoreettisessa lovijännityksessä on huomioitu lisäksi rakenteen ja hitsin geometriasta aiheutuva jännityksen kohoaminen.

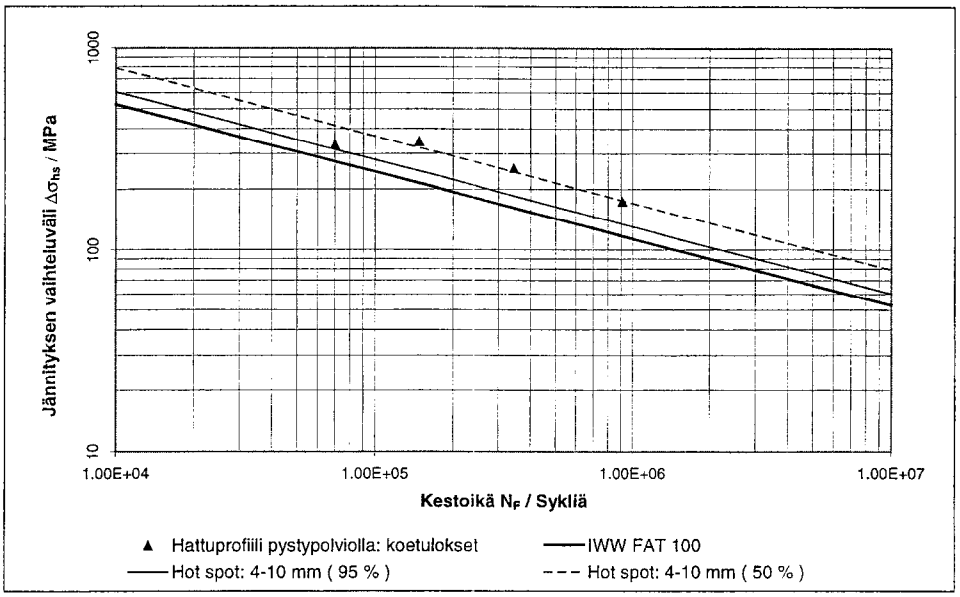

Kuva 9 Hot-spot väsymislujuusvertailu

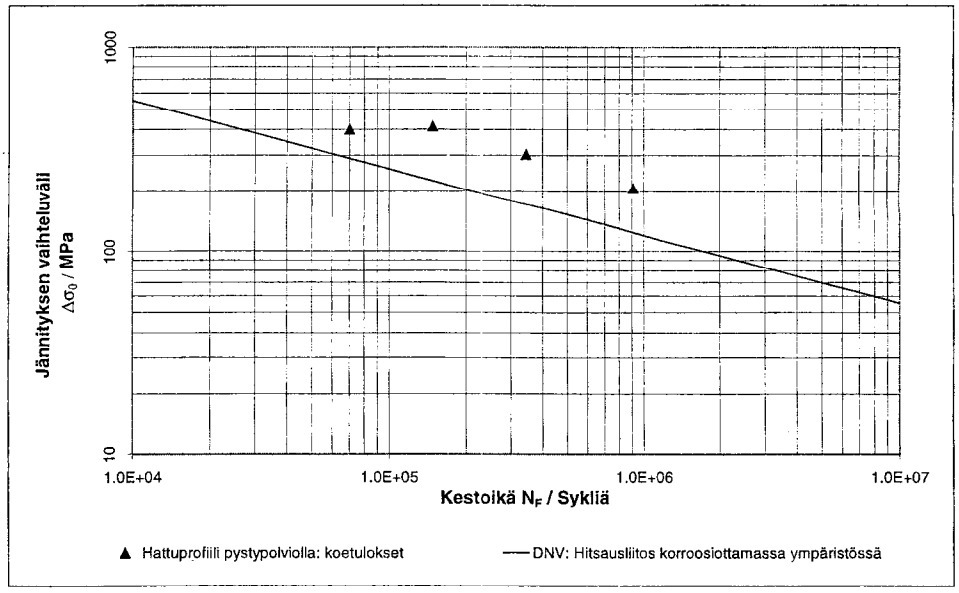

Kuva 10 Väsytyskoetuloksien vertailu DNV:n väsymismitoituskäyrään

5 HATTUPROFIILIN KÄYTTÖMAHDOLLISUUDET RISTEILIJÄALUKSESSA

Hattuprofiilin käyttömahdollisuuksia on tutkittu risteilijäaluksen kansirakenteissa. Esimerkki laivana on käytetty Royal Princess:iä (kuva 11). Royal Princess on 1983 Helsingin Wärtsilän telakalla rakennettu risteilijäalus, joka liikennöi Pohjois-Atlantilla ja Karibian merellä. Esimerkkilaivalle on määritetty ylempien kansirakenteiden vaadittavat väsymisluokat ja verrattu näitä hattuprofiililla jäykistetyn rakenteen väsymisluokkiin.

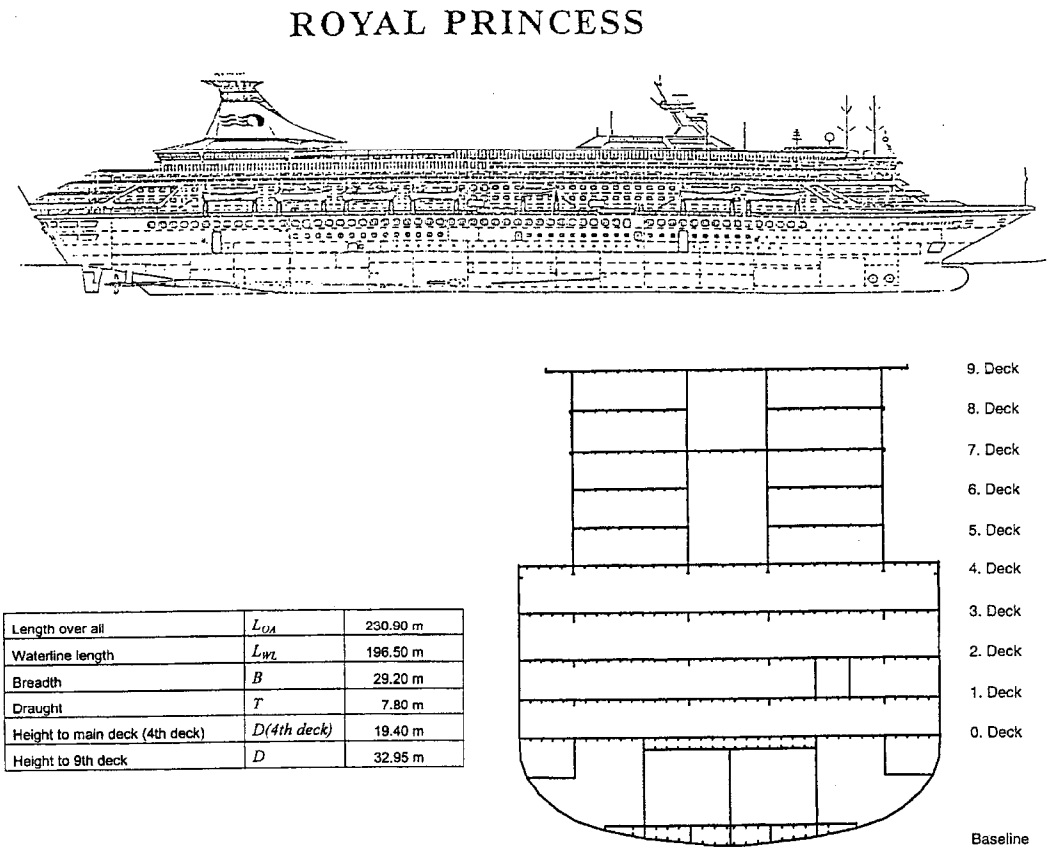

Length over all	L_{OA}	230.90 m
Waterline length	L_{WL}	196.50 m
Breadth	B	29.20 m
Draught	T	7.80 m
Height to main deck (4th deck)	D(4th deck)	19.40 m
Height to 9th deck	D	32.95 m

Kuva 11 Royal Princess:in päämitat /Kujala et al., 1998/

Tehdyt laskelmat perustuvat spektrianalyysiin, laivan poikkileikkauksen epälineaariseen normaalijännitysjakaumaan sekä kumulatiiviseen vaurioanalyysiin (Minerin summa) /Kukkanen, 1996 & Kujala et al., 1998/. Laskelmassa on oletettu että laiva kohtaa suunnitteluiän aikana 10^8 aaltoa. Tarkastelussa on tutkittu kolmea liikennöintialuetta: Pohjois-Atlanti ja Karibianmeri sekä Pohjois-Atlantin (30%) ja Karibianmeren (70%) yhdistetty merialue. Taulukossa 3 on esitetty Royal Princess:in kansirakenteilta vaadittavat väsymisluokat (FAT) vauriotodennäköisyydellä 1. Taulukossa 3 on lisäksi esitetty pystypolviolla vahvistetun hattuprofiilirakenteen saavutettu väsymislujuus prosentteina. Pystypolviorakenteen väsymisluokaksi saatiin 37 MPa, joka on hyvin lähellä nurkkapolviorakenteen väsymisluokkaa, 35 MPa. Taulukon 3 perusteella pystypolviolla vahvistetun hattuprofiilirakenteen käyttö olisi mahdollista Royal Princess:in kansirakenteissa Karibianmeren liikennöintialueella sekä osittain Pohjois-Atlantilla.

Nurkkapolviorakenteella väsymissärö ydintyi hattuprofiilin pysty- tai vinouuman hitsisaumaan, hitsin juuren puolelle. Teoreettisiin lovijännityskonsentraatikertoimiin /Radaj, 1990/ ja neliöprofiilin väsymisluokkiin /GL, 1997/ perustuvalla vertailulla voimme arvioida rakenteen väsymislujuuspotentiaalia. Viistämisellä ja riittävällä hitsin a-mitalla voidaan särön ydintyminen saada tapahtumaan hitsin ja perusaineen rajapinnalle. Tällöin nurkkapolviolla vahvistetun hattuprofiilirakenteen väsymislujuus kasvaisi arviolta noin 25 %. Väsymislujuuden 25:n prosentin korotuksella nurkkapolviolla vahvistetun hattuprofiilin käyttö olisi mahdollista muualla paitsi Pohjois-Atlantin liikennöintialueella kannella 8.

Taulukko 3 Pystypolviolla vahvistetun hattuprofiilirakenteen käyttömahdollisuudet Royal Princessin kansirakenteissa

		Merialue					
		1. Pohjois-Atlanti		2. Karibianmeri & Pohjois-Atlanti		3. Karibianmeri	
Kansi	**Kuvaus**	Vaadittu FAT / MPa	Saavutettu	Vaadittu FAT / MPa	Saavutettu	Vaadittu FAT / MPa	Saavutettu
4	Runko	42	87%	35	**106%**	35	**106%**
4	Kansirakennus	22	**168%**	19	**200%**	15	**241%**
5	Kansirakennus	28	**134%**	24	**152%**	19	**194%**
6	Kansirakennus	36	**103%**	32	**115%**	25	**148%**
7	Kansirakennus	45	83%	40	*93%*	31	**119%**
8	Kansirakennus	60	61%	46	*80%*	36	**102%**

Hattuprofiilin käyttö mahdollista lihavoituna esitetyillä alueilla (saavutettu > 100%)

6 LOPPUPÄÄTELMÄT JA YHTEENVETO

Tässä julkaisussa on esitetty hattuprofiililla jäykistetyn laivan kansirakenteen väsymislujuus-analyysin tuloksia. Lujuusanalyysi perustuu laskennallisesti ja kokeellisesti tehtyihin tutkimuksiin. Laskennallinen tutkimus tehtiin FE-menetelmällä käyttäen rakenteesta idealisoitua kuorielementtimallia. Kolmelle eri hattuprofiilikonstruktiolle tehtiin lisäksi väsytyskokeet.

FE-analyysissä tutkittiin viittä liitoksen vahvikerakennetta: vaakapolvio, uumainsertti, viistetty uumainsertti, nurkkapolvio ja pystypolvio rakennetta. FE-analyysissä käytettiin vertailumallina HP-profiililla jäykistettyä kansirakennetta. FE-analyysin perusteella nurkkapolvio ja pystypolviolla vahvistetut hattuprofiililiitoksen maksimijännitykset olivat likimain HP-profiililiitoksen suuruusluokkaa. FE-analyysi osoittautui melko hyväksi suhteellisen väsymislujuuden arviointimenetelmäksi. FE-analyysin pohjalta tehdyt arviot särön ydintymispaikasta ja eri rakennemallien väsymislujuusvertailut vastasivat koetuloksia. Lisäksi väsytyskoetulokset vastasivat aikaisempia tutkimustuloksia.

Väsymisvauriot syntyivät hattuprofiili ja nurkkapolviorakenteella profiilin ja poikittaislaipion liitoskohtaan. Särö ydintyi pienahitsin juuren puolelle. Hattuprofiililiitokselle ilman vahvikerakennetta saatiin väsymisluokaksi (FAT) 16 MPa ja nurkkapolviokonstruktiolle 35 MPa. Näiden rakenteiden väsymislujuutta olisi mahdollista kasvattaa liitoksen hitsisauman erilaisella toteutuksella, jolloin hitsin tunkeuma olisi parempi. Pystypolviorakenteella vahvistetun hattuprofiililiitoksen väsymisluokaksi saatiin 37 MPa.

Rakenteen toteuttamiskelpoisuutta saavutetun väsymislujuuden kannalta arvioitiin risteilijäaluksen kansirakenteessa. Nurkka- tai pystypolviolla vahvistettua hattuprofiilirakennetta olisi mahdollista käyttää Royal Princess:in kansirakenteissa Karibianmeren liikennöintialueella sekä osittain Pohjois-Atlantilla. Nurkkapolviorakenteen väsymislujuutta voidaan kasvattaa arviolta noin 25 % hitsin tunkeuman varmistamisella. Tällöin nurkkapolviollisen hattuprofiilin käyttö olisi mahdollista muualla paitsi Pohjois-Atlantin liikennöintialueella kannella kahdeksan.

7 KIITOKSET

Tässä julkaisussa esitetyt tulokset perustuvat Teknillisessä korkeakoulussa tehtyyn diplomityöhön. Työ liittyy Pinnoitetun ja ruostumattoman teräslevynkäyttö kerroslevyrakenteissa -nimiseen tutkimushankkeeseen. Tutkimustyö aloitettiin Teräksisten kerroslevyjen paikallislujuus ja liitokset -nimisen tutkimushankkeen aikana. Hankkeen rahoittajina olivat TEKES sekä teollisuuden yritykset. Kiitokset kaikille hankkeessa mukana olleille osapuolille.

8 LÄHDELUETTELO

American Welding Society. 1984. Structural Welding Code, Steel. D1.1-84. U.S.A

Det Norske Veritas. 1998. Fatigue assessment of ship structures. classification notes No. 30.7. Norway.

Fransman, J. 1986. A study of the influence of passenger ships' superstructures on the response of hull girder. Licentiate Thesis, Helsinki University of Technology, Ship Laboratory.

Fricke W., Petershagen H., Paetzold H. 1998. Fatigue Strength of Ship Structures: Part I & II. Hamburg, Germanischer Lloyd.

Gurney T. R. 1979. Fatigue of welded structures. Second Edition. Cambridge University Press. Cambridge.

Hibbitt, Karsson & Sorensen. 1995. ABAQUS/Standard User's manual Volume I-II Version 5.5. Abaqus. U.S.A

Hibbitt, Karsson & Sorensen. 1998. ABAQUS/Post Manual Version 5.8. Abaqus. U.S.A

Hobbacher, A. 1996. Recommendations for Fatigue Design of Welded Joints and Components. International Institute of Welding. XIII-1539-96 / XV-845-96.

Hughes, O. 1983. Ship Structural Design. The Society of Naval Architects and Marine Engineers. New Jersey.

I-DEAS. 1995. SDRC, I-DEAS Master Series Release 2.0/2.1.

Kujala P., Kukkanen T., Kotisalo K. 1999. Fatigue of all metal sandwich panels. Helsinki University of Technology. Ship Laboratory. Report M-237.

Kukkanen T., 1996. Spectral fatique analysis for ship structures. Uncertainties in fatigue actions. Licentiate's Thesis, Helsinki University of technology. Faculty of Mechanical Engineering.

Niemi E. 1996. Hitsattujen rakenteiden väsymistarkastelussa käytettävät jännitykset. Tekninen tiedotus, MET-julkaisu 3/96. Metalliteollisuuden Kustannus Oy. Tampere.

Niemi E., Kemppi J. 1993. Hitsatun rakenteen suunnittelun perusteet. Opetushallitus. Helsinki.

Niemi E., Kilkki J., Poutiainen I., Lihavainen V., 1998. Väsymättömän hitsausliitoksen suunnittelu. Lappeenrannan Teknillinen korkeakoulu.

Remes H, 1999. Hattuprofiililla jäykistetyn levykentän väsymislujuus. Diplomityö. Teknillinen korkeakoulu. Laivalaboratorio.

Radaj D. 1990. Design and Analysis of Fatigue Resistant Welded Structures. Abington Publishing. Cambridge. England.

Taggart R. 1980. Ship Design and Construction. The Society of Naval Architects and Marine Engineers. New York.

Latest FINFLO Applications to Propeller and Ship Hull Flows

Antonio Sánchez-Caja[1] and Tingqiu Li[2]
[1]VTT Manufacturing Technology, Helsinki, Finland
[2]Helsinki University of Technology, Helsinki, Finland

ABSTRACT

The FINFLO RANS equation solver has been used in many applications involving propeller and hull flows. In this paper some examples of the latest applications are presented. FINFLO is a multiblock cell-centred finite-volume multigrid-structured computer code with sliding mesh and moving-grid free-surface capabilities. As far as propeller flows are concerned, the two most interesting cases that had been recently analysed are the unsteady flow around a tractor thruster in quasi-steady and time-accurate computations and the axisymmetric flow around a ducted propeller. Good correlation with experiments is obtained in terms of force coefficients and velocity distributions. With regard to free-surface ship flows, two typically modern ship forms, the container and the tanker, have been tested. A dry- and a wetted-transom models are proposed for the treatment of the flow at the transom. The calculated results are compared with measurements for two turbulent models, the Baldwin-Lomax and Chien's low Reynolds number k-ε model. Good agreement with the experimental data in terms of the waves and total resistance coefficient is achieved. Furthermore, an improvement is observed with the k-ε turbulence model for the total resistance coefficient relative to the Baldwin-Lomax model.

1. INTRODUCTION

Over the last two decades, major advances in ship hydrodynamics have been achieved for the study of propeller and ship turbulent flows with and without free surfaces using Computational Fluid Dynamics (CFD) techniques. At the Helsinki University of Technology (HUT) and the Technical Research Centre of Finland (VTT) the application of RANS equation solvers to marine problems started in a cooperative programme in 1994.

For propeller flows, validation work was done for simple propeller geometries as that of DTMB propeller 4119 in 1995. Since then the application of FINFLO has been extended to more complex configurations as for example podded propulsors. In such propulsion units the flow is basically unsteady, which has to be taken into account into the computational model. The sliding mesh technique has been found robust for the analysis of the time-dependent viscous flow. The computations have been performed in a quasi-steady and in a time-accurate manner. The former was found to reduce the CPU time to about 1/10 relative to the latter. Its main merit consists of reducing the CPU time maintaining a full representation of the propeller geometry, i.e. without introducing simplified models for simulating the propeller action, such as actuator disk or body force models.

Another propeller configuration of interest to the Finnish industry is that of ducted propulsors. A Ka series ducted propeller with NSMB nozzle no. 19A has been selected as second validation case. Remarkable validation material is available for this case.

For ship flows with a free surface, most RANS solvers have been validated using

measurements from simple ship forms as those of the Wigley hull and the Series 60 (C_B=0.6). This has been also done for the FINFLO-code (Saisto & Sundell 1996, Sundell 1997, Piippo 1998). More recently, the primary emphasis in this area has been transferred to the detection of complex flow details for modern hull forms according to the recommendation of industry, and the results are directly used for performance analysis and ship design. As an example of this situation, some studies have been made for US Navy combatant model DTMB 5415 (C_B=0.506) by Cowles and Martinelli (1998), Ratcliffe (1998) and Wilson et al. (1998). Relevant works can also be found from Beddhu et al., (1998) and Muscal et al., (1999). DTMB 5415 is a modern naval combatant with sonar dome and transom stern quite different from typically modern merchant vessels.

Unfortunately, detailed RANS studies for modern merchant vessels are very limited in the open literature. These vessels present features that set most challenging topics to the marine hydrodynamics community, for example the partially wetted transom (ITTC, 1999). The complicated turbulent flow characteristics with free surface have been investigated for two types of the modern merchant ship forms using CFD techniques (Matusiak, 1999). A typical container vessel, the Hamburg Test Case (HTC), from HSVA, Germany, and a tanker from Finnish yard were selected as test cases. The former presents a flow detaching from the transom lower edge keeping it totally dry at the tested velocity. A dry-transom model is used for the analysis of such flow. The latter presents a partially wetted transom at the design speed, and a wetted-transom model is implemented for the treatment of the recirculating flow behind the transom.

2. NUMERICAL METHOD

2.1 Governing Equations

The flow simulation is based on the solution of RANS equations. They can be written in the following conservative form without the energy equation

$$\frac{\partial U}{\partial t}+\frac{\partial (F-F_v)}{\partial x}+\frac{\partial (G-G_v)}{\partial y}+\frac{\partial (H-H_v)}{\partial z}=Q \qquad (1)$$

where U is a vector of conservative variables $(\rho, \rho u, \rho v, \rho w, \rho k, \rho \varepsilon)^T$; F, G and H are the inviscid fluxes; F_v, G_v and H_v are the viscous fluxes; u, v and w are the absolute velocity components; ρ is the density, k is the turbulent kinetic energy and ε is dissipation of turbulence. The source term Q has non-zero components only for the turbulence equations. In the steady-state propeller analysis, the equations are solved in a co-ordinate system that rotates around the x-axis with an angular velocity Ω. In this case Q has the additional component (0, 0, $\rho\Omega w$, $-\rho\Omega v$, 0, 0, 0). In the time-accurate propeller analysis the source terms for the turbulence equations are retained, but there are no source terms in the momentum equations.

The concept of artificial compressibility is used to seek the solution of the equations for incompressible flows. The continuity equation is then modified by adding an artificial time derivative of pressure and an artificial speed of sound. The system of equations becomes hyperbolic and consequently has similar properties to those of compressible flows.

FINFLO has the possibility to use different turbulent models. In this paper Chien's low-

Reynolds-number k-ε model is used for propeller simulations and both the k-ε and Baldwin-Lomax model for hull flows. The solution is extended to the wall instead of using a wall-function approach.

2.2 Discretisation

A finite-volume technique is used for solving the equations. The differential equations are integrated over a computational cell

$$V_i \frac{dU_i}{dt} = \sum_{faces} -S.F^* + V_i Q_i \tag{2}$$

where

$$F^* = n_x(F-F_v) + n_y(G-G_v) + n_z(H-H_v) \tag{3}$$

and the summation is extended over the faces of the computational cell. In a rotating frame, i. e. for propeller calculations, the functional form of the flux equations is similar to the case without rotation. The difference is that in a rotating frame the motion of the cell faces is taken into account in the evaluation of energy flux and convective velocities.

Roe's method is applied for the evaluation of the inviscid fluxes. The flux is calculated with the help of a rotation matrix which transforms the dependent variables to a local system of co-ordinates normal to the cell surface (Siikonen, 1994). The interface values are evaluated by a MUSCL-type formula.

2.3 Solution Algorithm

For the steady-state flow simulation, the discretised equations are integrated in time by applying the DDADI-factorisation. This is based on the splitting of the Jacobians of the flux terms. The resulting approximately factored implicit scheme consists of a backward and a forward sweep in every co-ordinate direction. The sweeps are based on a first-order upwind differencing. In order to accelerate convergence, local time stepping and a multigrid method are also implemented in FINFLO (Siikonen et al., 1990). In the time-accurate simulation for unsteady flows, the above-mentioned pseudo-time integration is performed inside a physical time step (Sánchez et al., 1999). The sliding mesh technique was employed.

More detailed descriptions of FINFLO can be found in Siikonen et al. (1990), Lehtimäki et al., (1996), Siikonen & Pan (1992) and Pitkänen & Siikonen (1995).

2.4 Free-Surface Treatment

For flows with a free surface, the moving grid concept is used (Lehtimäki, 1998). The grid adapts to the free surface obtained by enforcing the dynamic boundary and the free surface is solved using the kinematic condition. The former condition is simplified and requires that the pressure at the free surface be atmospheric.The latter condition states that the flow particles on the free surface remain always on it.

The flow in the vicinity of the hull surface requires a special treatment. The non-slip boundary condition on the hull surface tends to deform the grid with severe shape gradients close to the hull surface. This problem can be avoided by extrapolating the wave shape from

that specified outside the problematic region. This is accomplished by the use of the linear least-square fit. In the transom stern region, both a dry- and a wetted-transom model are implemented for the Hamburg test case and the tanker, respectively. In the case of the former, the water is enforced to detach from the base of the transom junction as long as it touches the transom edge. In the case of the latter, a special treatment for the extrapolation of the wave height is necessary. Details of this procedure and results of it's application are given in Li (2000).

3. PROPELLER FLOW

3.1 Tractor thruster

The unsteady flow around a tractor thruster (pulling type) was reported in Sánchez-Caja et al. (1999) and analysed by solving the RANS equations in combination with the sliding mesh technique. The k-ε turbulent model was used in the simulation. The grid consists of 17 blocks divided into two groups representing the space near and far away from the pod. The space near the pod extends from the pod to a distance of about one propeller radius. The space far away from the hub extends from the propeller radius to the outermost external boundary. The grid has C-O topology in axial-circumferential direction for the group of blocks far away from the pod, and O-O topology for the blocks contiguous to the pod. The sliding surface is located between the propeller and the strut. The total number of cells is 814.080. The grid on the thruster surfaces is shown in Figure 1.

The computations were performed in two different ways. For the first calculation, the flow quantities were circumferentially averaged on the sliding surface in order to reduce computing time. The second calculation was time-accurate: no averaging of the flow is performed. Figures 2 and 3 show the pressure distributions obtained with the former method for the port and star-board side of the tractor thruster, and Figures 4, 5 and 6 show the corresponding results obtained with the latter method at different time steps. Differences from experimental values in thrust of 8.5 percent and in efficiency of about 6.5 percent appear. They were expected as the grid used in the computations was coarse: the entire space around the propeller and pod has to be meshed since no cyclic boundary conditions can be applied in the time-accurate calculation due to the presence of the strut, which breaks the axisymmetry of to inflow to the propeller.

The quasi-steady computation reduces the computing time in about one-tenth relative to the time-accurate computation. The differences from both calculations were about one percent for the performance coefficients due to the weak wake produced by the strut on the propeller plane. The quasi-steady approach gives a more accurate alternative for predicting the flow around tractor units than other methods that use actuator disk or body forces for modelling the propeller action.

3.2 Ducted Propeller

Validation data is presented for a ducted propeller in (Kawakita, 1992). The propeller has five blades, a diameter of 0.221 meters and a pitch ratio of 0.9741. The duct is NSMB nozzle no. 19A. LDV measurements were made at a rate of rotation of 25 rps and an advance coefficient of 0.5. The thrust and torque were measured as well as the velocities downstream the propeller. The grid used in the computations was over one million cells as shown in Table I. Figure 7 illustrates the grid shape on the duct and propeller surfaces.

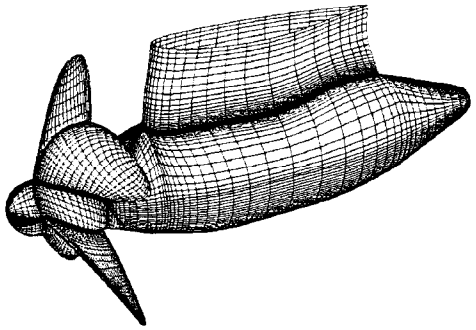

Figure 1. Computational grid on the surface of the tractor propulsor.

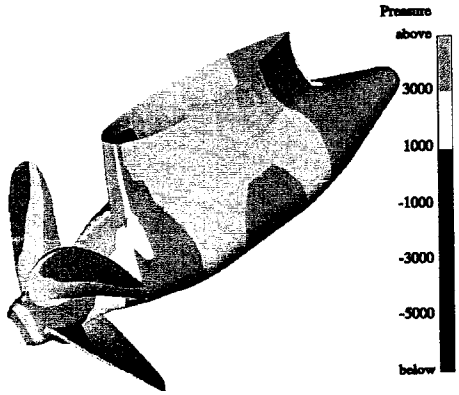

Figure 2. Distribution of pressure difference on the port side of the thruster surface. Quasi-steady simulation.

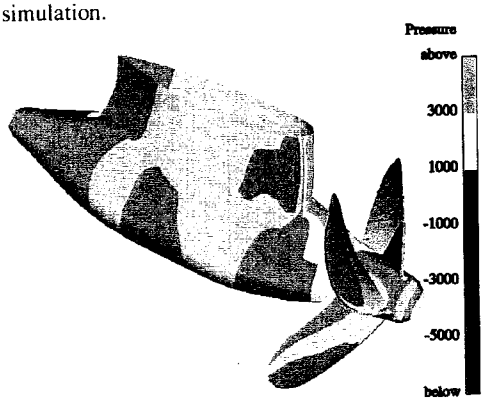

Figure 3. Distribution of pressure difference on the starboard side of the thruster surface. Quasi-steady simulation.

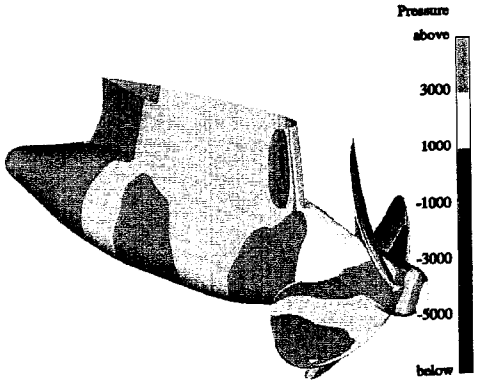

Figure 4. Distribution of pressure difference on the starboard side of the thruster surface for a reference angular position. Time-accurate simulation.

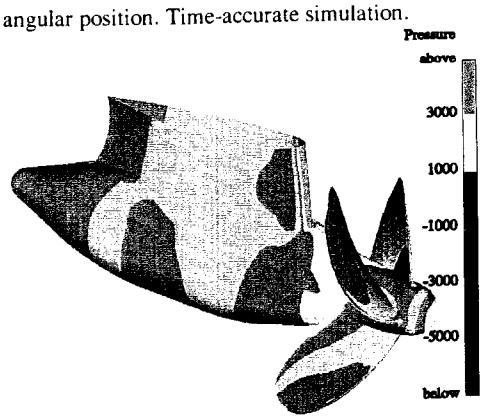

Figure 5. Distribution of pressure difference on the starboard side of the thruster surface for 30 deg propeller rotation. Time-accurate simulation.

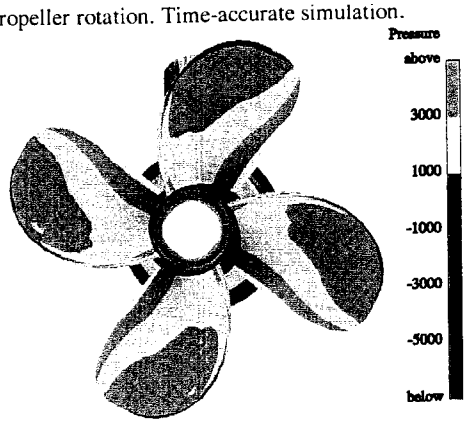

Figure 6. Distribution of pressure difference on the propeller blades. Time-accurate simulation.

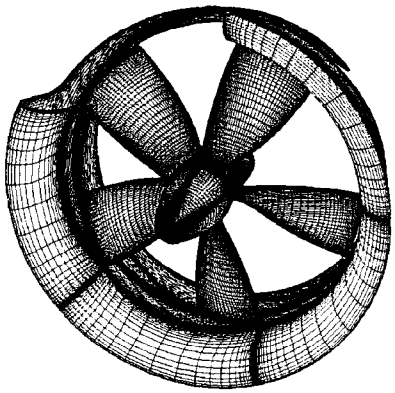

Figure 7. Computational grid on the surface of the ducted propulsor. Detail of duct construction

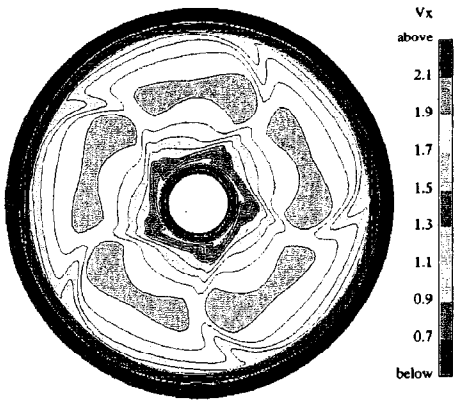

Figure 8. Predicted velocity distributions downstream of the ducted propeller (J=0.5, x/R=0.65).

The k-ε turbulence model gave good correlation of flow patterns and performance coefficients with measurements. Table II shows that the performance coefficients were calculated within 4.5 percent of the measurements. In particular the thrust coefficient for the propeller (K_{TP}) was predicted with accuracy. The about 4 percent difference in the prediction of the duct thrust (K_{TD}) made a total difference in the thrust coefficient (K_T) of one percent. The torque coefficient (K_Q) was overpredicted by about 4 percent. The good correlation with experimental values can be mainly attributed to the dense grid used in the calculations. Contrary to the tractor unit case, the axisymmetry of the inflow to the propeller allows us to use cyclic boundary conditions and, therefore, only the space between two contiguous blades has to be meshed.

Figure 8 shows a comparison of computed axial velocity contours with measurements. The agreement is good.

Table I. Number of cells in the mesh

Propeller Grid	Duct Grid	Rest of Grid	Total Grid
562,688	154,112	440,832	1,157,632

Table II. Calculated performance coefficients for the grids

	Experiment	Calculations
K_{TP}	0.197	0.197
K_{TD}	0.0481	0.0460
K_T	0.245	0.243
K_Q	0.03451	0.03615

4 HULL VISCOUS FLOW

4.1 Simulation of the HTC and Tanker

Table III presents the principal dimensions and grid points for the HTC and tanker, and their side profiles are shown in Fig.9. It is observed that the design waterline is located below the transom at the undisturbed free-surface for the HTC. The dry-transom model can therefore be used for the treatment of the flow off the transom. By contrast, for the tanker where the design waterline is above the transom stern and a wetted transom model is employed. The numerical simulation is performed with the two sets of meshes with O-O topology (see Fig. 10). Figure 11 displays the deformed hull surface and free surface in the transom regions when the flow is steady-state. The deformed free surface off the transom is rather flat for the HTC as compared with that for the tanker.

Table III. Principal dimensions and grid for the HTC and tanker

	HTC	Tanker
Ship length, L (m)	6.404	7.012
Breadth, B (m)	1.145	1.22
Forward draft, D_F (m)	0.383	0.58
After draft, D_A (m)	0.429	0.58
C_B	0.645	0.818
Coarse mesh	71x65x23	69x57x25
Fine mesh	141x129x45	137x113x49

4.2 Convergence History

Figure 12 presents the convergence history of the total resistance coefficient, C_T, for the HTC with the k-ε model. The value obtained is $C_T = 4.318 * 10^{-3}$ when the flow has reach the steady state. It approximates the experimental value within 2.27%. In other words, the total drag coefficient is predicted more accurately when the k-ε model is used instead of the B-L model (see Table IV). In the following subsections, unless otherwise indicated, all variables are nondimensionalized with L, U and ρ.

Table IV. Comparison of total drag coefficient for the HTC

	B-L model	k-ε mode	Experiment
Total resistance ($Ctx10^3$)	4.421	4.318	4.222
Relative error (%)	4.7	2.27	

Figure 9. Side profile. Top: the HTC ; Bottom: the tanker.

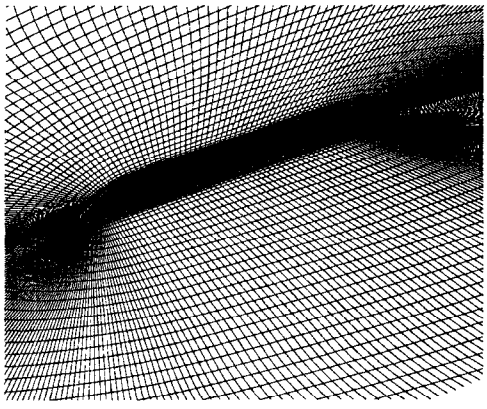

Figure 10. Mesh for the tanker.

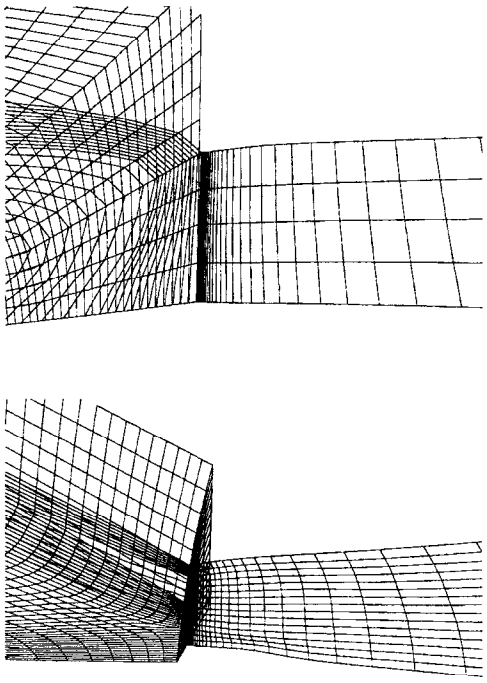

Figure 11. Deformed mesh at the transom. Top: HTC; Bottom: tanker.

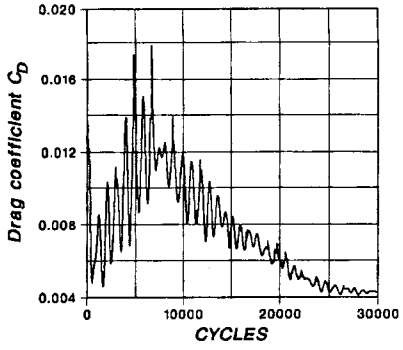

Figure 12. Convergence history of total drag coefficient, HTC (Fn= 0.25, Rn= $1.255*10^7$). K-ε turbulence model.

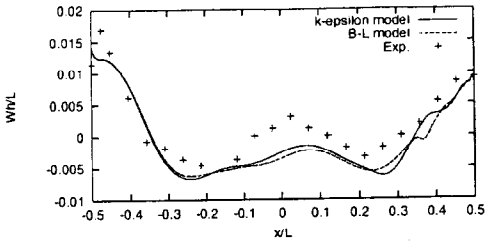

Figure 13. Comparison of wave profiles obtained with k-ε and B-L models, and experiments. HTC (Fn= 0.25, Rn= $1.255*10^7$).

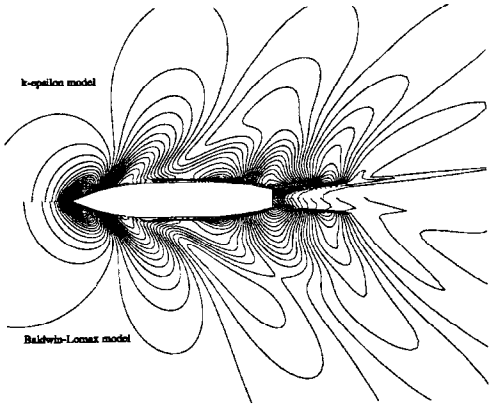

Figure 14. Wave contours. HTC (Fn= 0.25, Rn= $1.255*10^7$).

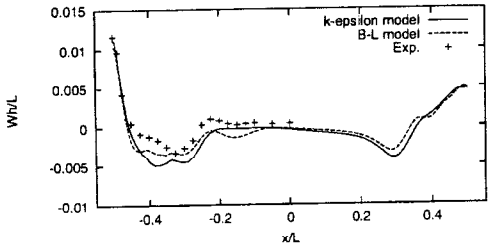

Figure 15. Comparison of wave profiles obtained with k-ε and B-L models, and experiments. Tanker (Fn= 0.15, Rn= $8.727*10^6$).

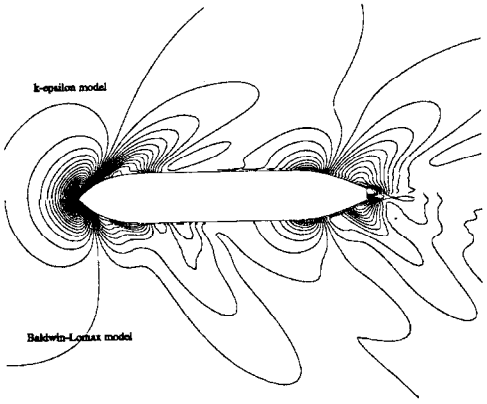

Figure 16. Wave contours. Tanker (Fn= 0.15, Rn= $8.727*10^6$).

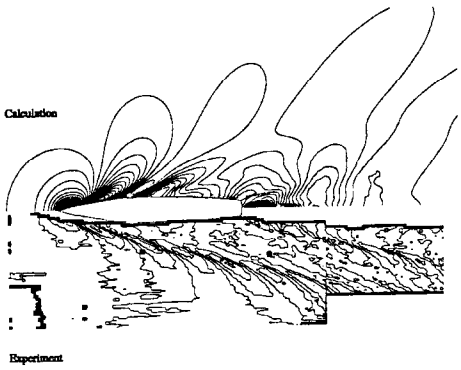

Figure 17. Comparison of wave contours between calculations and experiments. DTMB 5415 (Fn= 0.28, Rn= $1.28*10^7$).

4.3 Wave Patterns

4.3.1 The HTC

Figure 13 shows the surface-wave profiles obtained at the Fn=0.25 and Rn=1.255*10^7$, including a comparison between the k-ε and B-L models. It is seen that the effects of the turbulent model on the wave profiles are relatively small. Nevertheless, the results with the k-ε model seem to be closer to the experimental data in the most regions (Bertran et al., 1994), as shown in Fig.13. Interestingly, the transom waves at the stern (x/L=0.5) are rather flat as compared with the bow waves (x/L=-0.5). This is attributed to the effect of the transom stern. It confirms that the dry-transom model works well. However, a discrepancy remains at the midship. The wave contours with these two turbulent models are shown in Fig.14. It is observed that the wave field is not strongly dependent on the turbulence model due to rather small change between the contours.

4.3 The tanker

For the tanker, the surface-wave profiles at the Fn=0.15 and Rn=8.727*10^6 are well simulated as compared with the experimental data, as shown in Fig. 15. Unfortunately, measurements are available only in the bow region. Our recent study for the model DTMB 5415 shows the waves are simulated well, as shown in Fig. 17. This implies that the wetted-transom model works well. Moreover, the effects between the k-ε and B-L models are very small, except in the region of first trough where the difference between them seems to be large and the results with the B-L model are closer to the experimental data.

5. ACKNOWLEDGEMENTS

This work was sponsored by the Technology Development Centre (TEKES). The authors wish to thank the CFD team of the Departments of Applied Thermodymanics and Acronautics at Helsinki University of Technology and of the Deparment of Maritime and Mechanical Engineering at VTT Manufacturing Technology. Among them Patrik Rautaheimo, Esa Salminen, Reijo Lehtimäki, and more recently, Jussi Martio and Tommi Mikkola should be mentioned. Especially the authors are greatly indebted to Prof. Jerzy Matusiak., Prof. Timo Siikonen and Tech. Dr. Jaakko Pylkkänen for their support during all these years.

6. REFERENCES

Bertram Volker, Chao Kuo-Yih, Lammers Gerd and Laudan Jochen, 1994, Experimental validation data of free-surface flows for cargo vessels, Proceedings of CFD Workshop, Tokyo, Japan.

Bin Chen and Frederick Stern, 1999, Computational fluid dynamics of four-quadrant marine-propulsor flow, Journal Ship Research, Vol.43, No.4.

Cowles, G. and Martinelli, L., 1998, A viscous multiblock flow solver for free-surface calculations on complex geometries, Proc. 22nd Symp. Naval Hydrodynamics, Washington D.C.

ITTC, 1999, Report of the resistance and flow committee, 22nd International Towing Tank Conference, Seoul, Korea and Shanghai, China.

Lehtimäki, R., 1998, Grid Deformations Tools for Simulation of Free-Surface Flows, 1998, 6th International Conference on Numerical Grid Generation in Computational Fields Simulations, pp. 599-608, London UK

Lehtimäki, R., Laine, S., Siikonen, T., Salminen, E., 1996, Navier-Stokes Calculations for a Complete Aircraft, 20th ICAS Congress, Sorrento, ICAS-92-4.2.1.

Li, T., 2000, Numerical simulation of viscous steady flow with free surface around two types of modern realistic hull forms: Hamburg Test Case and Tanker, Report M-247, Ship Laboratory, Helsinki University of Technology, Finland.

Matusiak Jerzy, 1999, Calculation of ship viscous flow using FINFLO, INSEAN, Rome.

Muscari, R., Broglio, R. and Di Mascio, A., 1999, Comparison of three turbulence models for the study of the wake past a ship hull, JAKOM'99, Fukuuku, Japan.

Piippo, H, 1998. Computation of Steady Flow of Series 60 Ship Model in a Towing Tank. Espoo, 1998. VTT Manufacturing Technology Report VAL3A-010.

Pitkänen, H., Siikonen, T., 1995, Simulation of Viscous Flow in a Centrifugal Compressor. Espoo, HUT, Laboratory of Aerodynamics, Report No. B-46.

Saisto I., Sundell T., 1996. Computation of the viscous flow field around ship hulls, Integrated numerical and experimental methods in ship design Œ96, Otaniemi 27.3.96.

Sánchez-Caja, A, Salminen, E., Rautaheimo, P., Siikonen, T., 1999, Computations of the Incompressible Viscous Flow Around a Tractor Thruster Using a Sliding-Mesh Technique. 7th International Conference on Numerical Ship Hydrodynamics, July 19-22, Nantes (France).

Siikonen, T., 1995, An Application of Roe´s Flux-Difference Splitting for k-ε Turbulence Model, International Journal for Numerical Methods in Fluids, Vol. 21, No. 11. (Espoo, HUT, Laboratory of Aerodynamics, Report No. A-15.)

Siikonen, T., 1994, An Application of Roe´s Flux-Difference Splitting for k-ε Turbulence Model, International Journal for Numerical Methods in Fluids, Vol. 21, No. 11. (Espoo, HUT, Laboratory of Aerodynamics, Report No. A-15.)

Siikonen, T., Pan, H.-C.,1992, An Application of Roe´s Method for the Simulation of Viscous Flow in Turbomachinery, First European Computational Fluid Dynamics Conference, Brussels, 7-11 Sep 1992.

Sundell, T., 1997. Computations of the Free Surface Flow Around a ShipUsing the NS Solver FINFLO, VTT Technical Report VALB279

Taylor and Abdollah Arabshahi, 1998, CFD validation of the free surface flow around DTMB model 5415 using Reynolds averaged Navier-Stokes equations, Third Osaka Colloquium on advanced CFD Applications to Ship Flow and Hull Form Design, Osaka.

Wilson, R., Paterson, E. and Stern, F., 1998, Unsteady RANS CFD method for Naval combatant in waves, Proc. 22nd Symp. Naval hydrodynamics, Washington, D.C.

ALUKSEN LIIKKEIDEN KUUDEN VAPAUSASTEEN SIMULOINTIMALLI

Jussi Martio[1]
[1]VTT Valmistustekniikka

TIIVISTELMÄ

Tutkimuksessa on kehitetty matemaattinen malli aluksen kuuden vapausasteen simulointia varten säännöllisessä ja epäsäännöllisessä aallokossa. Aluksen ohjailusimulaattorin matemaattisen mallin liikeyhtälöihin on lisätty kallistus-, jyskintä- ja kohoiluliikkeiden liikeyhtälöt. Epälineaarisen Strip-teorian avulla lasketaan runkoon kohdistuvat aaltoherätevoimat. Lisäksi virtausta peräsimen ympärillä korjataan aaltopotentiaalista määritetyillä nopeuskomponenteilla, ja peräsimen sekä tuulen on herätevoimakomponentteihin on lisätty kallistusmomentit. Jyskintä- ja kohoiluliikkeet on mahdollista määrittää myös etukäteen merikelpoisuusohjelman antamien siirtofunktioiden avulla. Tässä raportissa on esitetty pääperiaatteet ja tarvittavat yhtälöt kyseisten mallien implementoimiseksi ohjailusimulaattoriin.

Täysmittakaavavertailujen osalta tulokset ovat kohtuullisia paitsi keinuntakulmien ja peräsinkulmien osalta. Esimerkkinä menetelmän mahdollisista sovellutuksista suoritettiin broaching-simulointeja sekä säännöllisessä että epäsäännöllisessä aallokossa. Broaching saatiin simuloitua muuttamalla alkuperäisen laivamallin parametrejä säännöllisessä aallokossa.

1. JOHDANTO

Hydrodynamiikassa on aluksen liikkeiden tarkasteleminen perinteisesti jaettu käsiteltävien vapausasteiden mukaan merikelpoisuuteen ja ohjailuun. Ohjailuun kuuluvat yleensä pitkittäis- ja poikittaisliikkeet sekä kääntymisliike, merikelpoisuuteen vastaavasti jyskintä, kohoilu ja keinunta.

Laivan liikkeitä määrittävät teoreettiset laskentamallit ovat kehittyneet merikelpoisuudessa pidemmälle kuin ohjailussa. Tähän on vaikuttanut mm. kaksi seikkaa: merikelpoisuuden herätevoimat, aaltovoimat, ovat luonteeltaan jaksonomaisia, jolloin liikkeitä (voimia) ei tarvitse simuloida ajan funktiona. Lisäksi viskoositeetista aiheutuvat hydrodynaamiset voimat eivät ole merikelpoisuudessa yhtä merkitseviä kuin ohjailussa, jolloin on ollut mahdollista käyttää yksinkertaisia potentiaaliteoriaan perustuvia malleja. Ohjailussa vastaavia teorioita ei ole pystytty kehittämään, ja mallikokeet ovat tällä hetkellä ainoa keino uuden laivamallin luomiseksi ohjailusimulaattoriin.

Merikelpoisuuden ja ohjailun käsitteleminen erikseen rajoittaa tiettyjen ilmiöiden tutkimista. Eräs hankalimista tarkasteltavista on broaching-tilanne, joka tapahtuu aluksen kulkiessa myötäaallokossa pienellä kohtaamistaajuudella, ja joka saattaa pahimmillaan johtaa aluksen kaatumiseen. Koska kyseisessä tapahtumaketjussa on tärkeää mallintaa sekä aallokon että peräsimen herätevoimat samanaikaisesti, on laskenta suoritettava kuuden vapausasteen simulointina. Muita mahdollisia tutkittavia ilmiöitä on aallokon vaikutus ohjailuun, aluksen vakavuuden menetys aallokossa, kallistuksen vaikutus ohjailuun sekä slamming.

Jos peräsinkulmat, peräsinkomennot ja aaltoherätevoimat halutaan sisällyttää matemaattiseen malliin, ainoa mahdollisuus laskea laivan liikkeitä kuudessa vapausasteessa on simulointi. Tällöin merikelpoisuusteorioiden aaltoherätevoimat on siirrettävä aikatason laskentaan, mikä vaatii käytettävältä tietokoneelta hyvää laskentakapasiteettia.

2. MATEMAATTINEN MALLI

Laivan liiketilaa simuloidaan Newtonin toisen lain mukaisesti:

$$\overline{F} = m\overline{a} \tag{1}$$

missä massa m sisältää laivan massan ja lisätyt massat, $\overline{a}$ on kiihtyvyys vektori ja $\overline{F}$ voimavektori. (1) voidaan lausua maahan kiinnitettyssä inertiaalikoordinaatistossa kuhunkin liikesuuntaan:

$$\begin{aligned} X_0 &= m_x \dot{u}_0 \\ Y_0 &= m_y \dot{v}_0 \\ Z_0 &= m_z \dot{w}_0 \\ N_0 &= I_{yy} \dot{r}_0 \\ K_0 &= I_{xx} \dot{p}_0 \\ M_0 &= I_{zz} \dot{q}_0 \end{aligned} \tag{2}$$

jossa I_{xx} , I_{yy} ja I_{zz} ovat hitausmomentit ja lisätyt hitaudet x_0-, y_0- ja z_0-akseleiden suhteen, $\dot{u}_0, \dot{v}_0$ ja $\dot{w}_0$ ovat kiihtyvyydet pitkittäis-, poikittais- ja pystysuuntiin sekä $\dot{r}_0$, $\dot{p}_0$ ja $\dot{q}_0$ kulmakiihtyvyydet x_0-, y_0- ja z_0-akseleiden ympäri. Voimat X, Y ja Z sekä momentit N, K ja M jaetaan komponentteihin seuraavasti:

$$\begin{aligned} X &= X_{hull} + X_{propeller} + X_{rudder} + X_{wind} + X_{wave} \\ Y &= Y_{hull} + Y_{rudder} + Y_{wind} + Y_{wave} \\ Z &= Z_{restoring} + Z_{hull} + Z_{wave} \\ N &= N_{hull} + N_{propeller} + N_{rudder} + N_{wind} + N_{wave} \\ K &= K_{hull} + K_{rudder} + K_{wind} + K_{wave} + K_{restoring} \\ M &= M_{hull} + M_{wave} + M_{restoring} \end{aligned} \tag{3}$$

Toisen kertaluvun differentiaaliyhtälöt (2) voidaan ratkaista määrittämällä ensin kiihtyvyydet ajan hetkellä t_j, jolloin uudet nopeuskomponentit saadaan integroimalla kiihtyvyysvektori ajan suhteen.Tätä varten implementoitiin sekä Eulerin eksplisiittinen että Runge-Kutta menetelmät. Toista vaihetta varten, paikkavektorin $\overline{X}$ määrittämistä ajan hetkellä t_{j+1}, nopeusvektori $\overline{V}$ muunnetaan kappalekoordinaatistosta inertiakoordinaatistoon. Kuudessa vapausasteessa käytetään kannanvaihtomatriiseja $\underline{T}$ ja $\underline{R}$ (Kalske 1992):

$$(u_0, v_0, w_0) = \underline{T}^{-1}(u, v, w)$$
$$(\dot{\phi}_0, \dot{\Theta}_0, \dot{\Psi}_0) = \underline{R}^{-1}(p, q, r) \tag{4}$$

Jotta voimat voidaan voidaan jälleen laskea ajan hetkellä t_{j+1}, on nopeudet u_0, v_0 ja w_0 sekä kääntymisnopeudet $\dot{\phi}_0, \dot{\Theta}_0$ ja $\dot{\Psi}_0$ muunnettava takaisin kappalekoordinaatistoon:

$$(u, v, w) = \underline{T}(u_0, v_0, w_0)$$
$$(p, q, r) = \underline{R}(\dot{\phi}_0, \dot{\Theta}_0, \dot{\Psi}_0) \tag{5}$$

Lisättyjen massojen vaikutukset koordinaatistojen vaihdoksessa jätetään huomioimatta.

3. RUNKOVOIMAT

3.1 Hydrostaattiset voimat

Hydrostaattiset voimat ovat nollannen kertaluvun eli laivan asemasta ja asennosta aiheutuvia voimia. Ohjailussa nollannen kertaluvun voimat eivät ole merkitseviä, mutta jyskinnän, kohoilun ja keinunnan kannalta ne ovat tärkeitä.

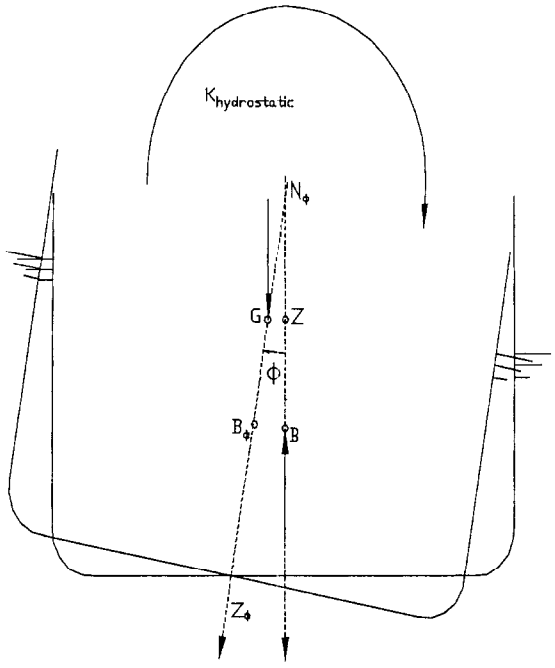

Kuva 1. Hydrostaattisen momentin määrittäminen, käytetyt merkinnät

Kuvassa 1 on veden pinta aallokossa eri korkeudella eri puolilla rungon poikkileikkausta. Laiva pyrkii takaisin tasapainotilaan kallistumalla kulman ϕ. Alusta kallistava momentti

$K_{hydrostatic}$ lasketaan

$$K_{hydrostatic} = -\rho g \nabla \overline{GZ} = -\rho g \nabla \overline{GN}_{\phi} \sin\phi \tag{6}$$

jossa pisteen N_ϕ koordinaatit ($y_{N\phi}$, $z_{N\phi}$) ovat

$$\tan\phi = \frac{y_{B\phi} - y_{N\phi}}{z_{B\phi} - z_{N\phi}} = \frac{y_{B\phi}}{z_{B\phi} - z_{N\phi}} \Rightarrow$$
$$z_{N\phi} = -\frac{y_{B\phi}}{\tan\phi} + z_{B\phi} \tag{7}$$

Koska kaavoissa (6)-(7) on tunnettava uppouman painopisteen B koordinaatit ($y_{B\phi}$, $z_{B\phi}$), on vapaan nestepinnan muoto laskettava rungon 2D poikkileikkauksissa jokaisena ajan hetkenä. Jos veden pinnan oletetaan olevan suora poikkileikkauksen läpi, voidaan aallon korkeus η laskea halutussa pisteessä ajan hetkellä t_j seuraavasti:

$$\eta_j(x,y) = \sum_{i=1}^{nw} \eta_i^a \cdot \cos\left(k_i x \cos\mu + k_i y \sin\mu - \omega_{wei}(t) \cdot t_j + \varepsilon_i\right) \tag{8}$$

missä η_i^a on kyseisen aaltokomponentin amplitudi, k on aaltoluku, μ laivan kurssi aallokkoon nähden, nw aaltokomponentien lukumäärä ja ε_i aaltokomponentin vaihe. Myös yhtälö (8) on ratkaistava ajan suhteen aaltokomponentin kohtaamistaajuuden $\omega_{ei}(t)$ takia.

Jyskinnän hydrostaattinen momenttikomponentti lasketaan vastaavalla tavalla kuin keinunnan tapauksessa. Kohoilun tapauksessa voimakomponentti saadaan hetkellisen ja tyynen veden uppouman erotuksena.

3.1 Aaltoherätevoimat

Aaltovoimat määritetään merikelpoisuudessa yleisesti käytetyn 2-D potentiaaliteorian, ns. Strip-teorian avulla. Kyseinen teoria olettaa laivan hoikaksi kappaleeksi ja virtauksen ideaalivirtaukseksi. Voimien laskenta suoritetaan laivan rungon 2-D poikkileikkauksissa.

Aaltoherätevoimat jaetaan kahteen osaan: Froude-Krylov voimiin ja diffraktiovoimiin. Froude-Krylov voimat saadaan määrittämällä häiriöittömän aallokon aiheuttama painekenttä laivan rungolla, ja diffraktiovoimien avulla korjataan laivan aiheuttamaa häiriötä rajapintaan. Kokonaisaaltoherätevoimat saadaan laskemalla Froude-Krylov- ja diffraktiovoimat yhteen komponenteittain:

$$
\begin{aligned}
X_{wave} &= F_{FKx} + F_{DIFFx} \\
Y_{wave} &= F_{FKy} + F_{DIFFy} \\
Z_{wave} &= F_{FKz} + F_{DIFFz} \\
N_{wave} &= M_{FKz} + M_{DIFFz} \\
K_{wave} &= M_{FKx} + M_{DIFFx} \\
M_{wave} &= M_{FKz} + M_{DIFFz}
\end{aligned}
\tag{9}
$$

Sekä Froude-Krylov voimat että diffraktiovoimat ovat luonteeltaan epälineaarisia, tässä tapauksessa diffraktiovoimat oletettiin lineaarisiksi. Froude-Krylov voimien epälineaarisuus huomioidaan päivittämällä aaltoa rungolla tarvittavia suureita laskettaessa.

3.1.1 Froude-Krylov voimat

Froude-Krylov voimat lasketaan hydrostaattisesta ja hydrodynaamisesta paineesta aallokon nopeuspotentiaalin avulla. Aluksen vaikutusta rajapintaan ei huomioida.
Veden paine p on hydrostaattisen paineen p_S ja hydrodynaamisen paineen p_d summa:

$$
\begin{aligned}
p &= p_s + p_d \\
&= \rho g z + \rho g \cdot \sum_{i=1}^{N} \eta_i^a k_i e^{-k_i z_{pp}} \cos(k_i x_{pp} \cos\mu - k_i y_{pp} \sin\mu - \omega_{ei} t + \varepsilon_i)
\end{aligned}
\tag{10}
$$

jossa x_{pp} ja y_{pp} ovat runkoviipaleen uppouman painopisteen koordinaatit.
Froude-Krylov voima saadaan integroimalla painejakauma rungon yli:

$$
F_{Fk} = -\iint_S (p_s + p_d)\bar{n}\, dS \tag{11}
$$

missä S on laivan vedenalaisen osan pinta-ala ja n veden pinnan ja x-akselin välinen yksikkö normaalivektori. Soveltamalla Gaussin sääntöä yhtälöön (11) (Newman 1977)

$$
F_{Fk} = -\iint_S (p_s + p_d)\bar{n}\, dS = -\iiint_V \nabla(p_s + p_d) dV = -\int_L \left(\iint_{S(x)} \nabla(p_s + p_d)\, dS \right) dx \tag{12}
$$

Lausumalla (12) summamuodossa saadaan

$$
F_{Fk} = -\sum_{i=1}^{NSec} \left(\iint_{S(x)} \nabla(p_s + p_d)\, dS \right) \cdot \Delta x_i \tag{13}
$$

jossa NSec on rungon poikkileikkausten lukumäärä.

Voimat kuhunkin liikesuuntaan lasketaan määrittämällä painegradientti haluttuun suuntaan lausekkeesta (13) Esimerkkinä pitkittäisvoima (Tuite 1997):

$$F_{Fkx} = \sum_{x=1}^{NSec} \frac{\partial p}{\partial x} \cdot \nabla_x(t)$$
$$= \sum_{x=1}^{NSec} - \rho g \cos\mu \sum_{i=1}^{N} \eta_i^a k_i e^{-k_i z_{pp}} \sin(k_i x_{pp} \cos\mu - k_i y_{pp} \sin\mu - \omega_{ei} t + \varepsilon_i) \cdot \nabla_x(t) \quad (14)$$

Tässä $\nabla_x(t)$ on runkoviipaleen hetkellinen uppouma ja A_{ww} on runkoviipaleen vesiviivan hetkellinen pinta-ala.

3.1.1 Diffraktiovoimat

Diffraktiovoimat lasketaan rungon poikkileikkauksien lisättyjen massojen sekä kyseisten leikkausten painopisteissä määritetyn vesipartikkelin nopeuden ja kiihtyvyyden avulla. Nopeudet lasketaan aaltokomponenttien nopeuspotentiaalin ϕ avulla:

$$\phi_{tot} = g \sum_{i=1}^{N} \frac{\eta_i^a}{\omega_i} e^{-k_i z} \sin(k_i x \cos\mu + k_i y \sin\mu - \omega_{ei} t + \varepsilon_i)$$
$$\Rightarrow \frac{\partial \phi_{tot}}{\partial y} = \dot{y}_{wave} = g \sum_{i=1}^{N} \frac{\eta_i^a}{\omega_i} e^{-k_i z} k_i \sin\mu \cdot \cos(k_i x \cos\mu + k_i y \sin\mu - \omega_{ei} t + \varepsilon_i)$$
$$\Rightarrow \frac{\partial^2 \dot{y}_{wave}}{\partial t} = \ddot{y}_{wave} = g \sum_{i=1}^{N} \frac{\eta_i^a}{\omega_i} e^{-k_i z} k_i \omega_{ei} \sin\mu \cdot \sin(k_i x \cos\mu - k_i y \sin\mu - \omega_{ei} t + \varepsilon_i) \quad (15)$$

Diffraktiovoimat määritetään seuraavasti (Tuite 1997):
Poikittaisvoima:

$$F_{DIFFy} = \sum_{x=1}^{m} \ddot{y}_{wave} \cdot AWM(t) + \sum_{x=1}^{m} \dot{y}_{wave} \cdot \frac{d\,AWM(t)}{dx} \cdot v \quad (16)$$

2D poikkileikkauksen lisätty massa AWM voidaan laskea esim. konformikuvauksella tai reunaelementtimenetelmällä.

3.1.3 Peräsin kallistava momentti

Peräsimen kallistava momentti arvioidaan sijoittamalla peräsimen sivuvoiman vaikutuspiste peräsimen syväyden d_{rudder} puoliväliin:

$$K_{rudder} = Y_{Rrudder} \cdot d_{rudder}/2 \quad (17)$$

missä $Y_{Rrudder}$ on peräsimen koordinaatistossa laskettu sivuvoima.

3.1.4 Peräsimeen aallokosta indusoitunut virtausnopeus

Aallokosta peräsimeen kohdistuva nopeuskomponentti määritetään laskemalla aaltopotentiaalin gradientti x ja y-akseleiden suunnassa:

$$u_{rudderwave} = \frac{\partial \phi_{wave}}{\partial x} = \sum_{i=1}^{N} \frac{ga_i}{\omega_i} k_i \cos\mu \, e^{-k_i z} \cos(k_i x_{rudder} \cos\mu + k_i y_{rudder} \sin\mu - \omega_{ei} t + \varepsilon_i)$$
$$v_{rudderwave} = \frac{\partial \phi_{wave}}{\partial y} = \sum_{i=1}^{N} \frac{ga_i}{\omega_i} k_i \sin\mu \, e^{-k_i z} \cos(k_i x_{rudder} \cos\mu + k_i y_{rudder} \sin\mu - \omega_{ei} t + \varepsilon_i) \quad (18)$$

jossa (x_{rudder},y_{rudder}) on peräsimen keskipisteen koordinaatit.

3.1.5 Tuulen kallistava momentti

Tuulen laivaa kallistava herätemomentti määritetään asettamalla tuulen sivuvoiman vaikutuspiste aluksen vedenpäällisen osan puoliväliin:

$$K_{wind} = Y_{wind} \cdot D/2 \quad (19)$$

3.1.6 Autopilot

Simuloinneissa käytettiin ns. kaarresädeautopilottia, joka yrittää ohjata laivaa annettuun annettuun suuntakulmaan. Yleensä broaching-tutkimuksissa asetetaan PID-säätimen integraaliosa I nollaksi (Tuite 1997), jolloin ajan suhteen kumuloituvaa virhettä ei huomioida. Yleisesti voidaan todeta, että autopilotin oikeat asetukset ovat olennaisia simulointitulosten kannalta.

4. ESIMERKKI TAPAUS: BROACING SIMULOINTI

Broaching-simulointeja suoritettiin autopilotin ohjauksessa säännöllisessä ja epäsäännöllisessä aallokossa. Kuvassa 2 on esitetty tilanne, jossa alus riistäytyy hallinnasta sen ratsastaessa alas aallon harjaa.

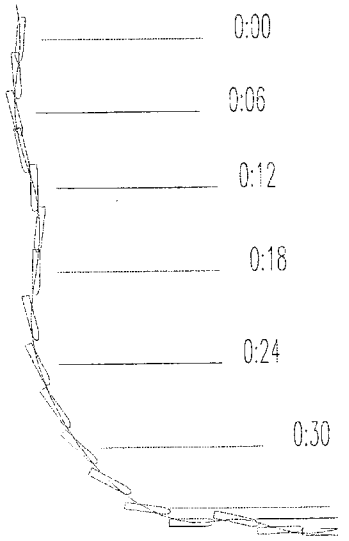

Kuva 2. Aluksen kulkema reitti broaching simuloinnissa

Kyseessä ei ole aivan todellinen broaching, jossa kääntymisnopeus saattaa nousta hyvinkin suureksi, ja josta pahimmillaan on seurauksena aluksen kaatuminen. Kuitenkin ilmiön perusteet pystytään mallintamaan, eli kun peräsin alusta oikaiseva momentti ei enää pysty kumoamaan aallosta runkoon indusoitunutta momenttia (Tuite 1997), kääntyy alus poikittain aallokkoon nähden.

5. JOHTOPÄÄTÖKSET

PC-pohjaiseen ohjailusimulaattoriin on implementoitu epälineaariseen strip-teoriaan perustuva aaltovoimien laskentamalli. Mallin testaus on yhä käynnissä, tähänastiset validoinnit ovat olleet rohkaisevia. PC-ympäristössä laskentaa voidaan suorittaa tietyin edellytyksin reaaliaikaisena säännöllisessä aallokossa. Lisäksi simulaattoriohjelman modulaarisuuden ansiosta kuuden vapausasteen liikkeiden laskentamalli on yhdistettävissä helpohkosti mihin tahansa simulaattorissa jo olevaan malliin.

Kalske, Seppo, Motion Simulation of Underwater Vehicles, Espoo 1992, VTT, VTT Publications 97, 138 p. + app. 27 p.

Newman J.N., Marine Hydrodynamics, Massachusetts Institute of Technology Press, Cambridge, 1977

Tuite Andrew, Broaching: An Extreme Nonlinear Motion Experienced by Small Vessels in Astern Seas, Väitöskirja, Australian Maritime College, Tasmania, 1997

POWER METHODS IN CONTROL OF SOUND AND VIBRATION

P. Hynnä, Research Scientist
VTT Manufacturing Technology, Maritime and Mechanical Engineering
Espoo, Finland

ABSTRACT

Low noise and vibration design methods are nowadays described in international standards. In these the airborne input power is the quantity, which is used to characterize the sources of airborne sound. As to structure-borne sound power and characterization of machines as a source of structure-borne sound there are not yet generally accepted international standards or methods. However, the research work on these topics is going on both in theoretical and practical aspects.

This literature review belongs to the VÄRE subproject Control of vibration and noise of vehicles. The aim of this literature review is to become acquainted with the methods for the characterisation of diesel engines and propellers of a ship as structure-borne sound sources. The other aim is to develop and transfer knowledge of design methods for the minimization of structure-borne sound transmission from sources to connected receiving structures.

1. INTRODUCTION

Nowadays acoustics of vehicles or of any kind of machines is important for the community and the industry. Low noise and vibration design (ISO/TR 11688-1, 1995; ISO/TR 11688-2 1998; and ISO 9611, 1996) is getting more emphasis at the design stage and it has an important impact on the marketability and competitiveness of many products. At the pre-design stage it is often asked to predict the resulted sound levels of a machine or component. To do this, one needs to analyze all the excitation sources and their interactions with the structures and transmission paths. For airborne sound well-established methods are nowadays available. Instead for structure-borne sound the methods for characterization of machines or components as sources of structure-borne sound are still in phase of intensive research and development.

Sound is propagated over long distances in build-up structures mainly as structure-borne sound (Cremer and Heckl, 1973) because typically material damping is low. Instead airborne sound has only meaning near the sound source or in spaces contiguous to the source space. Audible sound to a normal human ear covers roughly the frequency range from 20 Hz to 20 kHz (Pierce, 1991). Often at the design stage the frequency range is restricted to the frequencies including the octave bands with centre frequencies from 31,5 Hz to 8 kHz. This means that in built-up systems composed typically of beams, plates and shells one or two dimensions are small compared with the structural wavelength.

Predictability is required in different design stages including pre-design and simulation. Using the numerical calculation packages like FEM and BEM engineers are able to predict the sound and vibration levels of real structures only at very low frequencies. That is why they are looking for new solution methods like energy-related methods (e.g., Lyon and DeJong, 1995). The same trend is in the measurement techniques of transmission of sound and

vibration. The research is aimed towards vectorial energy techniques instead of classical transfer and modal approaches.

Analysis methods of structure-borne sound transmission must be able to handle different parts of the structure and the whole structure as well. Substructuring technique allows the properties of the assembled structure to be calculated using the properties of its parts. In the modelling using substructuring one important requirement is to be able to utilize also measured input data because the properties of mechanical parts vary and sometimes the only way is to use measured input data. The so-called impedance or mobility method allows both substructuring and use of measured input data (Carlsson, 1993). The roles of experiments with computational experimentation are thoroughly discussed by Fahy (1998).

Vibrating coupled structures often produce unwanted sound, noise. Characterization of machines as sources of structure-borne sound is the major problem when estimating the structure-borne sound emission (Wolde and Gadefelt, 1987). Vibrational power transmission from a machine source to flexible machinery supporting structures has been under intensive research (see e.g., Mondot and Petersson (1987), Koh and White (1996, I-III), Fulford and Gibbs (1997), Fulford and Gibbs (1999, Parts 1-2). Power transmission from a source structure to the receiving structure depends on the mobilities of the source and the receiving structure, respectively.

This research is concentrated (see *Figure 1*) to the structure-borne sound power and source characterization of diesel engines and propellers. The industrial application examples are in the ship or small craft context. The results of this project are also applied to an agricultural tractor in another subproject. The mobility technique is also under study, because it is well known that the transmitted power from a source to the receiving structure is dependent on the mobilities of the source and the receiver.

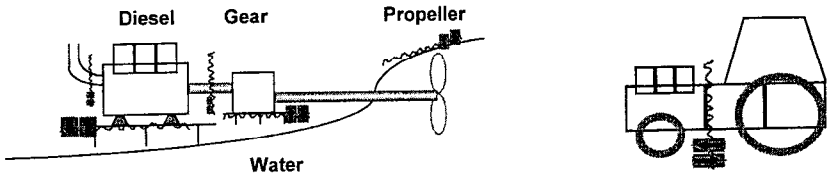

Figure 1. In the ship and small graft context interaction phenomena interconnect sources of sound and vibration with structure and the surrounding air and water. In an agricultural tractor the sound and vibration of a diesel engine is coupled to the cabin and environment.

2. MECHANICAL MOBILITY

2.1 General

ISO 7626-1 (1986) gives a definition to mechanical mobility Y_{ij} as the frequency-response function formed by the ratio of the velocity-response phasor at point i to the excitation force phasor at point j when all other measurement points on the structure are allowed to respond freely without any constraints other than those constraints which represent the normal support of the structure in its intended application. This definition is given mathematically in Eq. (1)

$$Y_{ij} = v_i / F_j \,, \tag{1}$$

where v_i is the velocity-response phasor and F_j the force phasor. The velocity response can be either translational or rotational, and the excitation can be either a rectilinear force or a moment. Mechanical mobility is sometimes called mechanical admittance. Mechanical mobility is the inverse of mechanical impedance Z_{ij}. The complex impedance Z can be written as

$$Z = R + iX \,, \tag{2}$$

where the real part R is called the resistance and the imaginary part X the reactance. Likewise the complex mobility Y can be written as

$$Y = G + iB \,, \tag{3}$$

where the real part G is called the conductance and the imaginary part B the susceptance.

Blocked impedance Z_{ij} is defined in ISO 7626-1 as the frequency-response function formed by the ratio of the phasor of the blocking or driving-point force response at point i to the phasor of the applied excitation velocity at point j, with all other measurement points on the structure "blocked" meaning constrained to have zero velocity. All forces and moments required to constrain fully all points of interest on the structure shall be measured in order to obtain a valid blocked impedance matrix.

Free impedance is defined in ISO 7626-1 as the ratio of the applied excitation force phasor to the resulting velocity phasor, with all other connection points of the system free. This means that they have zero restraining force. Free impedance is the arithmetic reciprocal of a single element of the mobility matrix.

Driving-point mechanical mobility or direct mechanical mobility Y_{ii} is the complex ratio of velocity and force taken at the same point in a mechanical system during simple harmonic motion (ISO 2041, 1990). Here point means both a location and a direction. Sometimes the term coordinate is used instead of point. Transfer mechanical mobility Y_{ij} is the complex ratio of the velocity v_i measured at the point i in the mechanical system to the force excitation at the point j in the same system during simple harmonic motion (ISO 2041, 1990).

According to matrix calculation the elements of impedance matrix are not the arithmetic reciprocals of the mobility matrix, and vice versa. The concept of immittance (impedance or admittance) and transmission matrices in the context of the vibration of mechanical systems is discussed in (Rubin, 1967). The mobilities on the contrary to the impedances of a given structure do not interdepend upon both the location and number of points of interest (O'Hara, 1967). Mobilities describe invariant characteristics of the whole structure, instead impedances describe only substructures. Because impedances depend upon the number of observation points considered they are not invariant characteristics of the structure (O'Hara, 1967).

In some applications a complete mobility matrix has to be measured for the description of the dynamic characteristics of a structure. So translational forces and motions along three mutually perpendicular axes as well as moments and rotational motions may be required to be measured depending on the applications. These measurements result in a 6 x 6-mobility matrix for each measurement location. For N measurement locations this means a full $6N$ x

$6N$-mobility matrix. However, in practice only seldom the full mobility matrix needs to be measured. Usually it suffices to measure only the driving-point mobility in the excitation location and a few transfer mobilities in locations of interest on the structure. Sometimes the dynamics of the system needs to be determined only in one coordinate direction, usually in vertical direction. Also in many practical engineering applications the influence of rotational motions and moments is negligible or can be replaced by two translations and forces.

2.2 Modelling with mobility

In the mobility technique the classical spring-mass-model is replaced by mobility model of a real structure (see *Figure 2*).

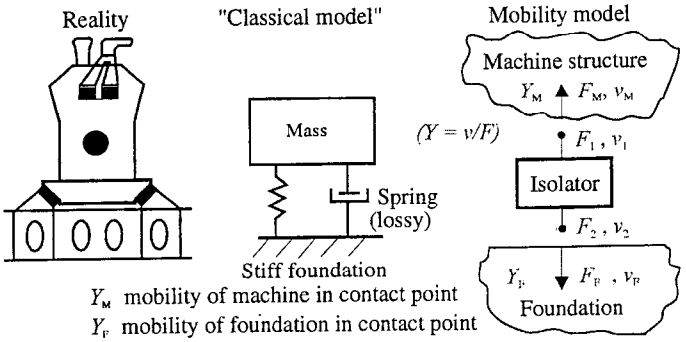

Figure 2. Calculation models of vibration isolated mounting (adapted from Plunt, 1981).

A source of structure-borne sound is connected to a receiver structure in N contact points having $n = 6N$ coupling coordinates, if all six motion coordinates are included in each point. For a time-harmonic vibration at angular frequency ω, the time-averaged power transmitted to the receiving structure in the ith contact point is

$$P_i = \tfrac{1}{2}\,\mathrm{Re}\,(\hat{F}_i \hat{v}_i^{*}) \tag{4}$$

where $\hat{F}_i$ is the complex amplitude of contact force and $\hat{v}_i$ of coupled velocity. When using the complex amplitude of free velocity $\hat{v}_f$ of the source and the driving point mobilities of the machine Y_M and foundation Y_F, the transmitted power is (Ohlrich, 1983)

$$P = \tfrac{1}{2}\left|\hat{v}_f^2\right| \frac{\mathrm{Re}\,\{Y_F\}}{\left|Y_M + Y_F\right|^2}. \tag{5}$$

From equation (5) it is seen that the power transmitted to the receiving structure is dependent on the free velocity of the source and the mobilities of the source and the receiving structure.

3. POWER CALIBRATION OF RECEIVING STRUCTURE

3.1 Calibration of receiver prior to installation of the source

Power calibration of the receiving structure developed by Ohrich (1999) is based on the relationship between power input at a point and the associated energy response of an arbitrarily chosen control region in the far-field of the receiving structure (see *Figure 3*).

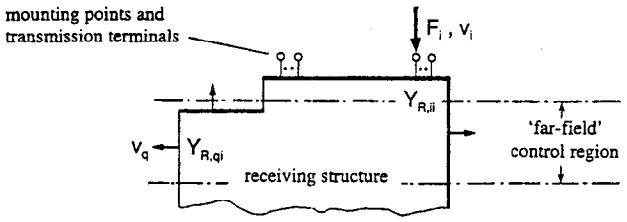

Figure 3. Power calibration of receiving structure by applying a known external force F_i at the ith drive point (Ohlrich, 1999).

From an external point force F_i at the point i with driving point mobility $Y_{R,ii}$ the power input is $P_i = F_i^2 \,\mathrm{Re}\,(Y_{R,ii})$, where the time-averaged mean-square value of force F_i^2 is introduced, e.g., $F_i^2 = \tfrac{1}{2}|F_i|^2$. This same notation is used later in this text. At the arbitrary point q in the far-field the exciting force generates as a response a normal velocity component of mean-square value

$$v_q^2 = |Y_{R,qi}|^2 F_i^2, \tag{6}$$

where $Y_{R,qi}$ is the transfer mobility from force excitation point i to receiving point q. The power input can be related to the spatially averaged velocity response $\langle v_q{}^2 \rangle$ and to the spatially averaged transfer mobility by (Ohlrich, 1999)

$$P_i = \langle v_q{}^2 \rangle \frac{\mathrm{Re}\,(Y_{R,ii})}{\langle |Y_{R,qi}|^2 \rangle} = \langle v_q{}^2 \rangle \mathrm{Re}\,(\alpha_{qi}), \tag{7}$$

where

$$\mathrm{Re}\,(\alpha_{qi}) = \mathrm{Re}\,((Y_{R,ii}) / \langle |Y_{R,qi}|^2 \rangle) \tag{8}$$

is the frequency dependent function of proportionality, which is obtained according to equation (7) using measured results. These uncorrelated proportionality functions are

averaged over three to four points to minimize uncertainty in the power estimate P according to the equation (Ohlrich, 1999)

$$P = \left\langle v_q^{\,2} \right\rangle \left\langle \frac{\mathrm{Re}\,(Y_{\mathrm{R},ii})}{\left\langle \left| Y_{\mathrm{R},qi} \right|^2 \right\rangle} \right\rangle_i = \left\langle v_q^{\,2} \right\rangle \left\langle \mathrm{Re}\,(\alpha_{qi}) \right\rangle_i . \tag{9}$$

In the derivation of the equation (9) no cross coupling was taken into account. After the averaged proportionality function is determined, the source is operated and the velocity response is measured. The structural power of the real source is obtained multiplying the result of proportionality function determined during power calibration with the spatially averaged squared velocity response $\left\langle v_q^{\,2} \right\rangle$. The details of the measurement technique are described in the article (Ohlrich, 1999).

3.2 Calibration when source is installed

In practice often the receiver mobilities are not available or measurable, because the source is already installed. In such cases one can use total mobilities of the coupled source-receiver system Y_{ii} and Y_{qi}. In these cases an approximate expression developed by Ohlrich (1999) can be used provided that the mobility of the source $Y_{\mathrm{S},ii}$ or alternatively the mobility of the receiver $Y_{\mathrm{R},ii}$ is known (see *Figure 4*).

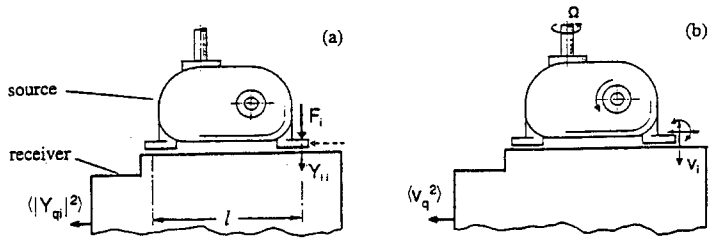

Figure 4. An illustration of measurements on coupled source-receiver system for the determination of: (a) total mobility, (b) averaged mean-squared velocity in the far-field (Ohlrich, 1999).

The total driving point mobility Y_{ii} and transfer mobility Y_i can be approximated as (Ohlrich, 1999)

$$Y_{ii} \approx \frac{Y_{\mathrm{S},ii} Y_{\mathrm{R},ii}}{Y_{\mathrm{S},ii} + Y_{\mathrm{R},ii}} \qquad \text{and} \qquad Y_{qi} \approx \frac{Y_{\mathrm{S},ii} Y_{\mathrm{R},qi}}{Y_{\mathrm{S},ii} + Y_{\mathrm{R},ii}} . \tag{10), (11}$$

With these approximated mobilities the power is obtained from (Ohlrich, 1999)

$$\tilde{P}^{S} \approx \langle v_q^{\,2} \rangle \left\langle \frac{|Y_{ii}|^2 \,\mathrm{Re}\,(1/Y_{ii} - 1/Y_{S,ii})}{\langle |Y_{qi}|^2 \rangle} \right\rangle_i \quad \text{or} \quad \tilde{P}^{R} \approx \langle v_q^{\,2} \rangle \left\langle \frac{|Y_{ii}|^2 \,\mathrm{Re}\,(1/Y_{R,ii})}{\langle |Y_{qi}|^2 \rangle} \right\rangle_i \qquad (12), (13)$$

where eq. (12) is used to estimate $\tilde{P}^{S}$ when the total source mobility $Y_{S,ii}$ is known, and eq. (13) when the total receiver mobility $Y_{R,ii}$ is known. Ohlrich obtained very good results with the structural power calibration and demonstrated the reliability of the procedures developed when he made in-situ measurements with two different type test receiving structures: a scale model of a ship testbed and with a 3/4-scale helicopter fuselage (see Ohlrich, 1999).

4 EXPERIMENTS AND COMPUTER SIMULATIONS

In the experimental part of this research project the aim is to apply the power flow methods in the ship context. The preliminary in-situ power calibration of a diesel engine was made on board a Ro-Ro ship (see *Figure 5*). During these measurements the ship was in the harbour and all propulsion machinery was stopped. The necessary electrical power was obtained from ashore. In addition the total mobility of a combined source-receiver system was measured in this phase. During the transfer voyage from the shipyard to Teesport in England the structure-borne sound power delivered by the diesel engine was measured. In a later phase the mobilities and source strength of this type of a diesel engine are measured in the test bed and compared to the results obtained in the ship installation. The mobility of the foundation in the ship is being calculated using the FEM method in the low frequencies. The calculated results are compared with measured ones.

Figure 5. Diesel engine in the test ship (left) and the excitation of the foundation with an electrodynamic shaker on board the Ro-Ro ship.

Later the mobility technique is applied in the design calculations of ship foundations to minimize the transmitted power from diesel engine to the ship steel structure. Also the interaction phenomena of a ship propeller with the steel plating above the propeller are considered for the determination of the structural power flow from propeller to the steel plating. In this part the FEM method and the mobility technique are planned to be used.

5 USE OF POWER FLOW ANALYSIS

Power flow analysis techniques can be used in the control of sound and vibration. It enables to determine the power transmitted from a source to the receiving structure. Using it various sources can be put quantitatively into the order of importance and compare the importance of different transmission paths. Ordinary vibration measurements fail in this task. The transmitted structural power can be minimized using mobility techniques. This has found applications e.g. in automotive industry (Ochsner and Bernhard, 1995). Statistical Energy Analysis (SEA) requires that the source strength of different machines and equipment are inputted as structural power or as airborne power depending on the source type (see e.g., Lyon and DeJong, 1995); Hynnä, Klinge and Vuoksinen 1995).

6 CONCLUSIONS

This literature review has shown that the modern energy related methods like power flow analysis and mobility technique are in the promising international research and development phase. It seems that the in-situ measurement techniques developed by Ohlrich can be applied in the ship context provided that the measurement equipment at hand fulfil the requirements of heavy and stiff structures encountered in practise.

7 ACKNOWLEDGEMENTS

VÄRE - Control of Vibration and Sound - Technology Programme 1999-2002 is a national technology programme launched by Tekes. "Power methods in control of sound and vibration" is one of its various subprojects. Tekes and Finnish companies Aker Finnyards, Kværner Helsinki and Turku yards, a diesel manufacturer Wärtsilä NSD Finland, and VTT Manufacturing Technology financially support this ongoing study. This funding and co-operation made this project possible and it is greatly acknowledged by the project group.

The supervising group is leaded by Licentiate in Technology Tapio Hulkkonen from Kværner Helsinki yard and the other members are: Masters of Science in Technology Jouko Virtanen, Berndt Lönnberg and Engineer Juhani Siren from Kværner; Masters of Science in Technology Jukka Vasama, Kari Kyyrö and Jari Lausmaa from Finnyards; and Masters of Science in Technology Peter Sundström and Petri Aaltonen from Wärtsilä NSD; project manager of the project "Control of vibration and noise of vehicles", Master of Science in Technology Teijo Salmi; and research professor, Doctor of Technology Matti K. Hakala from VTT Manufacturing Technology.

The author wants to express his warm thanks to the supervising group for the support and encouragement during the work.

8 REFERENCES

Carlsson, U. 1993. Mechanical mobility: A tool for the analysis of vibrations in mechanical structures (Doctoral thesis). Stockholm: Technical acoustics, Department of Vehicle Engineering, Royal Institute of Technology. Marcus Wallenberg Institute of Sound and Vibration Research. 333 p.

Cremer, L., Heckl, M. 1973. Structure-borne sound. Structural vibrations and sound radiation at audio frequencies. Berlin: Springer-Verlag. 528 p.

Fahy, F. 1998. Manfred Heckl memorial lecture: The role of experimentation in vibroacoustics. In: Proc. of the third European Conference on Noise Control, EURO-NOISE 98. Munich, Germany: German Acoustical Society. Pp. 3-14.

Fulford, R. A., Gibbs, B. M. 1997. Structure-borne sound power and source characterization in multi-point-connected systems, Part 1: Case studies for assumed force distributions. Journal of Sound and Vibration. Vol. 204, no. 4, pp. 659-677.

Fulford, R. A., Gibbs, B. M. 1999. Structure-borne sound power and source characterization in multi-point-connected systems, Part 2: About mobility functions and free velocities. Journal of Sound and Vibration. Vol. 220, no. 2, pp. 203-224.

Fulford, R. A., Gibbs, B. M. 1999. Structure-borne sound power and source characterization in multi-point-connected systems, Part 3: Force ratio estimates. Journal of Sound and Vibration. Vol. 225, no. 2, pp. 239-282.

Hynnä, P. Klinge, P. and Vuoksinen, J. 1995. Prediction of structure-borne sound transmission in large welded ship structures using statistical energy analysis. Journal of Sound and Vibration. Vol. 180, no. 4. pp. 583-607.

ISO 2041. 1990. Vibration and shock - Vocabulary. International Organization for Standardization. 59 p.

ISO 7626-1. 1986. Vibration and shock - Experimental determination of mechanical mobility - Part 1: Basic definitions and transducers. International Organization for Standardization. 23 p.

ISO 9611. 1996. Acoustics - Characterization of sources of structure-borne sound with respect to sound radiation from connected structures - Measurement of velocity at the contact points of machinery when resiliently mounted. International Organization for Standardization. 19 p.

ISO/TR 11688-1. 1995. Acoustics - Recommended practice for the design of low-noise machinery and equipment - Part 1: Planning. International organization for standardization. 36 p.

ISO/TR 11688-2. 1998. Acoustics - Recommended practice for the design of low-noise machinery and equipment - Part 2: Introduction to the physics of low-noise design. International Organization for Standardization. 46 p.

Koh, Y. K., White, R. G. 1996. Analysis and control of vibrational power transmission to machinery supporting structures subjected to a multiexitation system, Part I: Driving point mobility matrix of beams and rectangular plates. Journal of Sound and Vibration. Vol. 196, no. 4, pp. 469-493.

Koh, Y. K., White, R. G. 1996. Analysis and control of vibrational power transmission to machinery supporting structures subjected to a multi-excitation system, Part II: Vibrational power analysis and control schemes. Journal of Sound and Vibration. Vol. 196, no. 4, pp. 495-508.

Koh, Y. K., White, R. G . 1996. Analysis and control of vibrational power transmission to machinery supporting structures subjected to a multi-excitation system, Part III: Vibrational power cancellation and control experiments. Journal of Sound and Vibration. Vol. 196, no. 4, pp. 509-522.

Lyon, R. H., DeJong, R. G. 1995. Theory and application of statistical energy analysis. 2nd. ed. Boston, Massachusetts, USA: Butterworth-Heinemann. 227 p.

Mondot, J. M., Petersson, B. 1987. Characterization of structure-borne sound sources: The source descriptor and the coupling function. Journal of Sound and Vibration. Vol. 114, no. 3, pp. 507-518.

O'Hara, G. J. 1967. Mechanical impedance and mobility concepts. The Journal of Sound and Vibration. Vol. 41, no. 5, pp. 1180-1184.

Ohlrich, M. 1983. Experimental studies on transmission of structure-borne sound in models representing engine, foundation and hull structures. In: Plunt, J., Odegaard, J. (ed.). Noise sources in ships, II: diesel engines. Stockholm: Nordforsk. 23 p. (Miljövårsserien, Publication 1983:2)

Ohlrich, M. 1999. In-situ estimation of structural power transmission from machinery source installations. In : Jacobsen, F. (ed.) Proceedings of the Sixth Interenational Congress on Sound and Vibration. Lungby: The International Institute of Acoustics. Vol. 5, pp. 2149-2160.

Ochhsner, S. D., Bernhard, R. J. 1995. Application of a component mobility modeling technique to automotive suspension systems. Noise Control Engineering Journal. Vol. 43, no. 3, pp. 73-82.

Pierce, A. D. 1991. Acoustics. An introduction to its physical principles and applications. 2nd. ed. New York: The Acoustical Society of America. 678 p.

Plunt, J. 1981. Vibrationsisolering av maskiner. Dimensioneringsmetod, även för högfrekventa vibrationer. Göteborg: IFM Akustikbyrån. 123 p. + app. 44 p.

Rubin, S. 1967. Mechanical immittance- and transmission-matrix concepts. The Journal of the Acoustical Society of America. Vol. 41, no. 5, pp. 1171-1179.

Wolde, T. ten, Gadefelt, G. R. 1987. Development of standard measurement methods for structure-borne sound emission. Noise control engineering Journal. Vol. 28, no. 1, pp. 5-14.